Properties of voltage-gated Na^+ channels in pancreatic β-cells

---



A thesis submitted for the degree of Doctor of Philosophy by

Mahdieh Godazgar

St John's College, University of Oxford

and

Oxford Centre for Diabetes Endocrinology and Metabolism

Radcliffe Department of Medicine, University of Oxford

Michaelmas Term 2017

To my beloved family

Hossein, Masoumeh, Mahdi, Hadi and Faezeh

Statement of Authorship

I hereby declare that this is the original work of the author and contributions from others are declared here:

- All of the chimera constructs and the TTX-resistant $Na_V1.7$ and $Na_V1.3$ channels were generated by Dr. Margarita Chibalina.
- The data from Figure 3.2.5.1B-C are reanalysed data from (Zhang et al., 2014).

No part of this thesis has been submitted for any other degree at this or any other university.

Acknowledgements

The sincerity of my gratitude cannot be adequately conveyed on a single side of paper to colleagues, friends and family who have contributed to the past few years of my professional and personal development. I am extremely grateful to my supervisors Professor Patrik Rorsman and Dr. Margarita Chibalina for giving me the freedom to carry out my research independently and for providing me with the mentorship, guidance and support that has ultimately allowed me to develop as a scientist. Patrik, your enthusiasm for science has been inspiring; despite the challenges of the project, I always left your office with a sense of optimism and a determination to discover! Margarita, I am grateful for your invaluable insight that has, without a doubt, helped me develop into a more critical scientist. I also thank Dr. Quan Zhang for the insightful discussions and his continued enthusiasm for the project.

I would like to thank all members of the Rorsman laboratory (past and present) for all their invaluable discussions, expertise, companionship and patience. I would like to especially thank David Wiggins, Samantha Pearce, Andrei Tarasov, Linford Briant, Jakob Knudsen, Kerry McLaughlin and Reshma Ramracheya. A special thanks to Benoit Hastoy, for guiding me through my initial insecurities, for all his invaluable suggestions, for teaching me the most useful skill of fixing a bike puncture and for tolerating my poor taste in music over the countless hours spent in the TIRF room patching. You have been a wonderful colleague and friend. A special thanks also to Elisa Vergari, I am so lucky to have shared this journey with you. I am grateful for the fun, laughter and your support and encouragement in my development as a scientist. I have learnt a lot from you-most importantly to always be 'curious'!

I would also like to thank members of OCDEM: Costas, Natasha Hui Jin, Nellie Loh, Katherine Pinnick, Shahana, Vibe, Anna Gloyn and Leanne Hodson for taking an interest in me and the progress of my DPhil. I also thank Anne Clark, it has been a privilege to work with you and to accomplish the several baking challenges that we set for ourselves along the way! I would also like to thank the Radcliffe Department of Medicine for funding my DPhil, for providing opportunities for further growth and for taking a genuine interest in the development of their students.

This journey began as an undergraduate student in the laboratory of Professor Peter Jones. It was here that I was given the opportunity, confidence and mentorship to pursue my interest in science and research. I am extremely grateful for this and for the continued support that I have received during the course of my DPhil.

I am so grateful to all my friends in Oxford for making some of my most cherished memories in this wonderful city. Myrto, Gabby, Giuseppe and Jonas thank you for the countless evenings spent together, for sharing in my tears and laughter and for being my family away from home. Anca, thank you for the many evenings spent over delicious home-cooked food, your friendship and for tolerating the lab-chat that we put you through! Myrte and Melissa, I already miss the frantic evenings spent together baking, thank you for your friendship and all fond memories made. My special friend Caz, thank you for always taking me back to my 14-year old self and being there to laugh hysterically in the good and the not-so-good times alike.

My final and biggest thank you goes to my family for all their love, patience and support. Faezeh, thank you for always being there, for your calming and gentle reassurance when I needed it most and for being the best friend and sister that I am so very lucky to have. Hadash and Mahdash, thank you for giving me the confidence to never set limits on what I can achieve and for always encouraging me to be ambitious in my aims. Ali, Elias and Danial thank you for letting me be a part of your family and for all the laughter that we have shared along the way. Ma, Ba – no words can ever sufficiently thank you for all that you have given me. Thank you for allowing me the freedom to explore and purse my own interests, whilst always patiently supporting me. You are a continued source of inspiration and I am eternally grateful to have you as my role models in life. Thank you.

Abstract

Na_V channels in rodent β-cells predominantly exhibit a hyperpolarised voltage-dependence of inactivation, which is so characteristic that it can be used for functional identification of β-cells (Briant et al., 2017a, Chakravarthy et al., 2017). A smaller Na^+ current component (10-15%) also exists that inactivates over physiological membrane potentials and contributes to action potential firing (Vignali et al., 2006, Zhang et al., 2014). It has been proposed that the currents contributing to inactivation over vastly different membrane potentials reflect the contribution of different Na_V α-subunits. The aim of this thesis was to investigate the contribution of individual Na_V channel α-subunits to the behaviour of Na_V current inactivation in β-cells and to gain insight into the underlying mechanism(s) of channel regulation. TTX-resistant variants of the Na_V subunits found in β-cells ($Na_V1.3$, $Na_V1.6$ and $Na_V1.7$) were used to isolate currents from individual α-subunits expressed in insulin-secreting Ins1 cells and in non-β-cells (including HEK, CHO and αTC1-6 cells). $Na_V1.7$ inactivated at 15-20mV more negative membrane potentials than $Na_V1.3$ and $Na_V1.6$ in Ins1 cells. Meanwhile, all Na_V subunits inactivated at ~20-30mV more negative membrane potentials in Ins1 cells than in HEK, CHO or αTC1-6 cells reflecting α-subunit and cell-specific differences in the inactivation of Na_V channels. In Ins1 and primary β-cells, but never in the other cell types, widely different components of Na_V inactivation (separated by 30 mV) were also observed following expression of a single type of Na_V α-subunit. The more positive component exhibited a voltage-dependence of inactivation similar to that found in HEK/CHO cells. The more negative inactivation in Ins1 cells does not involve a diffusible intracellular factor because the difference between Ins1 and CHO persisted after excision of the membrane. We propose that biphasic Na_V inactivation in insulin-secreting cells reflects insertion of channels in membrane domains that differ with regard to lipid and/or membrane protein composition.

Common Abbreviations

ADP	Adenosine diphosphate
ATP	Adenosine triphosphate
K_{ATP} channels	ATP-sensitive-potassium channels
Na_V channels	Voltage-gated Na^+ channels
V_h	Half-maximal inactivation
$V_{0.5}$	Half-maximal activation
TTX	Tetrodotoxin
PTM	Post-translational modification
L1	Loop 1
L2	Loop2
L3	Loop 3
PKA	Protein kinase A
PKB	Protein kinase B
PKC	Protein kinase C
MAPK	Mitogen-activated protein kinase
CAMKII	Ca^{2+}/calmodulin-dependent protein kinase II
h	hour(s)
FCS	Foetal calf serum
nM	nanomolar
µM	micromolar
ml	millilitre
PMA	phorbol 12-myristate 13-acetate
GSIS	Glucose stimulated insulin secretion
DRG	Dorsal root ganglion
VSD	Voltage-sensing domain

Table of Contents

Chapter 1 13

1.1 Introduction 14

1.2 Regulation of glucose homeostasis by the pancreatic islets of Langerhans 15

1.2.1 The structure and function of the pancreatic islets of Langerhans 15

1.2.2 Diabetes Mellitus 17

1.2.3 Stimulus Secretion Coupling in β-cells 18

1.2.4 Glucose-inhibited glucagon secretion in α-cells 21

1.3 Structure and function of Na_V channels 24

1.3.1 Architecture of Na_v channels 24

1.3.2 Steady-state activation and inactivation of Na_V channels 27

1.4 Na_V channel inactivation properties in pancreatic β-cells 32

1.4.1 Arcane inactivation properties of Na_V channels in rodent β-cells 32

1.4.2 Species differences in Na_V channel inactivation in β-cells 33

1.4.3 Contribution of individual Na_V channel α-subunits to the arcane inactivation properties of Na_V currents in β-cells 34

1.5 Aims of thesis 35

Chapter 2 36

2.1 Molecular Biology 37

2.1.1 Plasmid constructs 37

2.1.2 Transformation of Bacteria 38

2.1.3 Site-directed mutagenesis 38

2.1.4 Gene expression analysis 39

2.2 Tissue culture and cell transfection 41

2.2.1 Cell culture 41

2.2.2 Cell transfection 42

2.3 Electrophysiology 43

2.3.1 Data Analysis 47

Chapter 3 48

3.1 Introduction 49

3.2 Results 51

3.2.1 Characterisation of endogenous Na_V channels in Ins1 and HEK cells 51

3.2.2 Characterisation of wild-type and TTX-resistant $Na_V1.7$, $Na_V1.3$ and $Na_V1.6$ in HEK cells. 56

3.2.3 Characterisation of $Na_V1.7$ in Ins1 and HEK cells 58

3.2.4 Characterisation of $Na_V1.3$ in Ins1 and HEK cells 64

3.2.5 Biphasic inactivation in primary β-cells 67

3.2.6 Voltage-dependence of activation of $Na_V1.3$ currents in Ins1 and HEK cells 68

3.2.7 Characterisation of $Na_V1.6$ in Ins1 and HEK cells 70

3.2.8 Characterisation of $Na_V1.5$ in Ins1 and HEK cells 74

3.2.9 Summary of $Na_V1.7$, $Na_V1.3$ and $Na_V1.6$ activation and inactivation properties in Ins1 and HEK cells 77

3.2.10 Characterisation of $Na_V1.7$, $Na_V1.3$ and $Na_V1.6$ in human EndoC-βh2 cell line 81

3.2.11 Characterisation of $Na_V1.7$, $Na_V1.3$ and $Na_V1.6$ in rodent non-β-cell lines 85

3.3 Discussion 87

3.3.1 Na_V channels inactivate at more negative membrane potentials in Ins1 cells 87

3.3.2 Individual Na_V subtypes exhibit two distinct inactivation behaviours 88

3.3.3 Species- and cell-specific regulation of Na_V channels 90

3.2.4 Biphasic and hyperpolarised inactivation of Na_V currents in Ins1 cells 92

Chapter 4 94

4.1 Introduction 95

4.2 Results 97

4.2.1 Effect of endogenous β_3-subunit knockdown on Na_V channel current properties in Ins1 cells 97

4.2.2 Effect of single β-subunit expression on the biphasic inactivation of Na_V currents in Ins1 cells 100

4.2.3 Effect of β_3-subunit expression on Na_V current in HEK cells 103

4.3 Discussion 107

Chapter 5 110

5.1 Introduction 111

5.2 Results 111

5.2.1 Regulation of Na_V channels is unlikely to be mediated through the cytoplasmic domains 111
5.2.2 Regulation of Na_V current inactivation by cytosolic factors present in rodent β-cells 115
5.2.3 Hyperpolarised inactivation of Na_V currents due to absence of cytosolic factors in rodent β-cells 120
5.2.4 Ca^{2+}- and PKC dependent regulation of Na_V channels in rodent β-cells 122
5.2.5 Regulation of Na_V channels via the insulin receptor signalling pathway 127
5.2.6 Effect of phosphatidylinositol 4,5-bisphosphate (PIP_2) on Na_V channel inactivation 129
5.2.7 Effect of chronic and acute differences in the extracellular glucose concentration on the voltage-dependence of Na_V channel inactivation 131
5.2.8 Surface charge effect of Na_V current inactivation in Ins1 and HEK cells 137
5.3 Discussion 139
5.3.1 Post-translational modification of Na_V channels in Ins1 cells 139
5.3.2 Na_V channels in Ins1 cells are not regulated by a diffusible intracellular factor 142
Chapter 6 146
6.1 Properties of Na_V inactivation in insulin-secreting cells 147
6.1.1 Hyperpolarised inactivation of $Na_V1.3$, $Na_V1.5$, $Na_V1.6$ and $Na_V1.7$ channels in Ins1 cells vs non-β-cells 147
6.1.2 Biphasic inactivation of individual Na_V channel α-subunits 149
6.2 Na_V inactivation in Ins1 cells: a possible model 150
6.3 Physiological significance of Na_V inactivation properties in rodent β-cells 153
6.4 Na_V channels in disease 154
6.4.1 Na_V channels and diabetes 155
6.4.2 Na_V channels and pain 155
6.4 Concluding remarks 158
Appendix 159
References 169

List of Tables

Table 1.3.1.1 - Sequence homology of Na_V channel α-subunits 26
Table 2.1.4.1 – Primers used to detect mRNA expression in Ins1 and HEK cells 40
Table 3.2.2.1 - V_h and k values of WT and TTX-resistant $Na_V1.7$, $Na_V1.3$ and $Na_V1.6$ expressed in HEK cells 58
Table 3.2.2.2 - $V_{0.5}$ and k values of WT and TTX-resistant $Na_V1.7$, $Na_V1.3$ and $Na_V1.6$ expressed in HEK cells 58
Table 3.2.9.1 – V_h values of $Na_V1.3$, $Na_V1.5$, $Na_V1.6$ and $Na_V1.7$ in Ins1 and HEK cells 80
Table 3.2.9.2 - Activation values of $Na_V1.3$, $Na_V1.5$, $Na_V1.6$ and $Na_V1.7$ in Ins1 and HEK cells 81
Table 3.2.11.1- V_h and k values of Na_v channel inactivation in CHO and αTC1-6 cells 86
Table 4.2.1.1–Effect of β_3 knockdown on endogenous Na_V current inactivation in Ins1 cells 100
Table 4.2.2.1 – V_h and k values of $Na_V1.7$, $Na_V1.3$ and $Na_V1.6$ co-expressed with the β_3-subunit in Ins1 cells 103
Table 4.2.3.1- Inactivation V_h and k values of $Na_v1.7$ and $Na_v1.3$ co-expressed with the β_3-subunit or GFP in HEK cells 107
Table 5.2.1.1 - $Na_V1.7$/$Na_V1.3$ chimeras expressed in Ins1 and HEK cells 114
Table 5.2.7.1 – Inactivation of endogenous Na_V currents after chronic exposure to 5, 11 and 25mM glucose 137
Supplementary Table 1 162
Supplementary Table 2 164
Supplementary Table 3 165

List of Figures

Figure 1.2.1.1– Immuno-stained image of a mouse islet of Langerhans. 17
Figure 1.2.3.1 – Stimulus-secretion coupling in mouse β-cells. 20
Figure 1.2.4.1- K_{ATP}-dependent intrinsic regulation of glucagon secretion model 23
Figure 1.3.1.1- Structure of the Na_V channel α-subunit. 25
Figure 1.3.2.1– Steady-state voltage-dependent activation and inactivation of the Na_V channel. 29
Figure 2.2.2.1 – Steady-state inactivation and activation pulse protocol 47
Figure 3.2.1.1 – Characterisation of endogenous Na_V channels in Ins1 and HEK cells 53
Figure 3.2.1.2 – Voltage-dependence of activation and inactivation of endogenous Na_V currents in Ins1 cell 55
Figure 3.2.2.1 – Voltage-dependence of inactivation and activation of WT and TTX-resistant versions of $Na_V1.7$, $Na_V1.3$ and $Na_V1.6$ channels in HEK cells 57
Figure 3.2.3.1 – TTX-resistant $Na_V1.7$ current traces in Ins1 and HEK cells 59
Figure 3.2.3.2- Voltage-dependence of activation of $Na_V1.7$ currents in Ins1 and HEK cells 60
Figure 3.2.3.3- Voltage-dependence of inactivation of $Na_V1.7$ currents in Ins1 and HEK cells 63
Figure 3.2.4.1 – Voltage-dependence of inactivation of $Na_V1.3$ in Ins1 and HEK cells 66
Figure 3.2.5.1- Biphasic inactivation of $Na_V1.3$ in primary mouse β-cells 68
Figure 3.2.6.1- Voltage-dependence of activation of $Na_V1.3$ in Ins1 and HEK cells 70
Figure 3.2.7.1- Voltage-dependence of inactivation of $Na_V1.6$ currents in Ins1 and HEK cells 72
Figure 3.2.7.2- Voltage-dependence of activation of $Na_V1.6$ currents in Ins1 and HEK cells 74
Figure 3.2.8.1- Voltage-dependence of activation and inactivation of $Na_V1.5$ currents in Ins1 and HEK cells 76
Figure 3.2.9.1- Summary of $Na_V1.7$, $Na_V1.3$ and $Na_V1.6$ Voltage-dependence of inactivation and activation in Ins1 and HEK cells 79
Figure 3.2.10.1- Characterisation of $Na_V1.7$, $Na_V1.3$ and $Na_V1.6$ in EndoC-βh2 cells 84
Figure 3.2.11.1 – Characterisation of $Na_V1.7$ and $Na_V1.3$ in αTC1-6 and CHO cells 86
Figure 4.2.1.1 – Effect of $β_3$ knockdown on endogenous Na_V current in Ins1 cells 99
Figure 4.2.2.1- Characterisation of $Na_V1.7$, $Na_V1.3$ and $Na_V1.6$ currents co-expressed with the $β_3$-subunit 102
Figure 4.2.3.1- Characterisation of $Na_V1.7$ and $Na_V1.3$ co-expressed with the $β_3$-subunit and GFP in HEK cells 106

Figure 5.2.1.1- $Na_V1.7$ and $Na_V1.3$ chimera hybrids....113
Figure 5.2.2.1 - $Na_V1.7$ and $Na_V1.3$ currents in cell-attached and inside-out configuration....116
Figure 5.2.2.2– Voltage-dependence of $Na_V1.7$ and $Na_V1.3$ current inactivation and activation in the cell-attached and inside-out configuration.....119
Figure 5.2.3.1- Patch cramming of $Na_V1.7$ channels expressed in Ins1 into HEK cells....121
Figure 5.2.4.1- Effect of 20μM BAPTA-AM on endogenous Na_V currents in Ins1 cells....123
Figure 5.2.4.2 – PKC-dependent regulation of Na_V current inactivation....126
Figure 5.2.5.1- Effect of diazoxide and S961 on Na_V inactivation....129
Figure 5.2.6.1- Effect of 50 μM PIP_2 diC8 on Na_V current inactivation and activation in Ins1 cells....130
Figure 5.2.7.1 – Effect of acute changes in extracellular glucose concentration on the voltage-dependence of $Na_V1.7$ and $Na_V1.3$ channel inactivation.....133
Figure 5.2.7.2 – Effect of chronic changes in glucose on channel inactivation....136
Figure 5.2.8.1- Effect of surface charge on the voltage-dependence of inactivation and activation of $Na_V1.3$ expressed in Ins1 cells....139
Figure 6.1.2.1- Biphasic inactivation of Na_V currents in Ins1 cells....153

Chapter 1

General Introduction

1.1 Introduction

The fundamental importance of voltage-gated Na^+ channels (Na_V channels) was first described by Hodgkin and Huxley in 1952 to explain the ionic mechanisms underlying the initiation and propagation of action potentials in the squid giant axon (Hodgkin and Huxley, 1952). Research into Na_V channels has since expanded vastly, providing a greater insight into their structure and function (Catterall et al., 2017, Black and Waxman, 2013, Catterall, 2014, Catterall, 2000).

Na_V channels are expressed abundantly and are present in nearly all electrically excitable cells where they play a key role in action potential initiation and generation (Hille, 2001). Their activity is dually dependent on the membrane potential of the cell. Depolarisation leads to opening of Na_V channels, resulting in a rapid inward Na^+ current, which is terminated when the channels enter a non-conducting inactivated state. Reversal of the inactivated state requires hyperpolarisation and the extent can vary according to the cell and Na_V subtype (Catterall et al., 2017). The balance between the voltage-dependence of activation and inactivation determines Na^+ current entry into the cell, which regulates cell excitability.

Na_V channels consist of a pore-forming α-subunit that can form heterodimers or heterotrimers with auxiliary β-subunits (Kruger and Isom, 2016, Calhoun and Isom, 2014). Insulin secreting β-cells express $Na_V1.3$, $Na_V1.6$ and $Na_V1.7$ that are encoded by the genes *Scn3a*, *Scn8a* and *Scn9a*, respectively. Moreover, they principally express *Scn1b,* which encodes the β_1-subunit (Adriaenssens et al., 2016, DiGruccio et al., 2016, Benner et al., 2014).

In rodent pancreatic β-cells, Na_V channels exhibit an unusually hyperpolarised voltage-dependence of inactivation and depolarisation from physiological membrane potentials evokes almost no Na^+ current (Zhang et al., 2014, Plant, 1988, Gopel et al., 1999). Full reactivation of Na_V channels in rodent β-cells requires hyperpolarisation to ~-120mV. This is 40-50mV more negative than the most repolarised membrane potential of a β-cell. As a result, most Na_V channels are 'locked' in a non-conducting inactivated state. A small additional current component (comprising 10-15% of the total Na^+ current) exists in β-cells, which inactivates over physiological membrane potentials and contributes to cell excitability.

It has been proposed that Na_V currents that inactivate over vastly different membrane potentials reflect the contribution of different Na_V channel α-subunits. Here we investigate the contribution of individual Na_V channel α-subunits to the behaviour of Na_V current inactivation in β-cells and gain insight into the underlying mechanism(s) of channel regulation.

1.2 Regulation of glucose homeostasis by the pancreatic islets of Langerhans

1.2.1 The structure and function of the pancreatic islets of Langerhans

The pancreatic islets of Langerhans are groups of endocrine cells found in the pancreas. The islets represent 1-2% of the total pancreatic mass and are surrounded by exocrine tissue, which accounts for the remaining 98-99% of the total pancreatic mass (Dolenšek et al., 2015). The endocrine component of the

pancreas is responsible for maintaining metabolic homeostasis following the absorption of nutrients into the blood from the gut.

Glucose homeostasis is achieved by the secretion of hormones from the islets of Langerhans. As shown in Figure 1.2.1.1, islets are composed of three principal cell-types: β-cells, α-cells and δ-cells (Cabrera et al., 2006), which produce and secrete the hormones insulin, glucagon and somatostatin, respectively. An elevation of blood glucose leads to the release of insulin, which in turn acts to lower blood glucose, by acting on peripheral tissues such as the muscle, liver and adipose tissue to increase the uptake of glucose. In contrast, when blood glucose levels decrease, glucagon is released from the α-cells, which again acts on peripheral tissue to increase blood glucose by stimulating gluconeogenesis and glycogenolysis (Campbell and Drucker, 2015). The role of somatostatin secreted from the δ-cells remains controversial. However it is thought to act as a break on both insulin and glucagon secretion (Braun et al., 2009, Briant et al., 2017b). Appropriate regulation of insulin and glucagon secretion is essential to metabolic homeostasis and its disruption is the cause of metabolic dysregulation associated with diabetes mellitus.

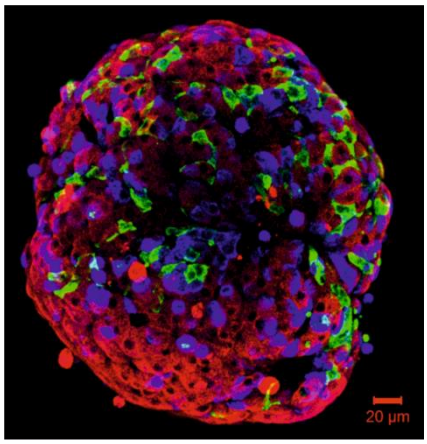


Figure 1.2.1.1– Immuno-stained image of a mouse islet of Langerhans.

The islets of Langerhans consist of three cell-types including β-, α- and δ-cells, labelled here in red, blue and green respectively. Image by Elisa Vergari taken from (Brereton et al., 2015).

1.2.2 Diabetes Mellitus

Diabetes mellitus (from here on in referred to as diabetes) is a metabolic disorder. It is characterised by high blood glucose levels as a result of insufficient insulin for the body's requirement, which may be due to either impaired insulin secretion, insulin action or both (Alberti and Zimmet, 1998). Diabetes is widely considered to be a major global health problem, as it increases the risk of heart disease and microvascular complications associated with blindness, renal failure and peripheral neuropathy (Forbes and Cooper, 2013). The disease has multiple aetiologies and is accordingly classified into multiple subtypes. Type 1 diabetes is an autoimmune disease, which involves the destruction of pancreatic β-cells. It accounts for 5-10 % of all diabetes cases (Copenhaver and Hoffman, 2017). Meanwhile, type 2 diabetes is the most common form, accounting for more than 90% of diabetes cases in adults (Grundy, 2008). It is influenced by lifestyle factors,

obesity, age and pregnancy, but also has a significant genetic component associated with it (McCarthy, 2017).

1.2.3 Stimulus Secretion Coupling in β-cells

The coordinated activation and inactivation of voltage-gated ion channels, driven by a key protein in the pathway: the ATP-sensitive-potassium channel (K_{ATP} channel) is central to the regulation of hormone secretion from the pancreatic islets of Langerhans (Ashcroft and Rorsman, 2013). K_{ATP} channels are sensitive to the cell ATP:ADP ratio (Ashcroft et al., 1984, Rorsman and Trube, 1985). Increasing concentrations of intracellular ATP act on K_{ATP} channels to close them and the resulting decrease in K_{ATP} conductance leads to membrane depolarisation. As such, K_{ATP} channels link metabolism to cellular electrical activity by regulating the membrane potential of the cell.

Pancreatic β-cells are electrically excitable and an elevation of plasma glucose initiates β-cell action potential firing that leads to stimulation of insulin secretion (Figure 1.2.3.1A). Under hypoglycaemic conditions, glucose metabolism is low and as a consequence the cytoplasmic ATP:ADP ratio is reduced and this keeps the β-cell membrane potential hyperpolarised (and electrically inactive) via activation of K_{ATP} channels (Figure 1.2.3.1B) (Ashcroft and Rorsman, 2013).

However, as the glucose concentration increases, the electrical activity of the cell is also stimulated in a dose-dependent manner (Figure 1.2.3.1A). Increased glucose uptake into the cell leads to an accelerated metabolism of glucose and to an elevated ATP:ADP ratio (Figure 1.2.3.1C). Closure of the K_{ATP} channel induces

membrane depolarisation. If membrane depolarisation exceeds -60 to -50mV, action potential firing is initiated with the opening of L-type Ca^{2+} channels. The associated influx of Ca^{2+} into β-cells triggers Ca^{2+}-dependent exocytosis of insulin granules.

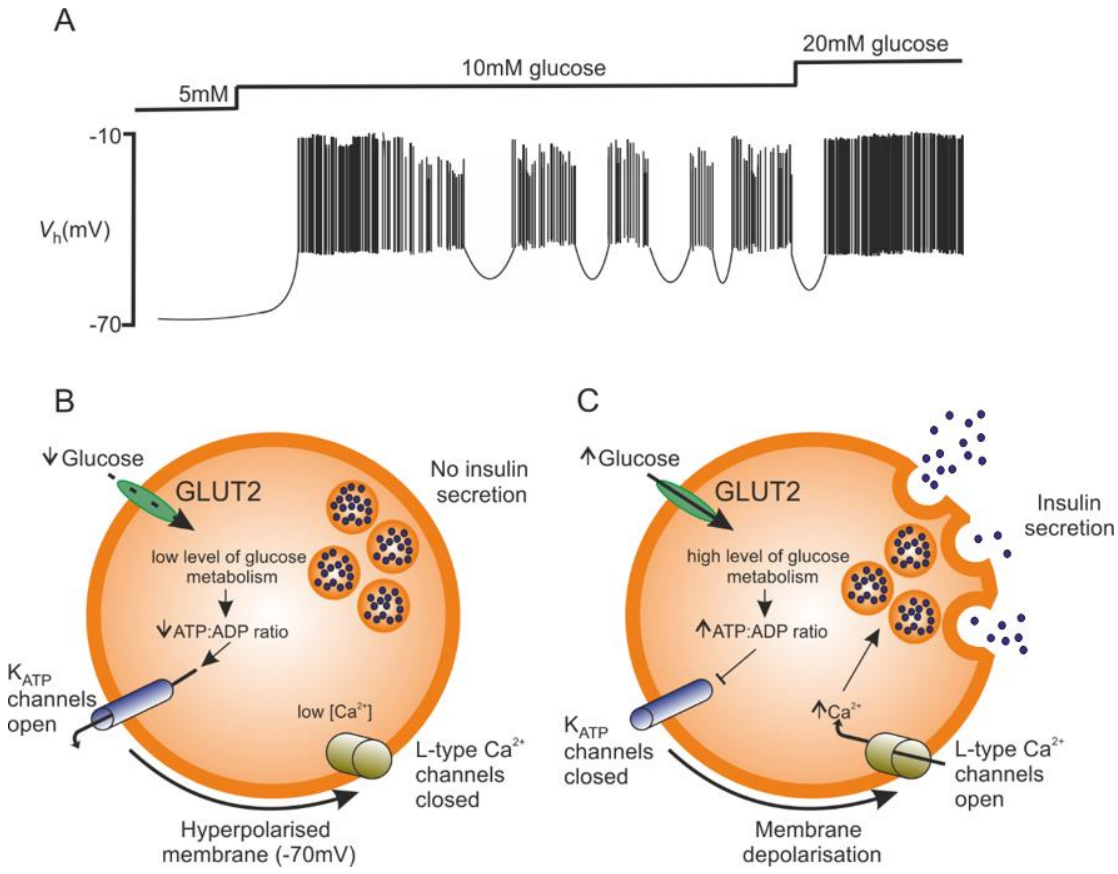


Figure 1.2.3.1 – Stimulus-secretion coupling in mouse β-cells.

A, illustration of an electrical recording of the β-cell membrane potential at 5, 10 and 20mM extracellular glucose concentrations. At 5mM glucose the β-cell is electrically inactive and the resting membrane potential of the cell is approximately -70mV. As the glucose concentration is elevated, the electrical activity of the cell increases in a dose-dependent manner reflected by the action potential firing frequency. *B*, represents the stimulus-secretion coupling pathway at low glucose concentrations. Under these circumstances, glucose intake into the cell via the GLUT2 transporter is low and as a result there is a low level of metabolism. As a consequence of the reduced ATP: ADP ratio, K_{ATP} channels remain open and the membrane is hyperpolarised. At these membrane potentials L-type Ca^{2+} channels remain closed and with no electrical activity insulin secretion is inhibited. *C*, as the glucose concentration increases, glucose uptake into the cell is elevated. Glucose is metabolised to increase the ATP:ADP ratio, which acts on the K_{ATP} channels to close them. Depolarisation of the cell membrane leads to the activation of L-type Ca^{2+} channels and the resulting increase in intracellular Ca^{2+} leads to insulin secretion. Schematic adapted from (Ashcroft and Rorsman, 2013).

1.2.4 Glucose-inhibited glucagon secretion in α-cells

How glucose regulates glucagon secretion from pancreatic α-cells remains a controversial subject (Gylfe, 2016, Walker et al., 2011, Gromada et al., 2007, Gylfe and Gilon, 2014, Jacobson et al., 2009, Briant et al., 2016, Gylfe, 2013). It has been postulated that glucose-sensing neurones in the central nervous system detect changes in extracellular glucose concentration and relay the signal to α-cells via neurones (Miki et al., 2001, Thorens, 2011). However, as glucagon secretion is also regulated independently of neuronal input, it has been proposed that glucose-sensing occurs within neighbouring β- and δ-cells that regulate glucagon secretion from α-cells. This effect would be mediated by the release of inhibitory paracrine factors such as insulin, Zn^{2+}, γ-aminobutyric acid or somatostatin (Franklin et al., 2005, Ravier and Rutter, 2005, Hauge-Evans et al., 2009, Briant et al., 2018).

Finally, there is also evidence to support intrinsic glucose-sensing by α-cells. There are two proposed mechanisms for the intrinsic regulation of glucagon secretion (Gylfe, 2013, Rorsman et al., 2014). One hypothesis is that under hypoglycaemic conditions a depolarising Ca^{2+} current initiates glucagon secretion by reducing the availability of ATP to the electrogenic Na^+/K^+ pump (Bode et al., 1999) or by activation of a depolarising store-operated influx of Ca^{2+} when energy is insufficient to maintain Ca^{2+} in the endoplasmic reticulum (Liu et al., 2004, Vieira et al., 2007).

The alternative hypothesis for intrinsic regulation is dependent on K_{ATP} channels (Gopel et al., 2000, MacDonald et al., 2007, Ramracheya et al., 2010, Rorsman et al., 2008, Zhang et al., 2013). According to this model, under hypoglycaemic

conditions K_{ATP} conductance in α-cells is low (but greater than zero) (Ashcroft and Rorsman, 2013). As a result the resting membrane potential is sufficiently depolarised to elicit action potential firing and, so, α-cells are electrically active at low glucose concentrations (Figure 1.2.4.1A). In α-cells, action potential firing is initiated with the activation of Na_V channels followed by the activation of voltage-gated P/Q type Ca^{2+} channels. The influx of Ca^{2+} initiates Ca^{2+}-dependent exocytosis of glucagon containing granules (Figure 1.2.4.1B). However as the glucose concentration is increased (i.e. from 1 to ≥ 6mM glucose), the ATP:ADP ratio is increased and K_{ATP} channel activity is completely blocked (Figure 1.2.4.1C). This leads to a further depolarisation of the cell membrane. However, due to the inactivation of Na_V channels (described in section 1.3.2) at more depolarised potentials, a reduction in the α-cell action potential spike amplitude occurs. This leads to reduced activation of P/Q-type Ca^{2+} channels, which play a prominent role in the exocytosis of glucagon granules. This has been postulated to explain the suppression of glucagon release under hypoglycaemic conditions.

A notable difference between the regulation of insulin and the proposed K_{ATP}-dependent model for intrinsic regulation of glucagon secretion is the role of Na_V channels in the stimulus-secretion coupling pathway. Interestingly, in human β-cells, Na_V channels do contribute to action potential firing and application of the Na_V channel blocker tetrodotoxin (TTX) reduces insulin secretion (Braun et al., 2008, Barnett et al., 1995). However, this is not typically seen in mouse β-cells. The very nature of Na_V currents in mouse β-cells, which render them functionally irrelevant in this cell type will be the subject of this thesis and will be discussed in further detail. First, it is important to consider the structure and function of Na_V channels.

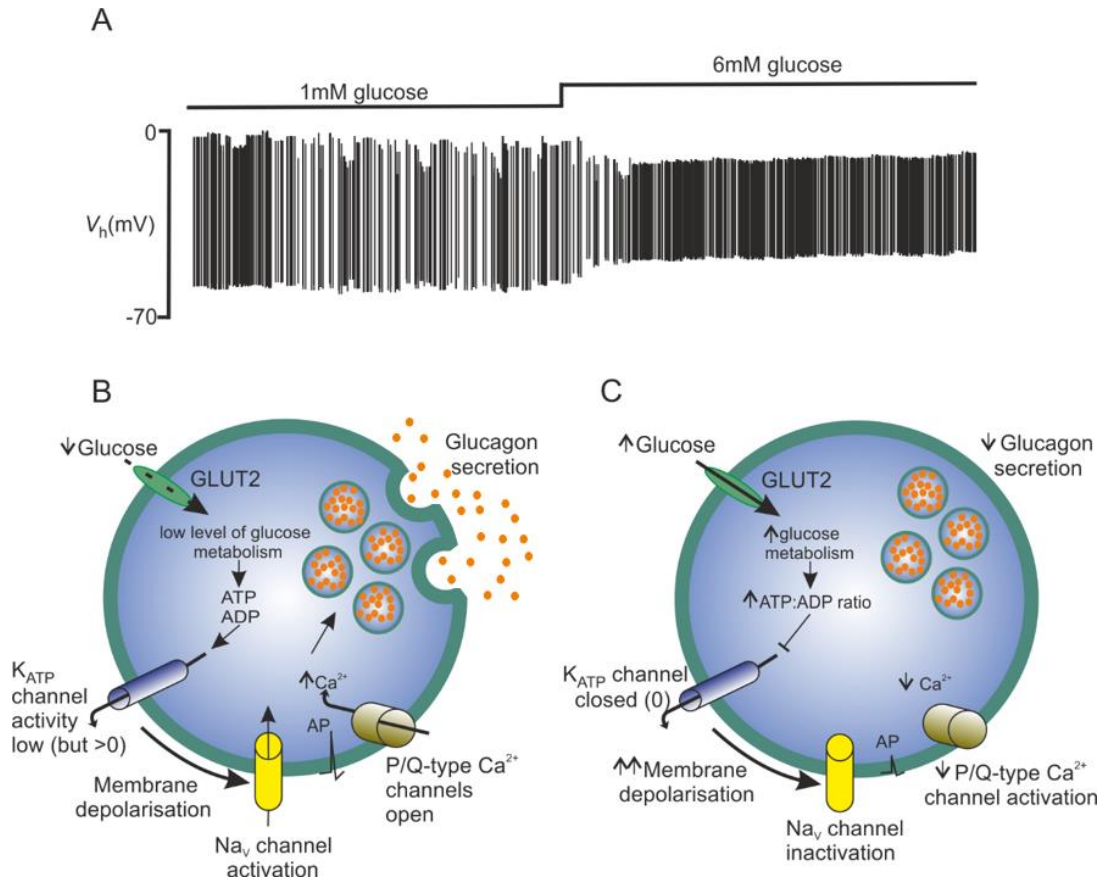


Figure 1.2.4.1- K_{ATP}-dependent intrinsic regulation of glucagon secretion model

A, illustration of an electrical recording of the α-cell membrane potential at 1mM and 6mM glucose. At 1mM glucose the α-cell is electrically active. As the glucose concentration is elevated to 6mM glucose, the resting membrane potential is further depolarised and action potential height is reduced. *B*, schematic of the regulation of glucagon secretion at low extracellular glucose concentrations. For reasons that remain obscure, K_{ATP} channel activity is sufficiently reduced (but >0) at low glucose to depolarise the membrane potential and activate Na_V channels to initiate action potential firing. Subsequent activation of P/Q type Ca^{2+} channels leads to an increase in intracellular Ca^{2+}, which initiates Ca^{2+}- dependent exocytosis of glucagon granules. *C*, schematic of glucose-induced inhibition of glucagon secretion. As the glucose concentration is elevated there is an increased uptake of glucose, an accelerated metabolism and a higher ATP:ADP ratio. ATP acts on K_{ATP} channels to reduce its conductance to zero; the further depolarisation of α-cell membrane potential leads to the inactivation of Na_V channels and reduced action potential height. This causes a reduced activation of P/Q type Ca^{2+} channels and as influx of Ca^{2+} into the cell is reduced, so is the secretion of glucagon. Schematic adapted from (Ashcroft and Rorsman, 2013).

1.3 Structure and function of Na_V channels

1.3.1 Architecture of Na_V channels

Na_V channels consist of a pore-forming α-subunit and auxiliary β-subunits. In mammals, nine pore-forming α-subunits have been identified. They are named $Na_V1.1$-1.9 and are encoded by the genes *Scn1a-5a* and *Scn8a-11a* (Catterall, 2000). The gene number and the Na_V channel number do not always correlate and thus the genes *Scn8a-11a* encode $Na_V1.6$-1.9, respectively. The genes *SCN6A* and *Scn7a* were mapped in human and mouse, respectively, but represent the same gene encoding Na_X (Goldin et al., 2000). For this reason *SCN6A* is no longer in use. Na_X is poorly homologous to Na_V channels and is activated by changes in the extracellular Na^+ concentration (~170mM) and not by changes in the membrane electrical field (Hiyama et al., 2002). All Na_V channel α-subunits are sensitive to TTX, with the exception of $Na_V1.5$, $Na_V1.8$ and $Na_V1.9$.

All nine α-subunits share a common overall structure, which is composed of a long polypeptide consisting of 1700-2000 amino acids that fold into four homologous domains (DI, DII, DIII and DIV), shown in Figure 1.3.1.1. Each domain consists of six transmembrane segments, S1-S6, (Catterall, 2000). The S4 region confers the voltage-sensing capacity of the channel, whilst S5, S6 and the S5-S6 membrane re-entrant linker are important in forming the pore of the channel. Since Na_V channel α-subunits contain the voltage sensors and the ion-conducting pore they are able to form functional channels expressed on their own.

However they can also form heterodimers or heterotrimers with one or two auxiliary β-subunits, respectively (Isom et al., 1992). The β-subunits serve as cell adhesion molecules interacting with the extracellular matrix, other cell adhesion

molecules and the cytoskeleton (Isom, 2002). As such they are able to modify the kinetics, voltage-dependence of gating and the cell surface expression of α-subunits (Kruger and Isom, 2016) . Four Na_V channel β-subunits exist (β_1-β_4). β_1 and β_3 associate with the α-subunits non-covalently, whilst β_2 and β_4, associate covalently via disulphide bridges (Namadurai et al., 2015). Both Na_V channel α- and β-subunit expression is regulated in a time- and tissue-specific manner (Catterall et al., 2005).

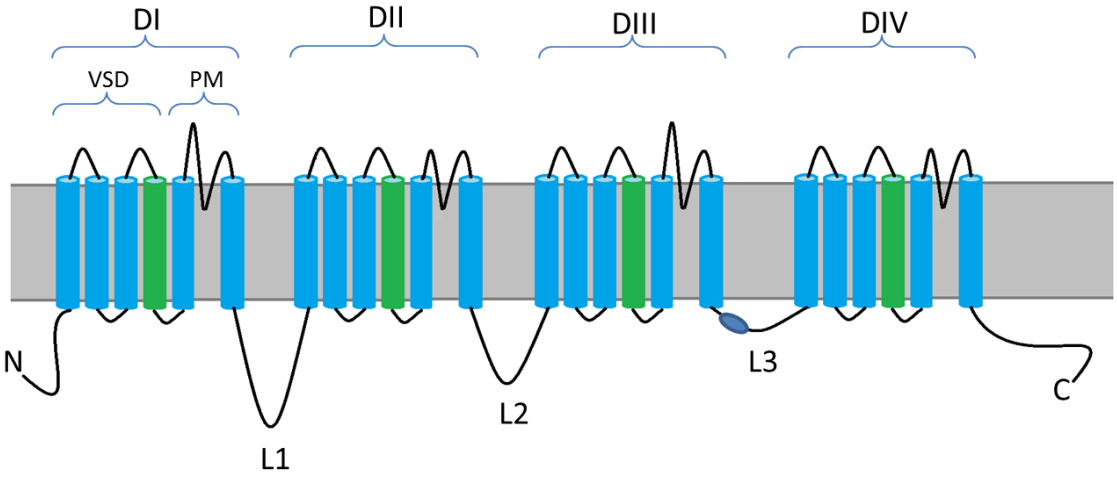


Figure 1.3.1.1- Structure of the Na_V channel α-subunit.

The Na_V channel α-subunit is composed of four non-identical domains (DI-DIV), each of which contains six transmembrane-spanning domains (S1-S6). The voltage-sensing domain (VSD) encompasses S1-S4. S4 (shown in green) characteristically harbours the positively charged arginine and lysine residues, which confers the voltage-sensitivity of the channel and initiates a conformational change upon changes in the membrane potential. The pore-forming module (PM) is formed by S5 and S6 as well as the membrane re-entrant linker between S5 and S6. The α-subunit contains intracellular N- and C-termini and each domain is linked to each other by the loops L1- L3. The 'inactivation particle' on L3 (indicated by a blue oval), is composed of non-polar amino acids isoleucine, phenylalanine and methionine and is responsible for steady-state inactivation. Schematic adapted from (Dib-Hajj et al., 2013).

Na_V channels are among the most conserved and ancient gene families, with a sequence identity of >50% between the transmembrane domains of the simplest multicellular eukaryote and that of a human Na_V channel α-subunit (Catterall et al., 2008, Zakon, 2012). The amino acid sequence homology between different human Na_V channel α-subunits is shown in Table 1.3.1.1. $Na_V1.1$, $Na_V1.2$, $Na_V1.3$, $Na_V1.4$ and $Na_V1.6$ display a sequence identity >70% relative to $Na_V1.7$.

Isoform	Identity (%)
$Na_V1.1$	77.58
$Na_V1.2$	78.85
$Na_V1.3$	77.22
$Na_V1.4$	70.18
$Na_V1.5$	63.95
$Na_V1.6$	72.41
$Na_V1.7$	100
$Na_V1.8$	53.50
$Na_V1.9$	58.30

Table 1.3.1.1 - Sequence homology of Na_V channel α-subunits

Na_V channel α-subunit amino acid sequences were aligned in Clustal Omega program (https://www.ebi.ac.uk/Tools/msa/clustalw2) using the NCBI reference sequences NP_001159435.1, NP_001035232.1, NP_008853.3, NP_000325.4, NP_932173.1, NP_055006.1, NP_002968.1, NP_006505.2 and NP_001274152.1. Amino acid identity is expressed as % relative to $Na_V1.7$.

1.3.2 Steady-state activation and inactivation of Na_V channels

The first recordings of Na_V current were made by Hodgkin and Huxley in 1952 and revealed three key features: (1) selective Na^+ conductance, (2) voltage-dependent activation and (3) rapid inactivation (Hodgkin and Huxley, 1952). Gaining insight into the structure of Na_V channels has been fundamental to mechanistically understanding how these key features of Na_V channels are regulated. Following the empirical model proposed by Hodgkin and Huxley, accurate predictions on the structure of Na_V channels that underlie these key features were made despite no knowledge of their nucleotide/amino sequences, yet alone their crystal structure. In the 1970s, Hille developed a model of the ion-conducting pore based on measurements of the relative permeability of the channel to many organic cations, which gave an indication of the geometry of the pore and thus provided details on how the selectivity of the channel is conferred (Hille, 1971, Hille, 1972). These studies were followed by Armstrong and Benzanilla who developed a technique to detect the movement of "gating charges", now known to reflect the movement of the voltage sensors in response to changes in membrane potential, which provided insight into the voltage-dependence of Na_V channel function (Armstrong and Bezanilla, 1973, Armstrong and Bezanilla, 1974). Indeed, the recent determination of bacterial and eukaryotic Na_V channel crystal structures at angstrom resolutions has served to further our insight into the structure and function of Na_V channels (Payandeh et al., 2012, McCusker et al., 2012, Zhang et al., 2012, Shen et al., 2017).

The different functional states of Na_V channels are summarised in Figure 1.3.2.1 (see Armstrong, 2006 for a more detailed schematic). S4 contains positively

charged arginine and lysine resides, otherwise known as “gating charges”. Under the influence of the membrane electrical field, the S4 segments move, and thereby confer the channels its voltage-sensing properties. Replacement of the positively charged amino acid residues in S4 with neutral or negatively charged residues changes the gating current and as a result shifts the half-maximal activation ($V_{0.5}$) of the Na$_V$ channel (Stuhmer et al., 1989). At the resting membrane potential, all four S4 helices are stably pulled into the intracellular side of the membrane. Upon depolarisation, the S4 segment sequentially moves outwards, guided by a narrow groove formed by S1-S3. S4 movement is rigidly coupled to the lateral movement of the S4-S5 linker, which is thought to induce movement of the pore-forming S5 and S6 segments (Armstrong, 2006). All four domains must undergo the outward movement in order for the activation gate to open (Yarov-Yarovoy et al., 2012).

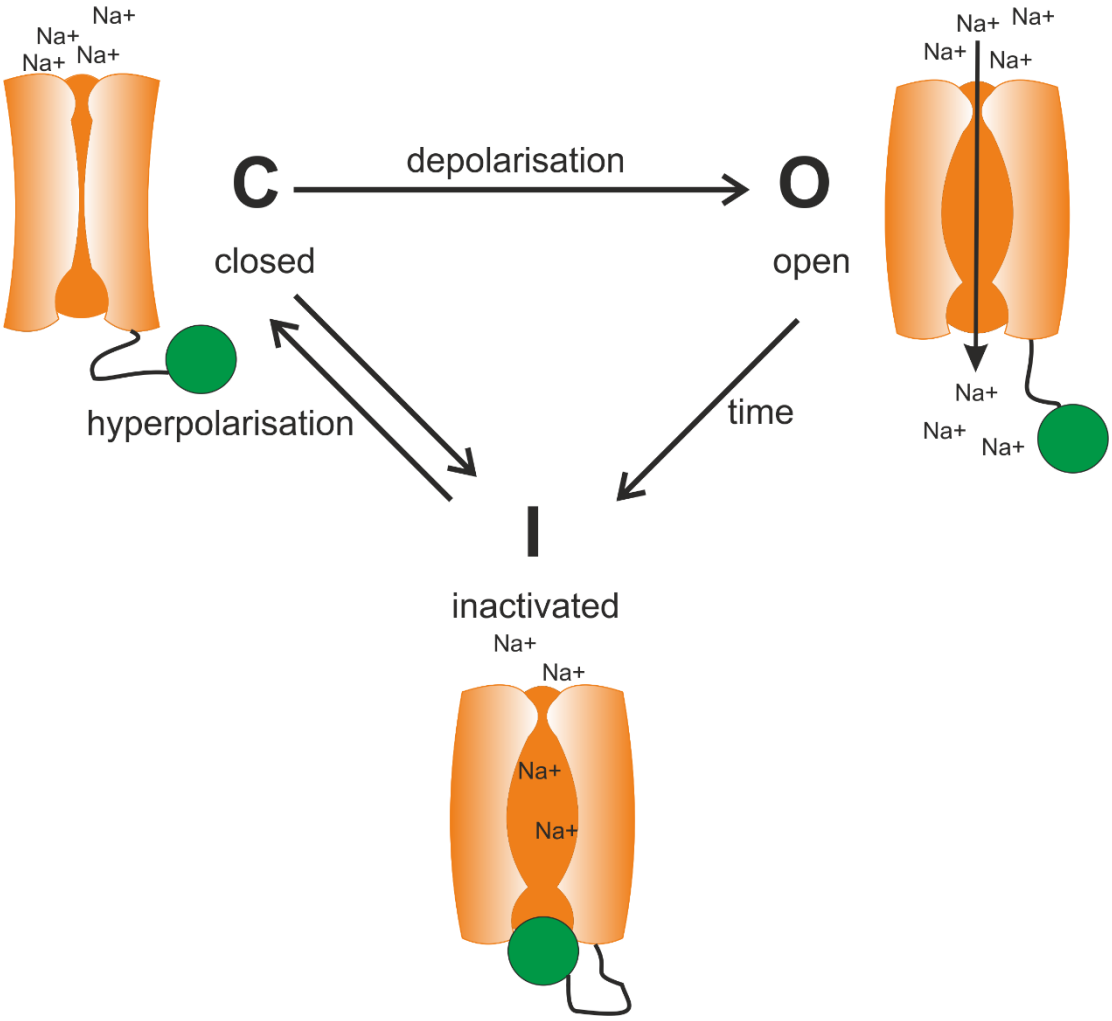


Figure 1.3.2.1– Steady-state voltage-dependent activation and inactivation of the Na_V channel.

Steady-state, voltage-dependent activation refers to a series of conformational changes required for the α-subunit's activation gate to enter an open conducting state, upon depolarisation. Fast inactivation occurs under a time-dependent process, which allows the inactivation gate or 'inactivation particle' (depicted by the green circle) to occlude the pore of the Na_V channel. Upon hyperpolarisation the channel returns to a closed state, from an inactivated state, where it can now enter a conducting state upon depolarisation. Note that the channel cannot enter an open state from the inactivated state.

Fast inactivation is a characteristic feature of Na_V channels. Despite a sustained depolarisation of the cell membrane the channel enters a non-conducting state. Its importance underlies many physiological processes, which include the refractory period in neurones and, as described in section 1.2.4, the intrinsic ability of pancreatic α-cells to regulate glucose-stimulated inhibition of glucagon secretion. Fast inactivation occurs when three non-polar amino acids: isoleucine, phenylalanine and methionine (IFM), which form the 'inactivation particle' positioned on L3, move into a blocking position and thus occlude the pore of the channel from the cytoplasmic side (West et al., 1992). Substitution of either amino acid disrupts inactivation, and in the case of phenylalanine, abolishes it completely (West et al., 1992). Similar observations can also be seen with intracellular application of a protease, an antibody targeted to L3 or cleavage of L3 (Armstrong et al., 1973, Vassilev et al., 1989, Stuhmer et al., 1989).

It has been proposed that fast inactivation derives its voltage-dependence from that of activation (Armstrong and Bezanilla, 1977). The process is thought to require movement of S4 in the DIV domain to unveil a pore region, which serves as a 'receptor' for the inactivation particle (Armstrong, 2006, Ahern, 2013). The S4 of the DIV domain contains eight gating charges rather than the four or six in domains I-II and III, respectively (Armstrong, 2006). It is thought that this difference allows the DIV region to enter two distinct states of activation. The first stage of activation is sufficient to allow ions to permeate, but does not allow the inactivation particle to occlude the mouth of the pore. Meanwhile, during the second stage of activation the inactivation particle moves into position to occlude the pore of the channel (Armstrong, 2006). Other experimental data exists which suggests that Na_V inactivation is not dependent on voltage dependent activation

(Featherstone et al., 1996, Kontis and Goldin, 1997, Ulbricht, 2005). The identity of the putative receptor for the IFM inactivation motif remains elusive. However, further structural analysis of the eukaryotic sodium channel may provide insight into a site for interaction of the IFM motif to block the open pore of the channel (Shen et al., 2017). Such analysis could not be performed on the bacterial sodium channel because they do not contain a fast inactivation gate (Catterall, 2014).

Return to a closed state from the open-inactivated state requires hyperpolarisation and is therefore a voltage-dependent process. The intracellular S4-S5 linker that connects the VSD to the pore, plays a crucial role in coupling voltage-dependent conformational changes in the VSD, to closing of the pore (Yarov-Yarovoy et al., 2012).

A separate process, termed slow inactivation, which is kinetically and structurally distinct from fast inactivation also results in a reduction of Na^+ current amplitude. In contrast, to fast inactivation that develops over a period of milliseconds, slow inactivation develops in response to prolonged depolarisations over a period spanning hundreds of milliseconds to seconds or in response to long trains of brief repetitive depolarisations. Recovery from slow inactivation occurs over similarly extended periods (Rudy, 1978, Struyk and Cannon, 2002) . Although the structural parts of the Na_V channel that participate in slow inactivation are not well-defined, a number of studies suggest that a profound rearrangement in the outer pore of the channel is involved (Struyk and Cannon, 2002).

1.4 Na_V channel inactivation properties in pancreatic β-cells

1.4.1 Arcane inactivation properties of Na_V channels in rodent β-cells

Since the earliest characterisation of Na_V channels in rodent β-cells, the role of these channels in this cell type has been somewhat puzzling. Mouse and rat β-cells display an arcane voltage-dependence of inactivation with a significantly hyperpolarised half-maximal inactivation (V_h) of approximately -100mV (Plant, 1988, Gopel et al., 1999, Hiriart and Matteson, 1988, Lou et al., 2003, Ashcroft and Rorsman, 1989). Therefore, at physiological membrane potentials most Na_V channels are 'locked' into an inactivated state and depolarisation from holding potentials equivalent to the resting membrane potential of a β-cell, evokes almost no Na^+ current. It is therefore not surprising that application of TTX to rodent β-cells at high glucose has no effect on the action potential height or insulin secretion (Pressel and Misler, 1991).

The hyperpolarised inactivation of Na_V channels observed in rodent β-cells contrasts the more positive V_h of Na_V channels expressed in α-cells (Leung et al., 2005, Zhang et al., 2014), in which Na_V channels are known to play a role in the regulation of glucagon secretion. The V_h of Na_V currents in α-cells is ∼-45mV (Gopel et al., 2000, Ramracheya et al., 2010, Zhang et al., 2013, Barg et al., 2000) However, there are other studies that show that Na_V channels in isolated α-cells inactivate at similarly negative voltages to β-cells (Vignali et al., 2006).

Na_V channels in rodent β-cells also display a significantly hyperpolarised shift in inactivation compared to non-pancreatic islet cells. For example the V_h in mouse DRG neurones is approximately -70mV (Herzog et al., 2003). This 30-50mV negative shift in the voltage-dependence of Na_V channel inactivation in rodent

β-cells compared to other cell types is truly remarkable, especially if one considers that all Na_V channels are fully inactivated at physiological membrane potentials (which rarely become more negative than -80mV).

1.4.2 Species differences in Na_V channel inactivation in β-cells

The arcane inactivation properties of Na_V channels observed in rodent β-cells is not consistent across species. As already pointed above, Na_V channels play a crucial role in the stimulus-secretion coupling pathway in human pancreatic β-cells. Human β-cells contain TTX-sensitive currents that inactivate with a V_h of ~-40mV (Braun et al., 2008, Barnett et al., 1995). Addition of TTX at 6mM glucose significantly reduces action potential amplitude and glucose-stimulated insulin secretion.

Moreover, in canine β-cells increasing glucose concentration causes membrane depolarisation and an increased frequency of Na_V channel-dependent action potentials (Pressel and Misler, 1991). Once a background membrane potential of approximately -40mV is reached Na_V currents are inactivated; at this potential voltage-dependant Ca^{2+} channels are activated to induce to a plataeu depolarisation. Although Na_V channel activation and inactivation properties were not measured directly in canine β-cells, it is clear from these results that Na_V channels in canine β-cells inactivate at more positive physiological membrane potentials, similar to human β-cells, which allows them to contribute to β-cells electrical activity in response to glucose (Pressel and Misler, 1991). Furthermore, a similar characterisation of stimulus-secretion coupling in porcine pancreatic islets also revealed a dependence of action potential activity on Na_V current (Silva

et al., 2009), suggesting that Na_V channels in porcine β-cells also inactivate at physiological membrane potentials, unlike rodent β-cells.

1.4.3 Contribution of individual Na_V channel α-subunits to the arcane inactivation properties of Na_V currents in β-cells

Further characterisation of Na_V currents in mouse β-cells has revealed that 90% of the current inactivates at negative membrane potentials (~-100mV) and the remaining 10% inactivates at more positive physiologically relevant membrane potentials. The two types of inactivation may reflect the expression of multiple α-subunits that inactivate at different membrane potentials (Vignali et al., 2006, Zhang et al., 2014). Vignali et al. was the first to show that two types of TTX-sensitive currents exist in β-cells: an 'early-inactivating' Na_V current and a 'residual' Na_V current, which have vastly different V_h measurements of -106±2mV and -59±3mV, respectively (Vignali et al., 2006). In support of this hypothesis, they also showed that two Na_V channels α-subunits, $Na_V1.7$ and $Na_V1.3$, are expressed in mouse β-cells.

More recently, characterisation of voltage-dependent inactivation in mouse β-cells revealed that, whilst most β-cells (~ 70 %) inactivate with a V_h of -97±1mV, a subset of β-cells display Na_V currents that inactivate with two components of inactivation that is best described as the sum of two Boltzmann functions (Zhang et al., 2014). In these β-cells the average V_h of the two components is −97±6mV and −50±1mV, comprising 49±10% and 51±10% of the maximum current, respectively. Again, it was suggested that the biphasic inactivation observed in these cells reflect the expression of different Na_V channel α-subunits, which

inactivate at vastly different membrane potentials (Zhang et al., 2014). Moreover in many β-cells addition of TTX reduced AP height and frequency (Ernst et al., 2009, Zhang et al., 2014).

It is important to determine the identity of Na_V channel α-subunits contributing to the arcane inactivation of Na_V currents in β-cells because, as the sequence identity between different Na_V channels is high (Table 1.3.1.1), differences in inactivation between different α-subunits could provide a good indication to the site of modulation. Moreover, if Na_V channel α-subunits are modulated differently, the β-cell could provide an excellent model for specific activation/inactivation of different Na_V channel α-subunits. This would be of great clinical interest as there are currently no reliable selective inhibitors for individual Na_V α-subunits.

1.5 Aims of thesis

Thus, the overarching aim of this thesis is to further our knowledge on the regulation of Na_V channels by seeking to understand the underlying mechanism(s) for the hyperpolarised inactivation of Na_V currents in rodent β-cells. The specific aims were to:

1. Investigate the contribution of individual Na_V channel α-subunits expressed in β-cells to Na_V current inactivation observed in β-cells;
2. Establish the role of β-subunits (if any) to the variable inactivation properties of Na_V channels in β-cells;
3. Elucidate a possible underlying mechanism for the modulation of Na_V channel inactivation behaviour in β-cells.

Chapter 2

Methods

2.1 Molecular Biology

2.1.1 Plasmid constructs

The constructs coding for human *SCN9A*, *SCN1B* and *SCN2B* expressed in tandem and *SCN3B* were kindly provided by Dr Frank Reimann (Cox et al, Nature 2006). The constructs coding the β-subunits also coded for GFP, thus allowing tracing of transfected cells. If β-subunits were not used a vector coding for GFP alone was used for co-transfection. The constructs coding for human *SCN3A* (RC215453), *SCN5A* (RC214786) and *SCN8A* (RC223887) were purchased from Origene Technologies, Inc.

Most α-subunits are sensitive to tetrodotoxin (TTX), with the exception of $Na_V1.5$, $Na_V1.8$ and $Na_V1.9$. TTX binds to the proximal part of the S5-S6 linker in domain I and thereby occludes the external mouth of the pore in μM concentrations. The aromatic amino acids Tyr or Phe confer the binding of TTX in this position; in the case of $Na_V1.5$ the amino acid in the equivalent position is a cysteine residue and it is therefore ~200-fold less sensitive to the toxin (Lehmann-Horn and Jurkat-Rott, 1999). Therefore, the TTX-sensitive channels can be rendered TTX-resistant by mutating the amino acid tyrosine (Cummins et al., 2001). To render $Na_V1.3$, $Na_V1.6$ and $Na_V1.7$ TTX-resistant, the tyrosine residue was substituted with serine at positions 384, 371 and 362, respectively. Site-directed mutagenesis of *SCN3A* and *SCN9A* was achieved using the Q5 Site-Directed Mutagenesis Kit (NEB). These constructs were kindly provided by Dr Margarita Chibalina. Site-directed mutagenesis of *SCN8A* was achieved using the QuickChange II XL-Site-Directed Mutagenesis Kit (Aligent Technologies) and is described below in section 2.1.3.

The TTX-resistant form of $Na_V1.7$ was used as a template for further molecular manipulation to generate $Na_V1.7/Na_V1.3$ hybrid constructs (Figure 5.2.1.1). The N-terminus, loop 1 (L1), loop 2 (L2), loop 3 (L3) and the C-terminus cytoplasmic domain of $Na_V1.7$ were substituted with the corresponding sequences of $Na_V1.3$ to generate the hybrid constructs. These constructs were also kindly provided by Dr Margarita Chibalina.

2.1.2 Transformation of Bacteria

The *SCN9A* plasmid was propagated in SURE 2 supercompetent cells (Aligent Technologies); *SCN3A*, *SCN5A*, *SCN3B* and *SCN1B* and *SCN2B* plasmids were propagated in XL10-Gold ultracompetent cells (Aligent Technologies) and the *SCN8A* plasmid was propagated in CopyCutter™ EP1400™ competent cells (Epicentre). Plasmid DNA was purified using QIAprep Spin Miniprep kit and CompactPrep Plasmid Midi Kit (Qiagen), according to manufacturers' guidelines.

2.1.3 Site-directed mutagenesis

To generate a TTX-resistant form of $Na_V1.6$, a point mutation of Y371S was made. The mutagenic primers used to create the mutation were forward and reverse primers: 5'-GCCTTATGACCCAGGACTCTTGGGAAAACTTGTATCAATTGAC-3' and 5'-GTCAATTGATACAAGTTTTCCCAAGAGTCCTGGGTCATAAGGC-3', respectively (Sigma Aldrich). The site-directed mutagenesis was performed using the QuikChange II XL Site-Directed Mutagenesis Kit (Aligent Technologies) according to manufacturer's guidelines. The mutation and the integrity of the plasmid was

verified by Sanger sequencing (Source BioScience, UK) and using restriction digest.

2.1.4 Gene expression analysis

Cells were grown to 60% confluence for RNA extraction, which was carried out using TRI reagent® (Sigma-Aldrich) according to manufacturer's guidelines. After phase separation, PureLink® RNA Mini Kit (Life Technologies) was used to isolate RNA from the aqueous phase. On-column PureLink® DNase treatment was used to remove DNA from the sample. RNA concentration was quantified using a NanoDrop 8000 spectrophotometer (Thermo Scientific). RNA samples were stored at -80^{o}C. Reverse transcription of RNA to cDNA was carried out using a High Capacity RNA-to-cDNA Kit (Applied Biosystems) according to manufacturer's guidelines. Depending on the RNA yield between 0.5-1.5µg of RNA was carried forward to the reaction.

The QuantiFast SYBR Green PCR kit (Qiagen) was used to quantify gene expression according to manufacturer's guidelines. All samples were run in triplicate wells in 384-well plates (4titude Ltd) for the genes of interest, along with two house-keeping genes: *GAPDH* and *PPIA*. Each well contained 1µl of QuantiTect Primer Assay (Qiagen, see Table 2.1.4.1), 1µl of cDNA diluted 1:25, 5µl of 2X QuantiFast SYBR Green PCR master mix and 3µl of RNase-free H_20. Quantitative PCR was performed on the Applied Biosystems 7900HT Fast Real-Time PCR system and the data was captured using the SDS v2.3 software. Amplification curves were inspected by eye and threshold lines were adjusted manually if necessary. Analysis was performed using the delta Ct ($2^{-\Delta Ct}$) method.

Gene name	Gene Symbol	Species	Primer ID
$Na_V1.1$ α-subunit	*Scn1a*	Rat	QT02445618
$Na_V1.2$ α-subunit	*Scn2a*	Rat	QT00190722
$Na_V1.3$ α-subunit	*Scn3a*	Rat	QT01568126
$Na_V1.4$ α-subunit	*Scn4a*	Rat	QT00184786
$Na_V1.5$ α-subunit	*Scn5a*	Rat	QT00186263
$Na_V1.6$ α-subunit	*Scn8a*	Rat	QT00195496
$Na_V1.7$ α-subunit	*Scn9A*	Rat	QT00194558
$Na_V1.8$ α-subunit	*Scn10a*	Rat	QT01605926
$Na_V1.9$ α-subunit	*Scn11a*	Rat	QT01603595
Na_V channel β_1-subunit	*Scn1b*	Rat	QT00181559
Na_V channel β_2-subunit	*Scn2b*	Rat	QT00193417
Na_V channel β_3-subunit	*Scn3b*	Rat	QT00179459
Na_V channel β_4-subunit	*Scn4b*	Rat	QT01581349
Glyceraldehyde-3-phosphate dehydrogenase	*Gapdh*	Rat	QT00199633
Peptidylprolyl isomerase A	*Ppia*	Rat	QT00177394
$Na_V1.2$ α-subunit	*SCN2A*	Human	QT00070707
$Na_V1.3$ α-subunit	*SCN3A*	Human	QT00064981
$Na_V1.6$ α-subunit	*SCN8A*	Human	QT00020923
$Na_V1.7$ α-subunit	*SCN9A*	Human	QT00001505
Na_V channel β_1-subunit	*SCN1B*	Human	QT00066080
Na_V channel β_2-subunit	*SCN2B*	Human	QT00022435
Na_V channel β_3-subunit	*SCN3B*	Human	QT00002184
Na_V channel β_4-subunit	*SCN4B*	Human	QT00011802
Glyceraldehyde-3-phosphate dehydrogenase	*GAPDH*	Human	QT01192646
Peptidylprolyl isomerase A	*PPIA*	Human	QT01866137

Table 2.1.4.1 – Primers used to detect mRNA expression in Ins1 and HEK cells

2.2 Tissue culture and cell transfection

2.2.1 Cell culture

The rat insulinoma cell line Ins1 832/13 (referred to as Ins1) was kindly provided by Dr Jochen Lang (Université de Bordeaux, France). The cells were cultured in RPMI-1640 (Gibco®, Life Technologies) supplemented with 11mM glucose (also 5 and 25mM glucose in the indicated experiments), 10% foetal calf serum (FCS; Gibco®, Life Technologies), 2mM Glutamax (Gibco®, Life Technologies), 1mM sodium pyruvate (Sigma-Aldrich), 10mM HEPES (Gibco®, Life Technologies), 50μM β-mercaptoethanol (Gibco®, Life Technologies), 100U/ml penicillin and 100μg/ml streptomycin (Sigma-Aldrich). In some experiments Ins1 cells were cultured for 48h with 10nM phorbol 12-myristate 13-acetate (PMA) (Sigma-Aldrich) or 100μM diazoxide (Sigma-Aldrich); for 24h with 10μM of the insulin receptor antagonist S961 (Sigma-Aldrich) or for 20min with 20μM BAPTA-AM (Tocris, UK). The cells were subcultured, once a week, using TrypLE™ Express (Gibco®, Life Technologies) and $2.5x10^5$ cells were transferred to a T25 flask (Starsdedt). The cell medium was changed three times a week.

The human embryonic kidney cell line (AD-293; referred to as HEK cells from here on) was obtained from Aligent Technologies. The culture medium used for HEK cells was Dulbecco's Modified Eagle Medium (Gibco®, Life Technologies) supplemented with 25mM glucose, 10% heat inactivated FCS, 2mM Glutamax, 1mM sodium pyruvate, 100U/ml penicillin and 100μg/ml streptomycin. The cells were subcultured at a ratio of 1:8, twice a week and the cell medium was changed once between cell subculture.

The mouse pancreatic α-cell line (αTC1-6) was obtained from ATCC (Manassas, USA) and cells were cultured in RPMI-1640 supplemented with 15mM glucose, 10% FCS, 10mM HEPES, 100U/ml penicillin and 100µg/ml streptomyocin. The cells were subcultured at a ratio of 1:3, twice a week and the medium was changed on alternating days.

The Chinese hamster ovary (CHO) cells were obtained from ECACC (Salisbury, UK) and cultured in Ham's F-12K (Kaighn's) medium (Gibco®, Life Technologies) supplemented with 7mM glucose, 10% fetal bovine serum, 2mM L-glutamine, 100U/ml penicillin and 100µg/ml streptomyocin. The cells were subcultured at a ratio of 1:10, three times a week.

EndoC-βh2 cell lines are derived from human fetal pancreatic buds and were kindly provided by Professor Raphael Scharfmann (Scharfmann et al., 2014, Ravassard et al., 2011). The cells are cultured at 5.6mM glucose in Dulbecco's modified Eagle's medium (DMEM; Sigma-Aldrich) with 2% BSA fraction V fatty acid free (Roche Diagnostics), 50µM 2-mercaptoethanol, 10mM nicotinamide (Calbiochem), 5.5µg/ml transferrin (Sigma-Aldrich), 6.7ng/ml selenite (Sigma-Aldrich), 100U/ml penicillin, and 100µg/ml streptomycin. The cells were subcultured once a week and $5.5x10^6$ cells were transferred to a T75 flask coated with 1% Matrigel and 2µg/ml fibronectin (Sigma-Aldrich).

2.2.2 Cell transfection

Transfection of plasmids and siRNA duplexes was performed using Lipofectamine® 2000 (Life Technologies) according to the manufacturer's

guidelines. Cells plated on 35mm dishes were co-transfected with 1.5μg of DNA encoding $Na_V1.3$, $Na_V1.6$ and $Na_V1.7$ α-subunits and 50ng of DNA encoding β-subunits (as specified) and assayed 24-48h after transfection. GFP fluorescence was used to select for transfected cells, which subsequently were tested for channel expression by whole-cell patch-clamp recording techniques.

siRNA-mediated knockdown experiments were performed in Ins1 cells. siRNA duplexes against rat *Scn3b* and scrambled negative control (Origene Technologies,Inc.) were applied at a final concentration of 60nM. For efficient knockdown, the cells were transfected twice: on day 1 and day 3 and used for experiments on day 4. The efficiency of knockdown was assessed by qPCR.

2.3 Electrophysiology

Whole-cell Na_V currents were recorded from untreated or transfected Ins1, HEK, αTC1-6 and CHO cells using the standard whole-cell configuration as previously described (Zhang et al., 2014). Voltage-clamp experiments were performed using EPC-9 amplifier and Pulse (Version 8.80) software (HEKA Electronics, Lambrecht /Pfalz, Germany). A DMZ-Zeitz-Puller (Zeitz) was used for fabrication of polished patch-clamp electrodes (Harvard Apparatus) that had a resistance of 2-4.5MΩ when filled with the electrode-filling solution. Currents were compensated for capacitive transients using a computer-controlled algorithm. Remaining capacitive transients were removed as well as leak subtraction corrected using a –P/4 protocol. Series resistance compensation between 50-80% was used every 2μs. The recorded currents were filtered by 2.9kHz and digitised at >10kHz. Recordings from cells with a seal resistance of less than 1GΩ, a voltage error

greater than 5mV and currents less than 50pA (except in Figure 5.2.2.1 and Figure 5.2.3.1) were not used. Since Na_V current activation and inactivation undergo a time-dependent shift towards more negative membrane potentials in the whole-cell configuration (Fernandez et al., 1984), all measurements reported here were obtained within ~1min of going whole-cell.

The standard extracellular medium for the electrophysiological measurements consisted of (mM) 118 NaCl, 20 tetraethylammonium-Cl (TEA-Cl; to block K^+ currents), 5.6 KCl, 1.2 $MgCl_2$, 5 HEPES (adjusted to pH 7.4 using NaOH), 5 D-glucose and 2 $CoCl_2$ (to block Ca^{2+} channels; also used at 0.2 and 10mM final concentrations in the indicated experiments). All experiments were conducted in the presence of $CoCl_2$ instead of $CaCl_2$. TTX (Alomone Labs, Jerusalem, Israel) was used at a final concentration of 0.1µgml−1, to block endogenous Na_V currents. BIM23056 (Tocris, UK) or PMA was included in the culture medium at 100nM and 10nM final concentration, respectively as indicated. The pipette solution contained (mM) 120 CsCl (to block K^+ currents) , 1 $MgCl_2.6H_2O$, 1 $CaCl_2$, 10 EGTA, 10 HEPES (adjusted to pH 7.15 with CsOH) and 3 Mg-ATP. In the indicated experiments phosphatidylinositol 4,5-bisphosphate (PIP_2) diC8 (Echelon) or neomycin (Sigma Aldrich) were present in the pipette solution at 50µM final concentration.

The effect of acute changes in the extracellular glucose concentration were measured in perforated-patch configuration, as previously described (De Marinis et al., 2010). Perforation was achieved using amphotericin B (Sigma-Aldrich), present in the intracellular solution at 60µgml^{-1} final concentration. The intracellular pipette solution was composed of (mM) 76 Cs_2SO_4, 10 NaCL, 10 KCl,

1 $MgCl_2$ and 5 HEPES, adjusted to pH 7.15 with CsOH. The extracellular solution used in the whole-cell configuration was also used for perforated patch clamp measurements at a final glucose concentration of 1mM or 20mM.

For cell-attached experiments, an extracellular ion composition was used for the pipette solution consisting of (mM) 118 NaCl, 20 tetraethylammonium-Cl, 5.6 KCl, 1.2 MgCl2, 5 HEPES (pH 7.4 with NaOH), 2 CoCl2 and 5 D-glucose. During seal formation, the cells were immersed in standard extracellular medium containing (mM) 137 NaCl, 5.6 KCl, 10 HEPES (pH 7.4 using NaOH), 1.1 $MgCl_2$ and 2.6 $CaCl_2$. Once the seal was formed, the high K+ extracellular solution was perfused, consisting of (mM) 125 KCl, 1 $MgCl_2$, 1 $CaCl_2$, 10 EGTA, 10 HEPES (pH 7.4 with KOH) and 5 D-glucose to depolarise the cell to ~0mV (Nernst potential) to allow accurate control of the membrane potential. After recordings were made in the cell-attached configuration, an extracellular solution with an intracellular ion composition was perfused, ready for patch excision into an inside-out configuration. The extracellular medium used for the inside-out patch experiments was identical to the high-K^+ solution specified above except the pH was adjusted to 7.2 and the addition of 3mM MgATP. All electrophysiological experiments were performed at 34°C.

For 'patch cramming' experiments, Ins1 and HEK cells were cultured in droplets of their respective culture media in the same 35mm dish. The same solutions that were used for cell-attached and inside-out configurations were then applied. However, upon excision of the membrane, the electrode was 'crammed' into a neighbouring HEK cell followed by subsequent measurements of voltage-dependent activation and inactivation (Kramer, 1990).

A standard two-pulse protocol was used to assess inactivation (Figure 2.2.2.1A). The pulse protocol consists of a 50ms conditioning pulse of potentials varying from -150mV and 0mV (in increments of 5mV) followed by a 5ms test pulse to 0mV. The peak inward current (I) produced after each depolarisation to 0mV was measured and normalised to the maximum Na^+ current amplitude (I_{max}). The data is presented as h_∞ ($=I/I_{max}$), which was plotted against the conditioning voltage (V). For each cell, the data points were approximated to a single or a double Boltzmann function to determine the half-maximal inactivation (V_h) and the slope factor (k). The most appropriate fit to the data (single or double Boltzmann) was determined using the Akaike Information Criterion (AIC) using Origin software. Inactivation curves were fitted to a single Boltzmann function when the fit to a double Boltzmann function resulted in either two V_h values with a difference of less than 15mV or a V_h composed of less than 15% of the total current.

Steady-state activation was assessed by applying a depolarising pulse, between -70 to +60mV (in increments of 10mV) for 20ms, from a holding potential of -150mV (Figure 2.2.2.1B). The peak inward current (I) produced after depolarisation to each voltage step was measured and used to calculate the Na^+ conductance (G) by the relation $G=I/(V-V_r)$ where V is the membrane potential and V_r is the estimated reversal potential, calculated using the Nernst equation from the extra- and intracellular Na^+ concentrations in the media (Gonoi and Hille, 1987). The sigmoidal curve produced was fitted to a Boltzmann function, which was used to determine the half-maximal activation ($V_{0.5}$) and the slope factor (k). The average current density was calculated by normalising the peak inward current produced after each voltage step to the slow-capacitance, which is proportional to the membrane surface area.

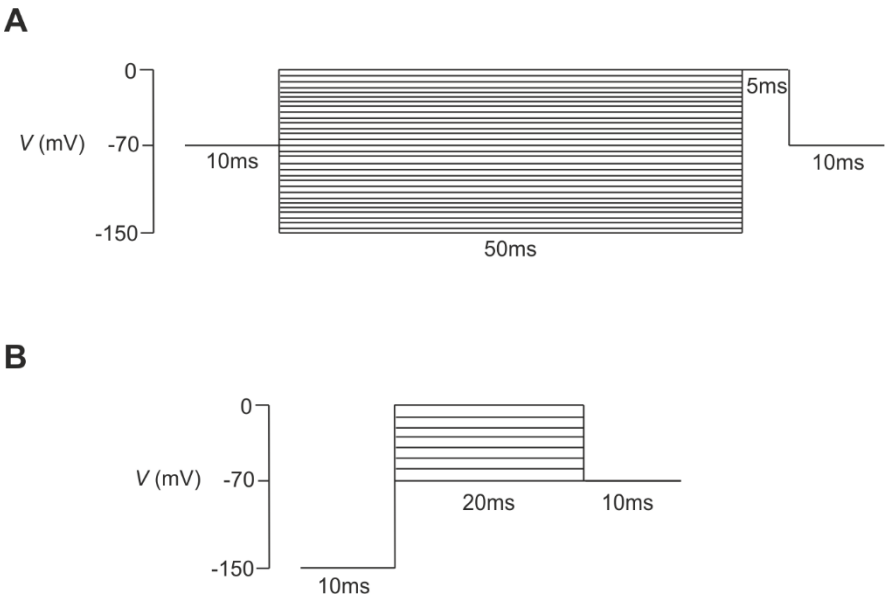


Figure 2.2.2.1 – Steady-state inactivation and activation pulse protocol

A, standard two-pulse protocol used to assess voltage-dependent inactivation. A conditioning pulse of potentials varying from -150mV and 0mV was applied in increments of 5ms, followed by a test pulse to 0mV. After each depolarisation to 0mV, the peak inward current produced was measured and normalised to the maximum current amplitude. *B*, pulse protocol used to assess steady state activation. A depolarising pulse between -70 to +60 mV was applied (in increments of 10ms) for 20 ms, from a holding potential of -150 mV. The peak current was measured after depolarisation to each voltage step and was used to calculate Na^+ conductance and Na^+ current density.

2.3.1 Data Analysis

All data are given as mean values ± SEM of the indicated number of experiments (*n*). Statistical significances were calculated using Student's t-test or ANOVA (for multiple comparisons, as appropriate).

Chapter 3

The contribution of individual Na_V channel α-subunits to the hyperpolarised inactivation of Na_V currents in rodent β-cells

3.1 Introduction

The lack of Na^+ current evoked by depolarisation, from physiological membrane potentials, despite the abundant expression of Na_V channel α-subunits reflects the hyperpolarised inactivation of Na_V channels in rodent β-cells (Gopel et al., 1999, Plant, 1988, Lou et al., 2003, Hiriart and Matteson, 1988). In addition, the presence of a small Na^+ current component (10-15%) that inactivates over physiological membrane potentials (and contributes to action potential firing) has been described (Vignali et al., 2006, Zhang et al., 2014). It has been suggested that the apparent difference in the voltage-dependence of inactivation between different Na_V current components can be attributed to the expression of different Na_V channel α-subunits.

Mouse β-cells express $Na_V1.3$, $Na_V1.6$ and $Na_V1.7$, as revealed by RNA sequencing data of FACs sorted mouse β-cells (Adriaenssens et al., 2016, DiGruccio et al., 2016, Benner et al., 2014). However, mouse β-cells principally express *Scn9a*, the gene that encodes $Na_V1.7$, with less expression of *Scn8a* and *Scn3a* (the genes that encode $Na_V1.6$ and $Na_V1.3$) (Zhang et al., 2014). The relative expression of *Scn9a* and *Scn3a* in β-cells is also reflected upon genetic ablation of the genes in β-cells, which causes a reduction in Na^+ current density by >85% and 35%, respectively (Zhang et al., 2014).

Genetic ablation of $Na_V1.3$ and $Na_V1.7$ in β-cells was used to identify the identity of the Na_V channel α-subunits inactivating at the different membrane potentials (Zhang et al., 2014). Partial ablation of *Scn3a* (*Scn3a*$^{+/-}$) in β-cells resulted in a biphasic inactivation with both a depolarised (~-49mV) and hyperpolarised (~-94mV) V_h component, attributed to the expression of different α-subunits.

Indeed, complete ablation of *Scn3a* in β-cells (*Scn3a*$^{-/-}$), assumed to result in only the $Na_V1.7$ current, revealed a single component of inactivation in all cells with an average V_h of -102±2mV (n=18). Conversely, ablation of *Scn9a* in β-cells (*Scn9a*$^{-/-}$), thereby genetically isolating $Na_V1.3$ current, also resulted in a single component of inactivation with a depolarised V_h of -66±7mV. This suggests that in mouse β-cells, $Na_V1.3$ is the physiologically relevant Na_V channel α-subunit (Zhang et al., 2014). Since $Na_V1.7$ is the predominant α-subunit in β-cells a large proportion of the Na^+ current inactivates over hyperpolarised membrane potentials. The inactivation properties of $Na_V1.3$ and $Na_V1.7$ were also reflected in glucose-stimulated insulin secretion (GSIS) experiments, where the *Scn3a*$^{-/-}$ significantly reduced insulin secretion at stimulatory glucose concentrations, whilst *Scn9a*$^{-/-}$ had no effect on GSIS (Zhang et al., 2014).

These results also suggest that $Na_V1.7$ inactivation is modulated in a β-cell specific manner. $Na_V1.7$ in sensory dorsal root ganglion neurones (DRG) inactivates at approximately -70mV (Herzog et al., 2003). Thus, $Na_V1.7$ in mouse β-cells inactivates at voltages 30mV more hyperpolarised than those for the same channel expressed in DRG neurones and this discrepancy cannot be explained by expression of different $Na_V1.7$ splice variants (Zhang et al., 2014).

Although the genetic ablation studies were useful in providing an insight into the contribution of individual α-subunits, the experiments were conducted on a background in which $Na_V1.6$ was still expressed and complete ablation of the *Scn3a* and *Scn9a* was not guaranteed. Therefore, to further investigate the contribution of individual α-subunits to Na_V current inactivation in β-cells and to establish whether the different components of inactivation do indeed correspond

to the inactivation of different Na_V channel α-subunits, it is important to characterise the current of Na_V channel α-subunits in isolation. To this end, $Na_V1.7$, $Na_V1.3$ and $Na_V1.6$, the α-subunits expressed in β-cells, were rendered resistant to TTX and were then individually expressed in Ins1 cells, a β-cell model. The activation and inactivation properties of the individual Na_V α-subunits were characterised in the presence of TTX to block endogenous Na_V currents and to allow the characterisation of the expressed TTX-resistant current in isolation. To access whether the α-subunits are modulated in a β-cell specific manner, TTX-resistant $Na_V1.7$, $Na_V1.3$ and $Na_V1.6$ currents were also characterised in HEK cells, a non-β-cell model, and their activation and inactivation properties were compared to those in Ins1 cells.

3.2 Results

3.2.1 Characterisation of endogenous Na_V channels in Ins1 and HEK cells

Na_V currents in Ins1 and HEK cells were measured in the presence and absence of TTX in response to a step depolarisation from -150mV to 0mV, as shown in Figure 3.2.1.1A and B. In Ins1 cells membrane depolarisation evoked a large rapid inward Na_V current, which was abolished upon the addition of TTX. HEK cells in contrast did not evoke a Na_V current upon depolarisation, which is consistent with its lack of Na_V channel α- and β-subunit mRNA expression (data not shown).

Relative mRNA expression of Na_V channels in Ins1 cells echoed the voltage clamp experiments and revealed expression of only TTX-sensitive channels (Figure 3.2.1.1C). However, unlike primary mouse β-cells, which predominantly express

Scn9a and to a lesser extent *Scn3a* and *Scn8a* (Adriaenssens et al., 2016, DiGruccio et al., 2016, Benner et al., 2014), Ins1 cells predominantly express *Scn3a*, with less expression of *Scn8a* and *Scn2a* and surprisingly, no detectable levels of *Scn9a*. To confirm that $Na_V1.7$ is not expressed in Ins1 cells, it was important to test whether the *Scn9a* primer was functional. The *Scn9a* primer was tested using a sample of rat islet cDNA as a positive control, in which *Scn9a* mRNA levels were detectable (Figure 3.2.1.1D); this confirmed that the primer is functional and $Na_V1.7$ is not expressed in Ins1 cells. The expression of β-subunits also differs between Ins1 cells and primary mouse β-cells. In the latter, the β_1 subunit is expressed more highly (Adriaenssens et al., 2016, DiGruccio et al., 2016, Benner et al., 2014), whilst the β_3 subunit is expressed more highly in Ins1 cells.

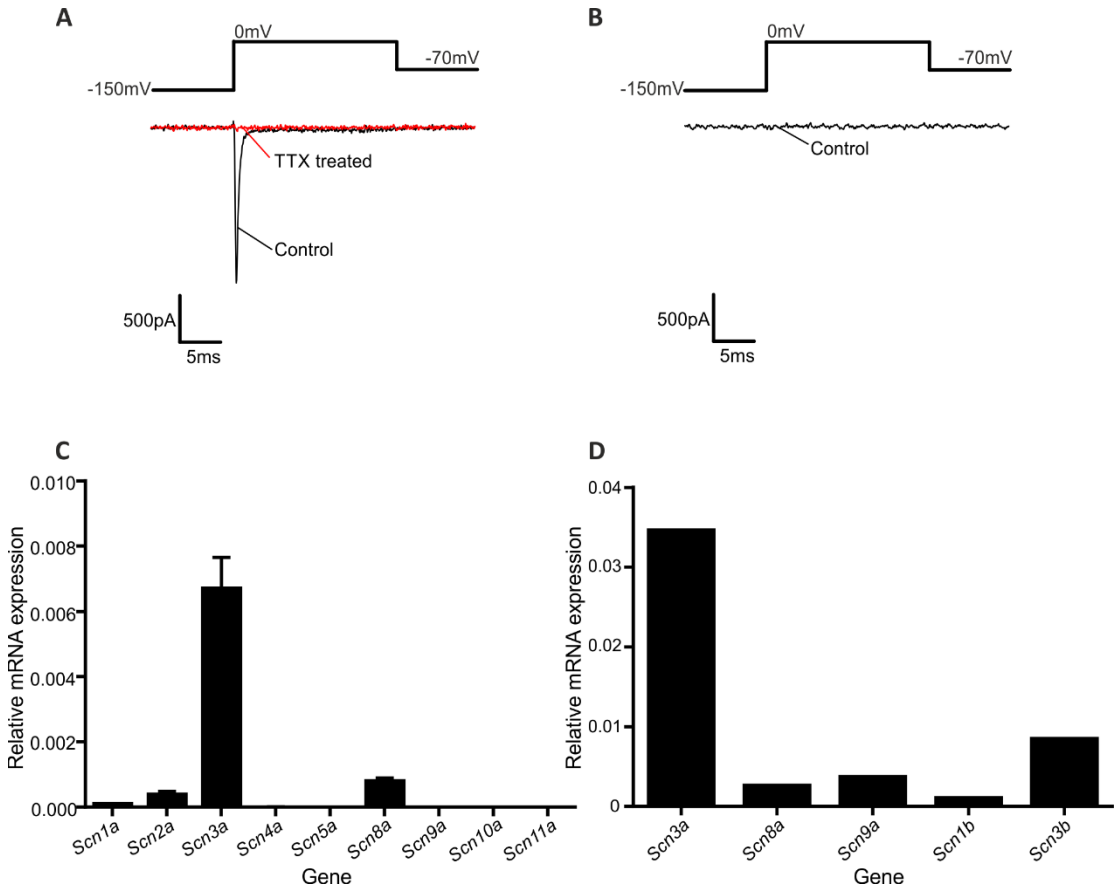


Figure 3.2.1.1 – Characterisation of endogenous Na$_V$ channels in Ins1 and HEK cells

A, endogenous Na$_V$ current from Ins1 cells in response to a step depolarisation from -150mV to 0mV in the absence (black) and presence (red) of TTX. *B*, same as in *A* except in HEK cells and only in the absence (black) of TTX. *C*, represent relative mRNA expression of Na$_V$ channel α-subunits in Ins1 cells (*n*=2 preparations). *D*, relative mRNA expression of Na$_V$ channel subunits in rat islets (*n*=1 preparation).

Characterisation of endogenous Na$_V$ currents in Ins1 cells revealed two components of voltage-dependent inactivation, as indicated by the arrows in Figure 3.2.1.2A. Interestingly, a large negative component can be observed despite the lack of endogenous Na$_V$1.7 mRNA expression in Ins1 cells. 12/24 cells inactivated with a monophasic inactivation with an average V_h of -88±2mV and a

slope factor, *k*, of 9±0.2 (Figure 3.2.1.2B). The remaining 12 cells inactivated with a biphasic inactivation; the average V_h of the two components is -87±3mV and -43±2mV, comprising 71± 6% and 29±6% of the current (Figure 3.2.1.2C).

Voltage-dependence of activation in Ins1 cells displayed a $V_{0.5}$ of -16±2mV (n=21), as shown in Figure 3.2.1.2D. This is more depolarised than the $V_{0.5}$ of ~-24mV observed in primary β-cells (Zhang et al., 2014). However, endogenous currents displayed a similar I-V relationship to primary β-cells with a large peak current density of -169±29pApF^{-1} at 0mV (data not shown).

Given that Ins1 cells share a similar inactivation behaviour to primary mouse β-cells and neither Ins1 nor HEK cells express endogenous TTX-resistant channels they were chosen as appropriate models to represent β- and non-β-cells.

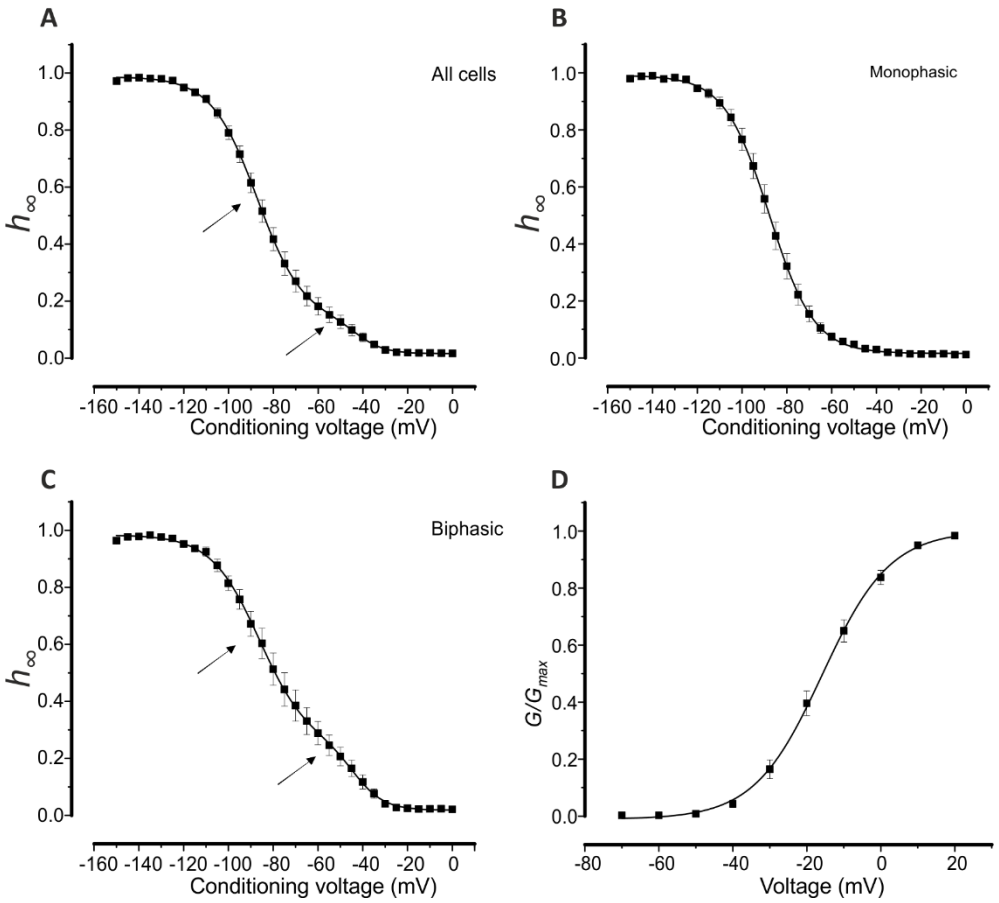


Figure 3.2.1.2 – Voltage-dependence of activation and inactivation of endogenous Na_V currents in Ins1 cell

A, average voltage-dependence of Na_V current inactivation recorded from all Ins1 cells (*n*=24). Arrows indicate the two components of inactivation. The curve represents a double Boltzmann function. *B*, same as in *A*, but average of all cells that were best described using a single Boltzmann function i.e had a monophasic inactivation (*n*=12). *C*, same as in *A*, but average of all cells that were best described using a double Boltzmann function i.e had a biphasic inactivation (*n*=12). Arrows indicate the two components of inactivation. *D*, voltage-dependence of Na_V current activation (G/Gmax) in Ins1 cells (*n*=21), fitted to a single Boltzmann function.

3.2.2 Characterisation of wild-type and TTX-resistant $Na_V1.7$, $Na_V1.3$ and $Na_V1.6$ in HEK cells.

To make certain that site-directed mutagenesis of the channels rendering them resistant to TTX, does not affect the channel gating properties, wild-type (WT) and TTX-resistant channels were characterised in HEK cells. Since HEK cells do not express any endogenous Na_V currents, WT and TTX-resistant currents could be isolated and compared without contamination of endogenous Na_V currents. The data is shown in Figure 3.2.2.1 and the voltage-dependence of inactivation and activation values are summarised in Table 3.2.2.1 and Table 3.2.2.2, respectively. Compared to the WT, rendering the channel TTX-resistant did not affect the inactivation properties of $Na_V1.7$, $Na_V1.3$ or $Na_V1.6$, nor did it affect the activation properties of $Na_V1.7$ or $Na_V1.6$. However, a small but significant depolarising shift of 4mV in the $V_{0.5}$ of TTX-resistant $Na_V1.3$ could be observed in comparison to WT $Na_V1.3$, as summarised in Table 3.2.2.2. Since rendering the channels TTX-resistant had no effect on the voltage-dependence of inactivation and activation (with the exception of $Na_V1.3$) compared to the WT channels, they provide an excellent means for characterising individual Na_V currents in isolation. From here on in, TTX-resistant $Na_V1.7$, $Na_V1.3$ and $Na_V1.6$ will be referred to simply as $Na_V1.7$, $Na_V1.3$ and $Na_V1.6$.

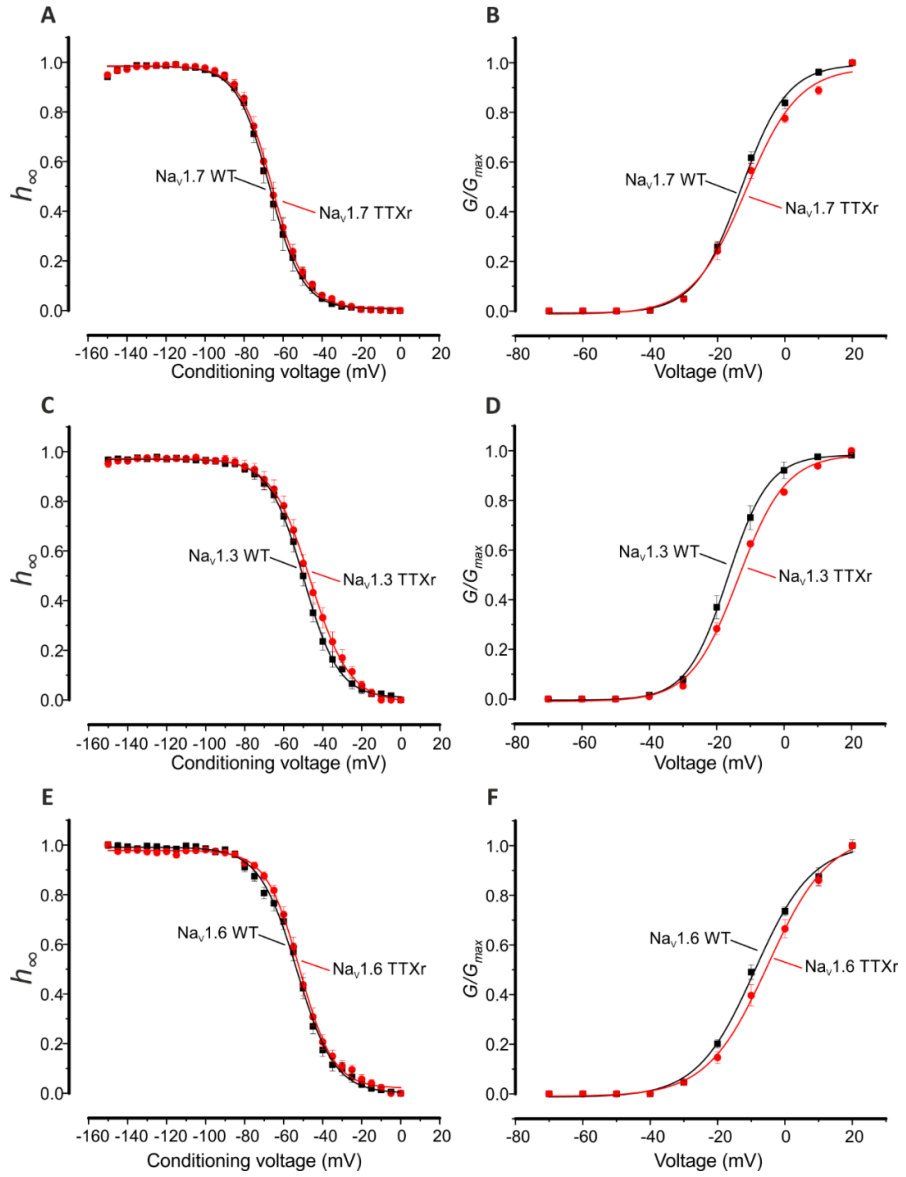


Figure 3.2.2.1 – Voltage-dependence of inactivation and activation of WT and TTX-resistant versions of $Na_V1.7$, $Na_V1.3$ and $Na_V1.6$ channels in HEK cells

A, voltage-dependence of inactivation (h_∞) of $Na_V1.7$ WT (black; *n*=6) and $Na_V1.7$ TTX-resistant (red; *n*=6) α-subunits co-expressed with β_1- and β_2-subunits. The curves represent a single Boltzmann fit to the data. *B*, voltage-dependence of activation (G/G_{max}) of $Na_V1.7$ WT (black; *n*=7) and TTX-resistant (red; *n*=9) α-subunits co-expressed with β_1- and β_2-subunits. The curves represent a single Boltzmann fit to the data. *C*, same as in *A*, but for $Na_V1.3$ WT (black; *n*=14) and $Na_V1.3$ TTX-resistant (red; *n*=7). *D*, same as in *B*, but for $Na_V1.3$ WT (black; *n*=5) and $Na_V1.3$ TTX-resistant (red; *n*=7). *E*, same as in *A*, but for $Na_V1.6$ WT (black; *n*=13) and $Na_V1.6$ TTX-resistant (red; *n*=10). *F*, same as in *B*, but for $Na_V1.6$ WT (black; *n*=5) and $Na_V1.6$ TTX-resistant (red; *n*=9).

Construct	V_h (mV)	k
$Na_V1.7$ WT	-67±2 (6)	8±1 (6)
$Na_V1.7$ TTX-resistant	-66±2 (9)	8±1 (9)
$Na_V1.3$ WT	-50±2 (14)	8±1 (14)
$Na_V1.3$ TTX-resistant	-48±1 (7)	10±2 (7)
$Na_V1.6$ WT	-53±1 (13)	8±1 (13)
$Na_V1.6$ TTX-resistant	-53±1 (10)	7±1 (10)

Table 3.2.2.1 - V_h and k values of WT and TTX-resistant $Na_V1.7$, $Na_V1.3$ and $Na_V1.6$ expressed in HEK cells

Values represent mean ± SEM of indicated number of cells (n).

Construct	$V_{0.5}$ (mV)	K
$Na_V1.7$ WT	-13±1 (7)	7±1 (7)
$Na_V1.7$ TTX-resistant	-12±1 (9)	8±1 (9)
$Na_V1.3$ WT	-18±1 (5)	5±1 (5)
$Na_V1.3$ TTX-resistant	-14±1 (7)**	7±1 (7)††
$Na_V1.6$ WT	-9±1 (5)	8±1 (5)
$Na_V1.6$ TTX-resistant	-5±1 (9)	9±1 (9)

Table 3.2.2.2 - $V_{0.5}$ and k values of WT and TTX-resistant $Na_V1.7$, $Na_V1.3$ and $Na_V1.6$ expressed in HEK cells

Values represent mean ± SEM of indicated number of cells (n). ** P <0.01, t-test $V_{0.5}$ of $Na_V1.3$ WT vs $Na_V1.3$ TTX-resistant. †† P <0.01, t-test k of $Na_V1.3$ WT vs $Na_V1.3$ TTX-resistant.

3.2.3 Characterisation of $Na_V1.7$ in Ins1 and HEK cells

The $Na_V1.7$ channel was co-expressed with β_1- and β_2- subunits in Ins1 and HEK cells and currents evoked from a step depolarisation from -150mV to 0mV are shown in Figure 3.2.3.1A and B. Addition of TTX reduced the peak current in Ins1

cells, but not in HEK cells, which reflects the block of endogenous Na_V currents in Ins1 cells and the lack of endogenous Na_V currents in HEK cells.

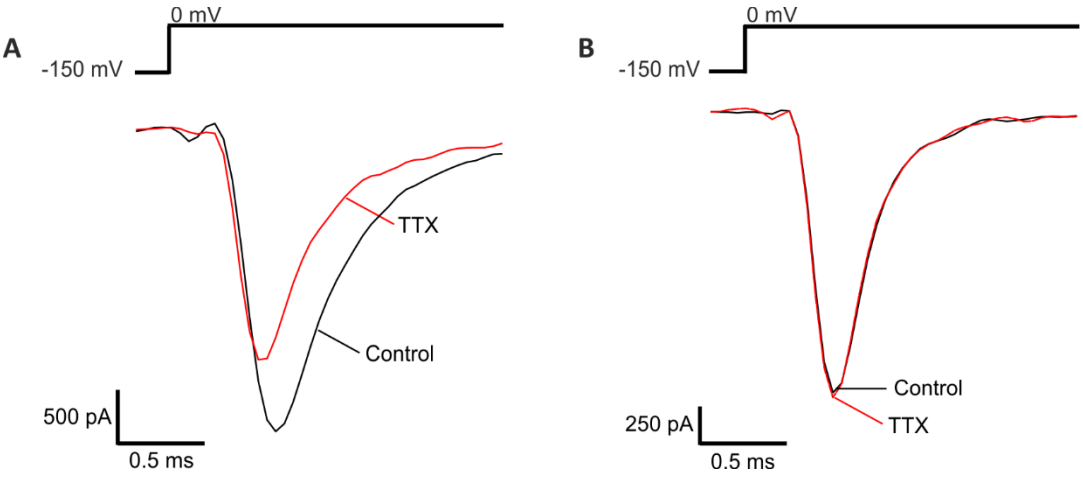


Figure 3.2.3.1 – TTX-resistant $Na_V1.7$ current traces in Ins1 and HEK cells

A, Na_V currents evoked in response to a step depolarisation from -150mV to 0mV in Ins1 cells with co-expression of $Na_V1.7$ and β_1- and β_2-subunits in the absence (black; control) and presence of TTX (red; TTX treated). The reduction of the peak current induced by TTX reflects a block of endogenous Na_V current. B, same as in A but expressed in HEK cells.

Families of voltage clamp currents recorded from $Na_V1.7$ expressed in Ins1 cells and HEK cells, during membrane depolarisations from -150mV to -20, -10 and 0mV are shown in Figure 3.2.3.2A and B, respectively. There was no significant difference in the voltage-dependence of activation of $Na_V1.7$ in Ins1 and HEK cells is shown in Figure 3.2.3.2C. The $V_{0.5}$ of $Na_V1.7$ in Ins1 and HEK cells is -13±1mV (n=39) and -12±1mV (n=8), respectively. The I-V relationship of $Na_V1.7$ was also similar between both cell types.

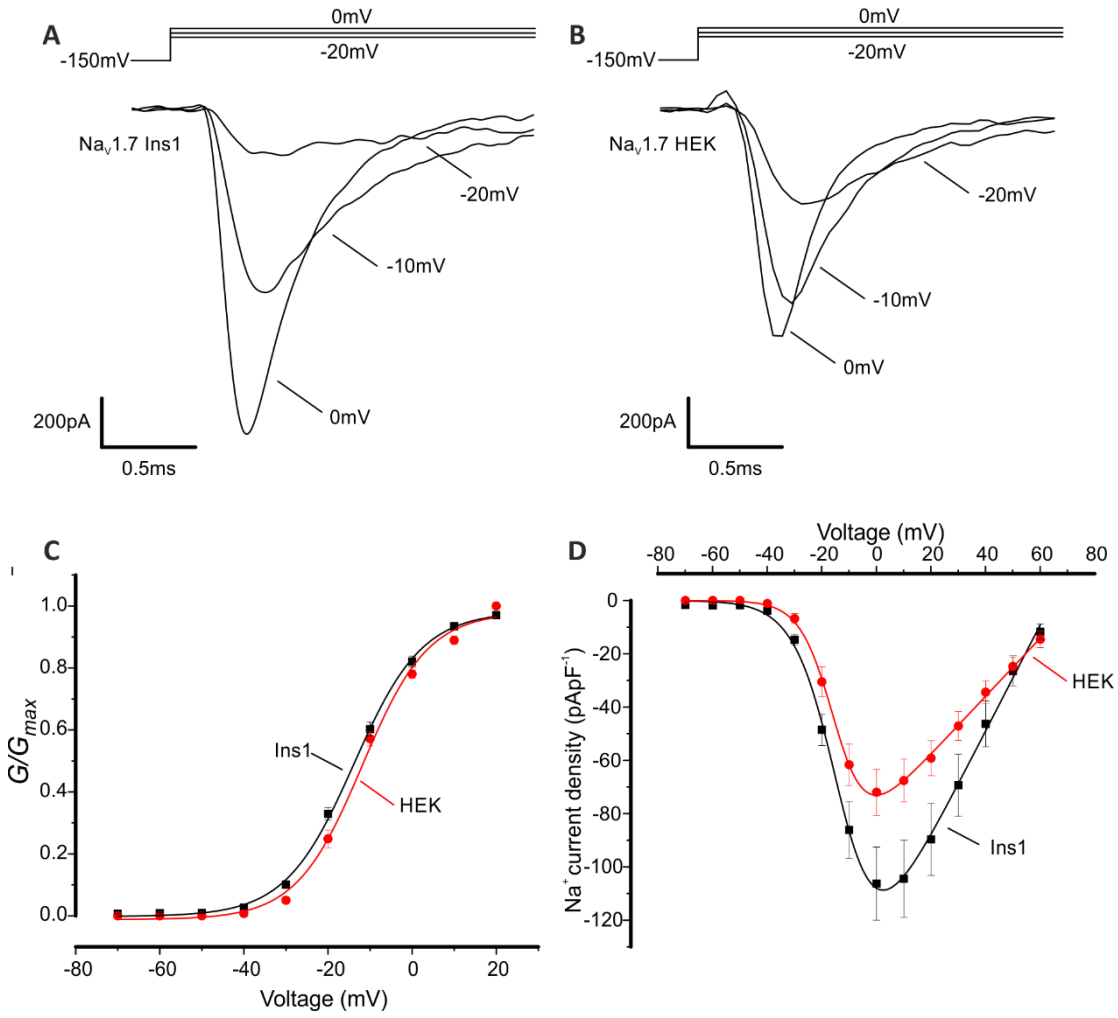


Figure 3.2.3.2- Voltage-dependence of activation of Na$_V$1.7 currents in Ins1 and HEK cells

A, family of voltage-clamp Na$_V$1.7 currents evoked by depolarisations from a holding potential of -150 to -20, -10 and 0mV when the α-subunit is co-expressed with β_1- and β_2-subunits in Ins1 cells. *B*, same as in *A*, but with Na$_V$1.7 expressed in HEK cells. *C*, voltage-dependence of Na$_V$1.7 current activation (G/G_{max}) in Ins1 (black; *n*=39) and HEK cells (red; *n*=8). D, I-V relationship of Na$_V$1.7 currents in Ins1 (black; *n*=39) and HEK cells (red; *n*=8).

In contrast, to the voltage-dependence of activation, the voltage-dependence of inactivation is significantly shifted in a hyperpolarised direction in Ins1 cells compared to HEK cells, as shown in Figure 3.2.3.3A. The majority of cells in Ins1 demonstrated a monophasic inactivation with a V_h of -94±2mV (n=38) (Figure

3.2.3.3B), which was significantly more hyperpolarised than the V_h of -66±2mV (n=9) for $Na_V1.7$ expressed in HEK cells (P<0.001, Mann Whitney Rank Sum Test). Surprisingly, 9/46 cells expressing $Na_V1.7$ in Ins1 cells displayed a biphasic inactivation where the inactivation curve was best described using a double Boltzmann function. The average V_h of the curves fitted to a double Boltzmann is -97±4mV and -67±4mV, comprising of 50±4% and 50±4% of the total current (Figure 3.2.3.3C). Interestingly the positive component of inactivation, which has a V_h of -67mV is very similar to the inactivation of $Na_V1.7$ in HEK cells. The two components of inactivation of $Na_V1.7$ become less apparent when averaging all of the cells that exhibited a biphasic inactivation. For this reason two examples of cells that displayed biphasic inactivation are shown in Figure 3.2.3.3D.

We explored the effect of Na^+ current density on V_h to ensure that the difference in V_h of $Na_V1.7$ between Ins1 and HEK cells is not due to a difference in the level of expression of the channel between the two cell types. Moreover, if the V_h of $Na_V1.7$ or the occurrence of biphasic inactivation was influenced by Na^+ current density it may suggest regulation of the channel by a limited pool of a certain modulating factor, which becomes saturated upon increased expression of the channel. However, there is no significant difference between the average Na^+ current density of cells that exhibited a monophasic (-96±13pApF^{-1}) and biphasic inactivation (-75±17pApF^{-1}) of $Na_V1.7$ current (Figure 3.2.3.3E; P =0.735, Mann Whitney Rank Sum Test), suggesting that there is no correlation between Na^+ current density and the fit of the curve to a single or double Boltzmann function. Moreover, there is also no obvious relationship between the Na^+ current density and V_h (Figure 3.2.3.3F).

Interestingly, the scatter of V_h amongst cells that exhibited monophasic inactivation appears to distinctly fall into V_h values observed in the positive (black) and negative (grey) components of biphasic inactivation (Figure 3.2.3.3F). This suggests that the channels can distinctly inactivate at two different membrane potentials separated by ~30mV. Thus biphasic inactivation may reflect the inactivation of different populations of the same α-subunit inactivating at different membrane potentials.

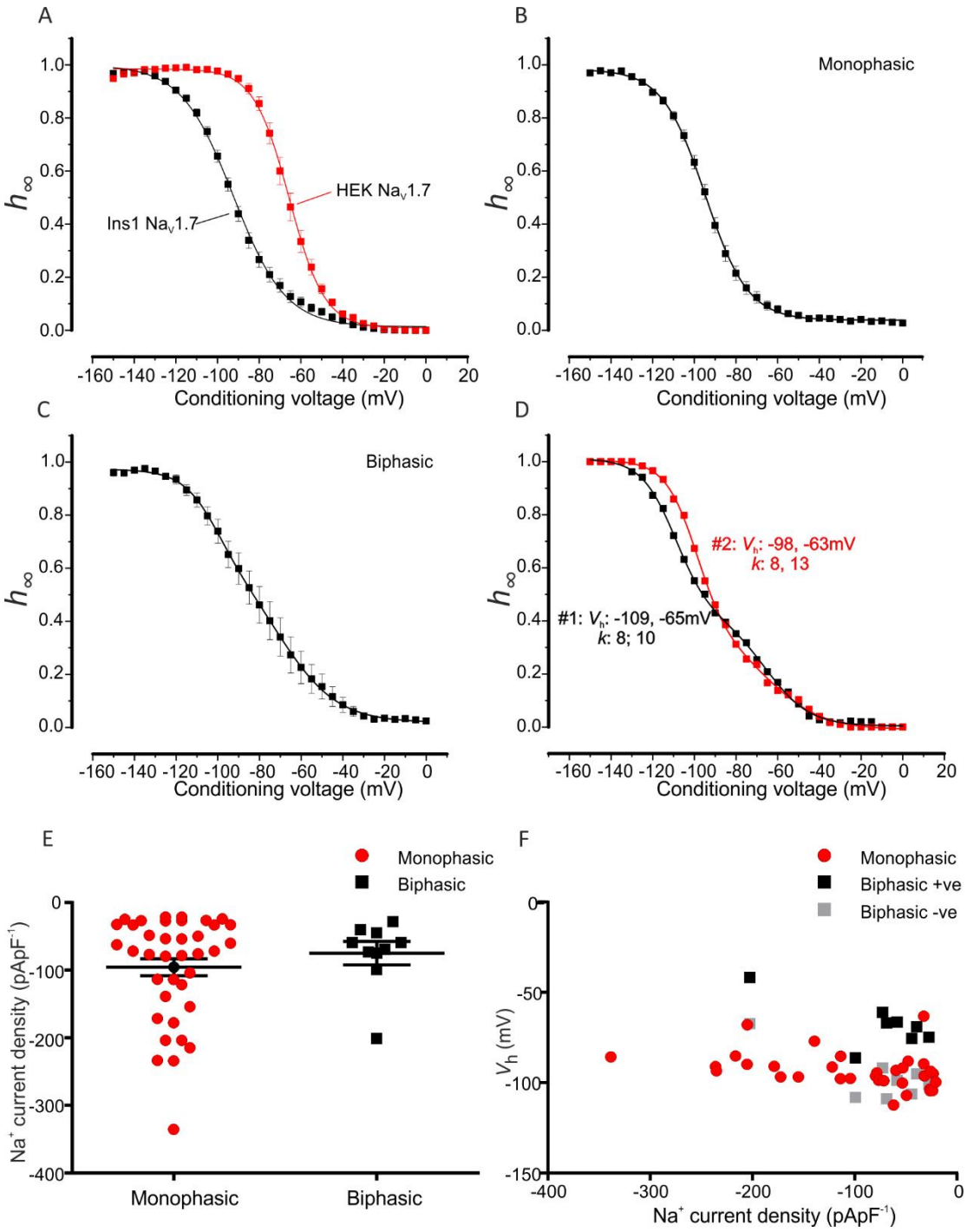


Figure 3.2.3.3- Voltage-dependence of inactivation of Nav1.7 currents in Ins1 and HEK cells

A, voltage-dependence of Nav1.7 current inactivation (h_∞) when the α-subunit was co-expressed with β1- and β2-subunits in Ins1 (black; *n*=47) and HEK cells (red; *n*=9). The curves represent a double and single Boltzmann fit to the data for Nav1.7 currents recorded from Ins1 and HEK cells, respectively. *B*, the average voltage-dependence of inactivation of Nav1.7 current in Ins1 cells that was best described with a single Boltzmann fit to the data (*n*=38). *C*, same as in *B* but for biphasic

inactivation (*n*=9). *D*, examples of biphasic inactivation curves of $Na_V1.7$ in Ins1 cells with their respective V_h and *k* values. *E,* represents the relationship between peak Na^+ current density and the most appropriate fit (single or double Boltzmann, reflecting monophasic or biphasic inactivation respectively) to current inactivation data in Ins1 cells. *F*, relationship between monophasic, biphasic negative (-ve) and biphasic positive (+ve) V_h values and the peak Na^+ current density of $Na_V1.7$ in Ins1 cells.

3.2.4 Characterisation of $Na_V1.3$ in Ins1 and HEK cells

Contrary to our initial expectation, $Na_V1.3$ (similar to $Na_V1.7$) also displayed a hyperpolarising shift in inactivation in Ins1 cells compared to HEK cells, as shown in Figure 3.2.4.1A. The average V_h of $Na_V1.3$ currents inactivating with a single component of inactivation in Ins1 cells is -78±6mV (*n*=8). This is significantly more hyperpolarised than the V_h of -48±1mV for $Na_V1.3$ current inactivation in HEK cells (n=7; *P*<0.001, t-test), which invariably inactivated with a single component of inactivation.

$Na_V1.3$ current inactivation in 26/34 Ins1 cells could be best described using a double Boltzmann fit to the data, the average of these cells is shown in Figure 3.2.4.1B and examples of individual cells exhibiting biphasic inactivation is shown Figure 3.2.4.1C. The two components of inactivation had a $V_{0.5}$ of -87±2mV and -55±2 mV, comprising 57±5% and 43±5% of the total current, respectively. It is worth noting that the positive component of biphasic inactivation is very similar to the inactivation of $Na_V1.3$ observed in HEK cells.

Interestingly, amongst the 8/34 cells inactivating with a single component of inactivation, 6/8 cells inactivated at negative voltage with an average V_h of -87±3mV (Figure 3.2.4.1D) and 2/8 cells inactivated at a more positive potentials

with a V_h value of -57 and-53mV (Figure 3.2.4.1E). Remarkably, these voltages coincide exactly with the V_h of $Na_V1.3$ currents inactivating with a biphasic voltage-dependence of inactivation. Indeed the scatter of individual data points (Figure 3.2.4.1F), shows that cells that inactivated with a monophasic inactivation have V_h values that fall distinctly amongst the V_h values of biphasic negative or biphasic positive values and not in between, again suggesting that the same population of Na_V channel α-subunits can inactivate at two distinct membrane potentials separated by ~30mV, giving rise to a biphasic inactivation.

Figure 3.2.4.1F shows the relationship between Na^+ current density and V_h. It is clear that there is no correlation between the current density and V_h of $Na_V1.3$ currents.

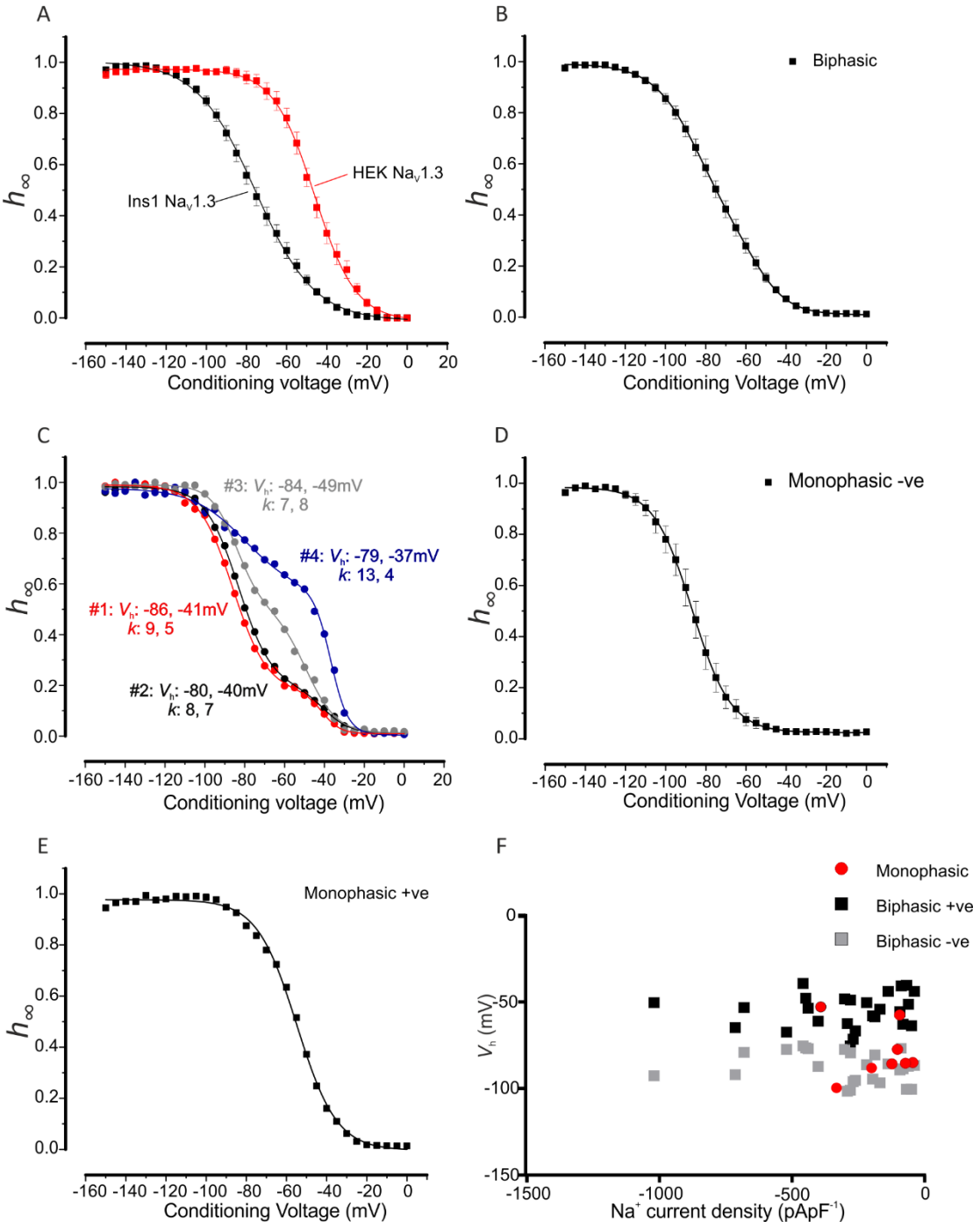


Figure 3.2.4.1 – Voltage-dependence of inactivation of Nav1.3 in Ins1 and HEK cells

A, voltage-dependence of Nav1.3 current inactivation (h_∞) when the α-subunit was co-expressed with β_1- and β_2-subunits in Ins1 (black; n=34) and HEK cells (red; n=7). The curves represent a double and single Boltzmann fit to the data for Nav1.3 currents recorded from Ins1 and HEK cells, respectively. *B*, the average voltage-dependence of inactivation of Nav1.3 current in Ins1 cells that was best described with a double Boltzmann fit to the data (n=26). *C*, examples of biphasic

inactivation curves of $Na_V1.3$ in Ins1 cells with their respective V_h and k values. *D,* same as in *B* but for cells that were best described with a single Boltzmann fit to the data and had a V_h < -70mV (n=6). *E*, same as in *D* but for cells that had a V_h >-70mV (n=2). *F*, relationship between monophasic, biphasic negative (-ve) and biphasic positive (+ve) V_h values and the peak Na^+ current density of $Na_V1.3$ in Ins1 cells.

3.2.5 Biphasic inactivation in primary β-cells

We expressed $Na_V1.3$ in primary mouse β-cells to test whether the hyperpolarised and biphasic inactivation can be extended to primary β-cells. Although the transfection rate was low, large TTX-resistant $Na_V1.3$ currents were observed in 3 β-cells (Figure 3.2.5.1A). The average current amplitude was -1±0.1nA. These currents underwent voltage-dependent inactivation with a V_h of -88mV. However, in two of the three cells, there was biphasic inactivation with a small (43% and 22%) component that inactivated at -95 and -103mV and a larger (57% and 78%) component that inactivated at -73mV in both cells.

It has previously been reported that ablation of *Scn3a* leads to the loss of Na_V current components that inactivates at positive membrane potentials (Zhang et al., 2014). These data have now been reanalysed and expressed as current amplitudes in absolute (in pA) rather than relative (normalized to maximum current) terms. Figure 3.2.5.1B shows Na_V currents recorded in control (*Scn3a*$^{+/-}$) and knockout *Scn3a*$^{-/-}$ β-cells. In agreement with the previous conclusion, ablation of *Scn3a* was associated with the loss of the Na_V current inactivating at positive membrane potentials (Figure 3.2.5.1B, shaded area). However, there was also a large reduction (~200pA) of Na_V current at negative membrane potentials. Figure

3.2.5.1C shows the net $Na_V1.3$ current isolated by subtracting the currents in *Scn3a*$^{-/-}$ from those measured in *Scn3a*$^{+/-}$ mice. The net current shows biphasic inactivation and can be described as the sum of two Boltzmann functions with V_h values of -86mV and -57mV that comprised 76% and 24%, respectively. These values are close to those observed for the isolated $Na_V1.3$ current and similar to the two components of inactivation observed in Ins1 cells expressing $Na_V1.3$ (Table 3.2.9.1).

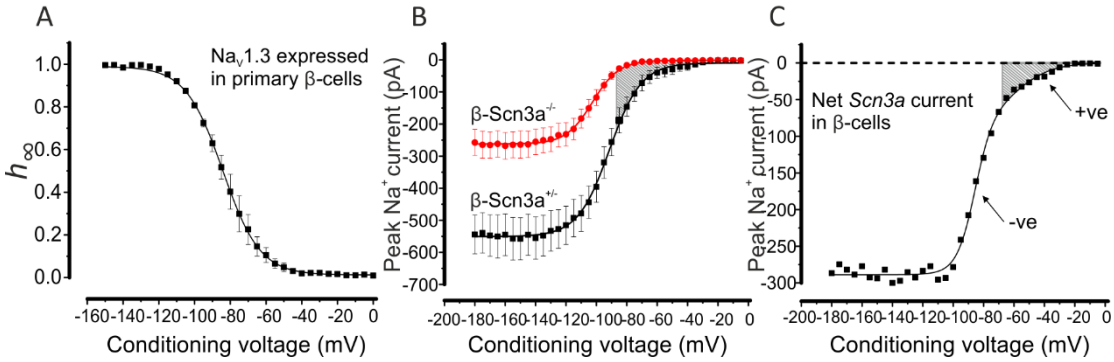


Figure 3.2.5.1- Biphasic inactivation of $Na_V1.3$ in primary mouse β-cells

A, Na^+ current inactivation in primary mouse β-cells co-transfected with $Na_V1.3$ α-subunit and β_1- and β_2-subunit (*n*=3). *B*, voltage-dependence of Na^+ current inactivation in *Scn3a*$^{+/-}$ (n=7) and *Scn3a*$^{-/-}$ β-cells (*n*= 8). Same data as in (Zhang et al., 2014) but current amplitudes are presented in absolute rather than relative terms. C, net $Na_V1.3$ current isolated by subtracting Na_V currents in *Scn3a*$^{-/-}$ β-cells from those in *Scn3a*$^{+/-}$ β-cells. Note biphasic inactivation. A double Boltzmann function was fitted to the data points, yielding V_h values of -86 and -57 mV.

3.2.6 Voltage-dependence of activation of $Na_V1.3$ currents in Ins1 and HEK cells

Families of voltage clamp currents recorded from $Na_V1.3$ expressed in Ins1 and HEK cells, during membrane depolarisations from -150mV to -20, -10 and 0mV

are shown in Figure 3.2.6.1A and B. Despite, the difference in $Na_V1.3$ current inactivation between Ins1 and HEK cells, there was no significant difference in the $V_{0.5}$ between Ins1 cells and HEK cells, -12±1mV (n=31) and -14±1mV (n=5), respectively (Figure 3.2.6.1C). Moreover, the I-V relationships of $Na_V1.3$ were similar except that the Na^+ density was twice as large in Ins1 cells compared to HEK cells (Figure 3.2.6.1D).

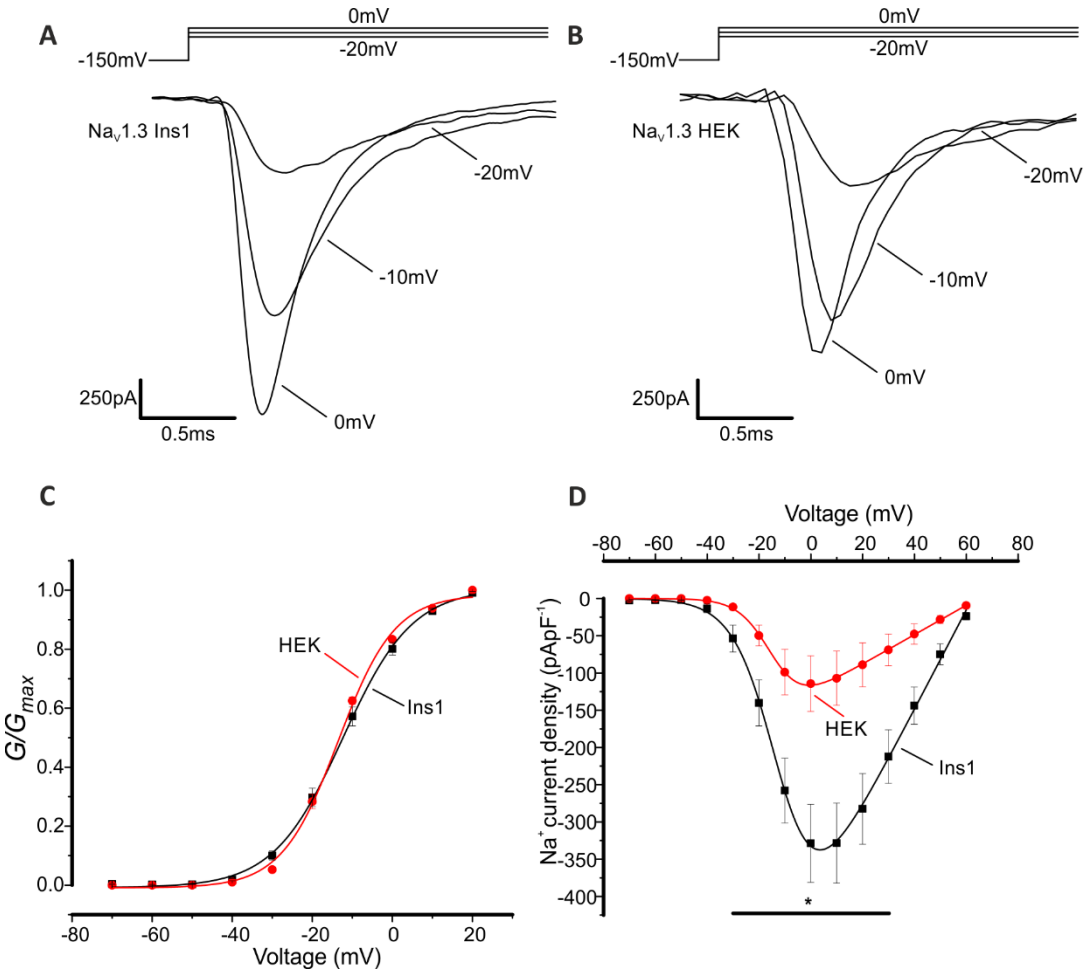


Figure 3.2.6.1- Voltage-dependence of activation of Na$_V$1.3 in Ins1 and HEK cells

A, family of voltage-clamp Na$_V$1.3 currents evoked by depolarisations from a holding potential of -150 to -20, -10 and 0mV when the α-subunit is co-expressed with β_1- and β_2-subunits in Ins1 cells. *B*, same as in *A*, but with Na$_V$1.3 expressed in HEK cells. *C*, voltage-dependence of Na$_V$1.3 current activation (G/G_{max}) in Ins1 (black; n=31) and HEK cells (red; n=5). *D*, I-V relationship of Na$_V$1.3 currents in Ins1 (black; n=31) and HEK cells (red; n=5). *P<0.05, using a one-way-ANOVA.

3.2.7 Characterisation of Na$_V$1.6 in Ins1 and HEK cells

Similar to Na$_V$1.7 and Na$_V$1.3, Na$_V$1.6 inactivated at a more negative potential in Ins1 cells compared to HEK cells, as shown in Figure 3.2.7.1A. The average V_h of Na$_V$1.6 currents inactivating with a single component of inactivation in Ins1 cells

is -73±4mV (n=10). This is significantly more hyperpolarised than the V_h of $Na_V1.6$ in HEK cells, -53±1mV (n=10), which again consistently inactivated with a single component of inactivation.

The majority of $Na_V1.6$ currents in Ins1 cells (25/35 cells) inactivated with two components of inactivation with an average V_h of -86±1mV and -56±1mV, comprising of 56±4% and 44±4% of the total current, respectively (Figure 3.2.7.1B). Examples of cells that exhibited biphasic voltage-dependence of inactivation are shown in Figure 3.2.7.1C. Ins1 cells inactivating with a single component of inactivation could again be divided into two groups: those inactivating at a more negative potential (<-70 mV) had an average V_h of -83±2mV (n=5), and those inactivating at a more positive potential (> -70 mV), which had an average V_h of -63±2mV (n=5), as shown in Figure 3.2.7.1D and E, respectively.

Figure 3.2.4.1F shows the relationship between Na^+ current density and V_h of $Na_V1.6$ currents in Ins1 cells. It is clear that there is no correlation between the Na^+ current density and V_h of $Na_V1.6$ currents. The scatter of individual data points indicate that cells that inactivated with a monophasic inactivation have V_h values that fall distinctly amongst the V_h values of biphasic negative or biphasic positive values.

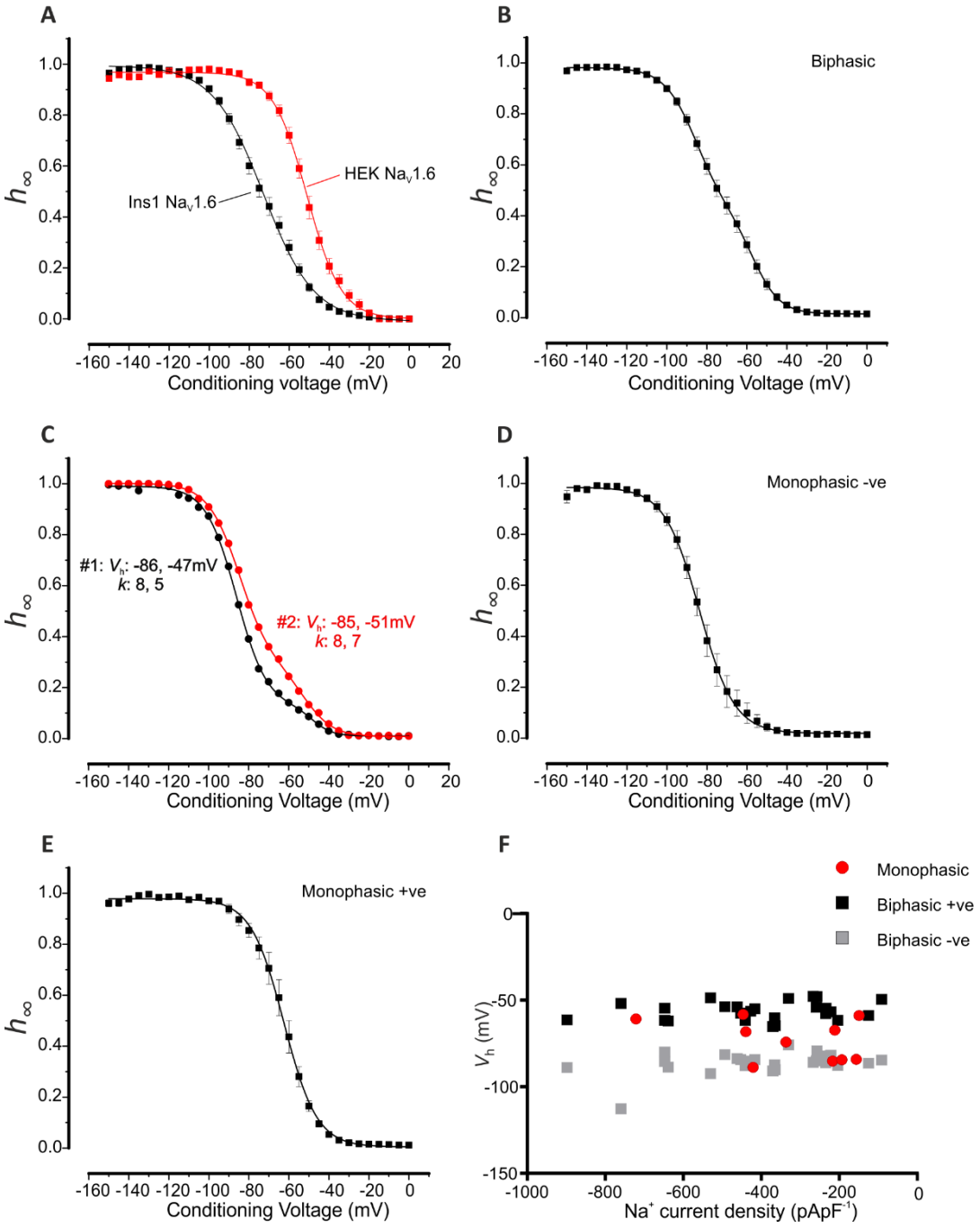


Figure 3.2.7.1- Voltage-dependence of inactivation of Nav1.6 currents in Ins1 and HEK cells

A, voltage-dependence of Nav1.6 current inactivation (h_∞) when the α-subunit was co-expressed with β_1- and β_2-subunits in Ins1 (black; *n*=35) and HEK cells (red; *n*=10). The curves represent a double and single Boltzmann fit to the data for Nav1.6 currents recorded from Ins1 and HEK cells, respectively. *B*, the average voltage-dependence of inactivation of Nav1.6 current in Ins1 cells that was best described with a double Boltzmann fit to the data (*n*=25). *C*, examples of biphasic inactivation curves of Nav1.6 in Ins1 cells with their respective V_h and *k* values. *D*, same as in *B* but

for cells that were best described with a single Boltzmann fit to the data and had a V_h <-70mV (n=5). *E*, same as in *D* but for cells that had a V_h >-70mV (n=5). *F*, relationship between monophasic, biphasic negative (-ve) and biphasic positive (+ve) V_h values and the peak Na^+ current density of $Na_V1.6$ in Ins1 cells.

Voltage-clamp current traces for $Na_V1.6$ in Ins1 cells and HEK cells are shown in Figure 3.2.7.2A and B, respectively. Unlike $Na_V1.7$ and $Na_V1.3$, which showed a similar voltage-dependence of activation in Ins1 and HEK cells, the activation of $Na_V1.6$ is significantly different between Ins1 and HEK cells (Figure 3.2.7.2C). The $V_{0.5}$ of $Na_V1.6$ is -16$\pm$1mV (n=18) and -5$\pm$2mV (n=9) in Ins1 cells and HEK cells, respectively. Furthermore, the I-V relationship of $Na_V1.6$ between Ins1 and HEK cells is also different, as the Na^+ current density peaked at 0 and 10 mV, respectively (Figure 3.2.7.2D). The current density is also significantly lower in HEK than in Ins1 cells.

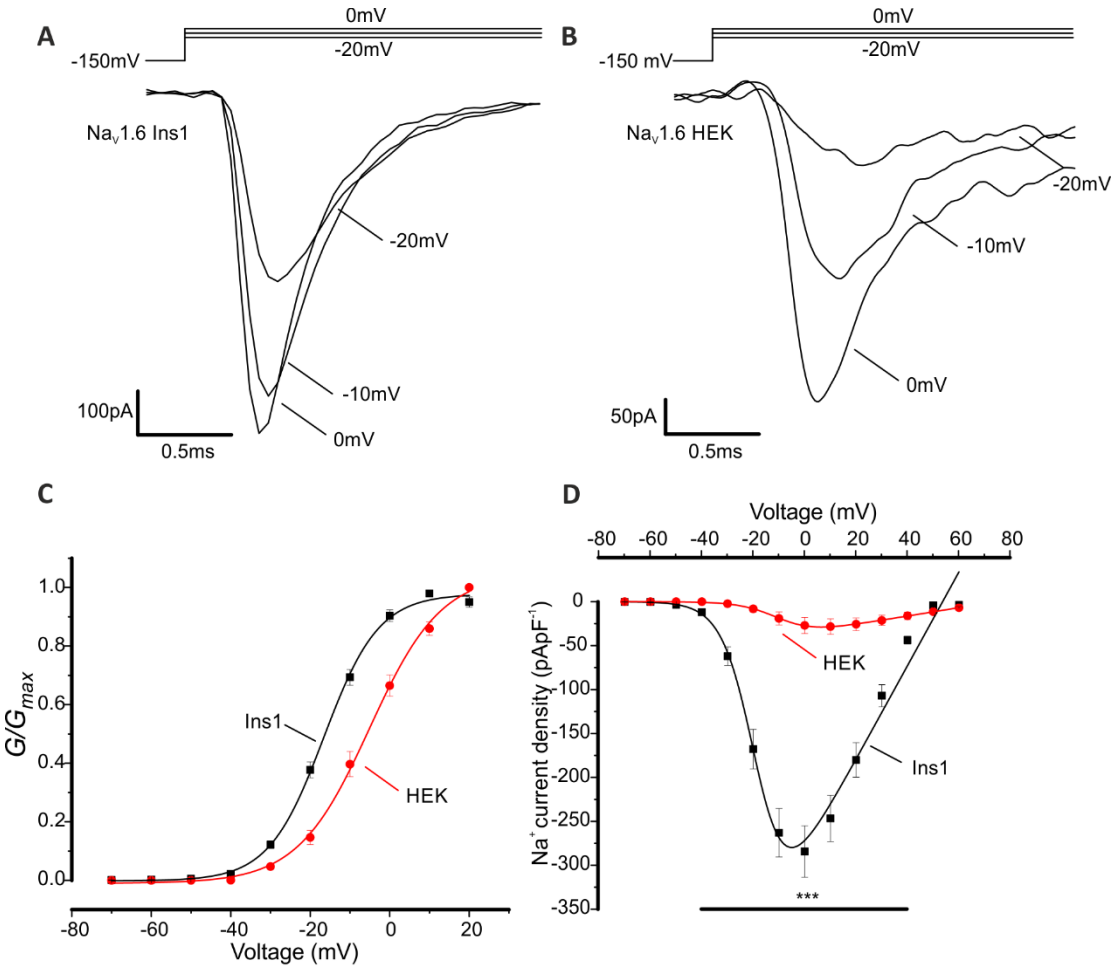


Figure 3.2.7.2- Voltage-dependence of activation of Na$_V$1.6 currents in Ins1 and HEK cells

A, family of voltage-clamp Na$_V$1.6 currents evoked by depolarisations from a holding potential of -150 to -20, -10 and 0mV when the α-subunit is co-expressed with β_1- and β_2-subunits in Ins1 cells. *B*, same as in *A*, but with Na$_V$1.6 expressed in HEK cells. *C*, voltage-dependence of Na$_V$1.6 current activation (G/G_{max}) in Ins1 (black; n=18) and HEK cells (red; n=10). *D*, I-V relationship of Na$_V$1.6 currents in Ins1 (black; n=18) and HEK cells (red; n=9). ***P<0.001, one way ANOVA for Na^+ current density at -40mV to 40mV between Ins1 and HEK cells.

3.2.8 Characterisation of Na$_V$1.5 in Ins1 and HEK cells

To investigate whether other Na$_V$ channels that are not normally expressed in β-cells, also display hyperpolarised inactivation in β-cells compared to

non-β-cells, the activation and inactivation properties of the cardiac Na_V channel, $Na_V1.5$, was assessed in Ins1 and HEK cells. Families of voltage-clamp current traces for $Na_V1.5$ in Ins1 cells and HEK cells are shown in Figure 3.2.8.1A and B, respectively. As observed for the other channels, $Na_V1.5$ currents inactivate at a significantly more negative V_h in Ins1 cells compared to HEK cells, -99±2mV (n=9) and -77±1 mV (n=10), respectively (P<0.001, t-test). Inactivation of $Na_V1.5$ currents in Ins1 cells was invariably monophasic. The significant difference in inactivation between the two cell types is observed with no significant difference in the $V_{0.5}$ of $Na_V1.5$ currents between Ins1 and HEK cells, -34±2mV (n=4) and -35±1mV (n=6), respectively. The I-V relationship of $Na_V1.5$ is similar between the two cell types, with peak current density at 0mV (data not shown).

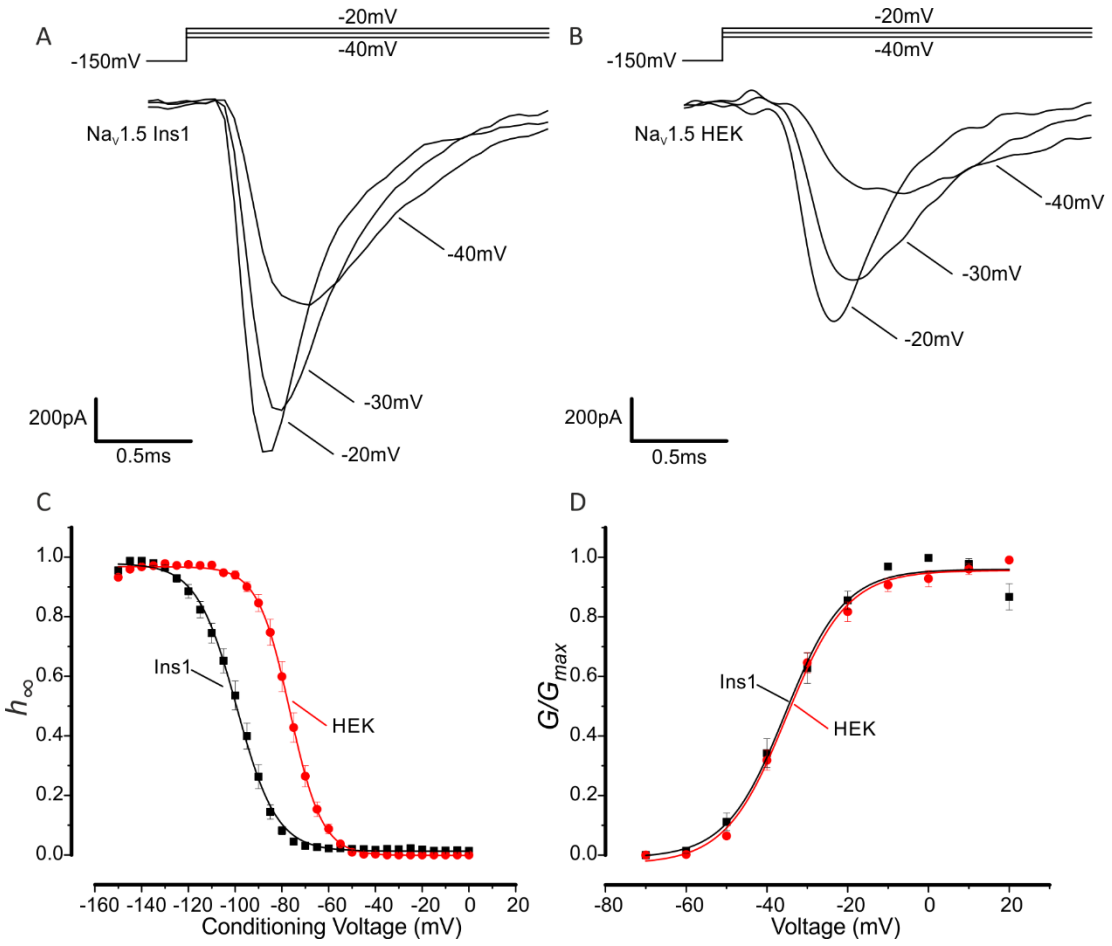


Figure 3.2.8.1- Voltage-dependence of activation and inactivation of Na$_V$1.5 currents in Ins1 and HEK cells

A, family of voltage-clamp Na$_V$1.5 currents evoked by depolarisations from a holding potential of -150 to -20, -10 and 0mV when the α-subunit is co-expressed with β_1- and β_2-subunits in Ins1 cells. *B*, same as in *A*, but with Na$_V$1.5 expressed in HEK cells. *C*, voltage-dependence of Na$_V$1.5 current inactivation (h_∞) in Ins1 and HEK cells. The curves represents a single Boltzmann fit to the data in Ins1 cells (black; n= 9) and HEK cells (red; n=10). *D*, voltage-dependence of Na$_V$1.5 current activation (G/G_{max}) in Ins1 (black; n=4) and HEK cells (red; n=6).

3.2.9 Summary of $Na_V1.7$, $Na_V1.3$ and $Na_V1.6$ activation and inactivation properties in Ins1 and HEK cells

Figure 3.2.9.1 and Supplementary Table 1 and 2 summarise the voltage-dependence of $Na_V1.7$, $Na_V1.3$ and $Na_V1.6$ current activation and inactivation in Ins1 and HEK cells. Despite the unexpected hyperpolarising shift in inactivation exhibited by $Na_V1.3$ and $Na_V1.6$ expressed in Ins1 cells compared to HEK cells, $Na_V1.7$ still inactivated more negatively than both other channels (Figure 3.2.9.1A), in good agreement with studies in KO mice (Zhang et al., 2014). The average V_h and slope factor, k, of $Na_V1.7$, $Na_V1.3$ and $Na_V1.6$ current inactivation in Ins1 and HEK cells are summarised in Table 3.2.9.1. Similar to Ins1 cells, there is also a significant difference in the V_h between the three Na_V channel α-subunits recorded in HEK cells ($P < 0.001$, one way ANOVA) and again the inactivation curve of $Na_V1.7$ was shifted in a hyperpolarising direction compared to $Na_V1.3$ and $Na_V1.6$ in HEK cells, as shown in Figure 3.2.9.1B. However, unlike Ins1 cells, all of the channels expressed in HEK cells still inactivate at physiologically relevant membrane potentials (Table 3.2.9.1).

Unexpectedly, all of the α-subunits (with the exception of $Na_V1.5$) expressed in Ins1 cells exhibited a biphasic inactivation (i.e. a V_h at positive and negative membrane potentials ranging between -55 to -67mV and -86 to -97mV, respectively). The frequency of cells inactivating with a biphasic inactivation was significantly higher when the cells expressed $Na_V1.3$ (26/34) and $Na_V1.6$ (25/34) compared to $Na_V1.7$ (9/47) (P<0.001; chi-squared test).

The voltage-dependence of activation of $Na_V1.7$, $Na_V1.3$ and $Na_V1.6$ currents in Ins1 is shown in Figure 3.2.9.1C and $V_{0.5}$ and k values are summarised in Table

3.2.9.2. All three Na_V channels displayed a similar voltage-dependence of activation in Ins1 cells, with no significant difference between the $V_{0.5}$ (P=0.157, one way ANOVA) or k (p = 0.167, one way ANOVA). However, there is a significant difference between the $V_{0.5}$ of $Na_V1.7$, $Na_V1.3$ and $Na_V1.6$ currents in HEK cells (P<0.001, one way ANOVA on ranks), as activation of $Na_V1.6$ is shifted to a more depolarised membrane potential. There is also a significant difference in the voltage-dependence of activation slope factor, k, between the three Na_V channels expressed in HEK cells (P < 0.05, one way ANOVA).

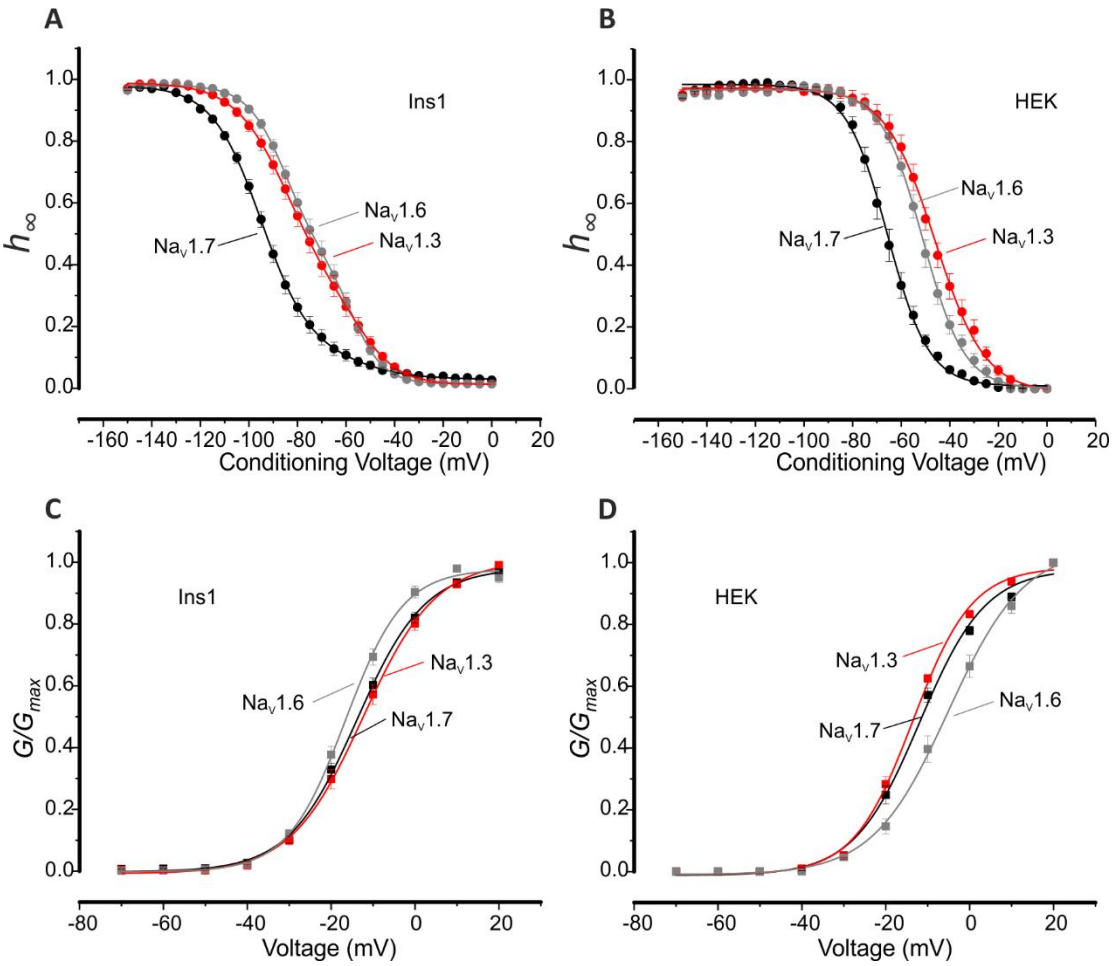


Figure 3.2.9.1- Summary of $Na_V1.7$, $Na_V1.3$ and $Na_V1.6$ Voltage-dependence of inactivation and activation in Ins1 and HEK cells

A, voltage-dependence of $Na_V1.7$ (same data as in Figure 3.2.3.3), $Na_V1.3$ (same data as in Figure 3.2.4.1) and $Na_V1.6$ (same data as in Figure 3.2.7.1) current inactivation (h_∞) in Ins1 cells. *B*, same as in *A* but for HEK cells. *C*, voltage-dependence of activation of $Na_V1.7$ (same data as in Figure 3.2.3.2), $Na_V1.3$ (same data as in Figure 3.2.6.1) and $Na_V1.6$ (same data as in Figure 3.2.7.2) in Ins1 cells. *D*, same as in *C* but for HEK cells.

Na_V current	**Monophasic V_h (mV)**	***K***	**Biphasic V_h-1 (mV)**	***k1***	**Biphasic V_h-2 (mV)**	***k2***
Ins1 $Na_V1.3$	-79±6 (8)	9±1 (8)	-87±2 (26)	9±1 (26)	-55±2 (26)	7±1 (26)
Ins1 $Na_V1.5$	-99±2 (9)	8±1 (9)	N/A	N/A	N/A	N/A
Ins1 $Na_V1.6$	-73±4 (10)	8±1 (10)	-86±1 (25)	8±1 (25)	-56±1 (25)	6±1 (25)
Ins1 $Na_V1.7$	-94±2 (38)	9±1 (38)	-97±4 (9)	8±1 (9)	-67±4 (9)	10±2 (9)
HEK $Na_V1.3$	-48±1 (7)	10±2 (7)	N/A	N/A	N/A	N/A
HEK $Na_V1.5$	-77±1 (10)	6±1 (10)	N/A	N/A	N/A	N/A
HEK $Na_V1.6$	-53±1 (10)	7±1 (10)	N/A	N/A	N/A	N/A
HEK $Na_V1.7$	-66±2 (9)	8±1 (9)	N/A	N/A	N/A	N/A

Table 3.2.9.1 – V_h values of $Na_V1.3$, $Na_V1.5$, $Na_V1.6$ and $Na_V1.7$ in Ins1 and HEK cells

Cells are divided between those that exhibited Na_V current inactivation that were best described using a single Boltzmann function (monophasic) and those that were best described using a double Boltzmann function (biphasic) (AIC test). Values represent mean values ±SEM of indicated number of cells (*n*). V_h represents membrane potential at which inactivation is half-maximal in cells with monophasic inactivation and *k* represents the slope factor. In cells with biphasic inactivation, V_h-1 and V_h-2 represent the membrane potential at which inactivation is half-maximal for the current components inactivating at negative and positive membrane potentials, respectively. *k1* and *k2,* represent the respective slope factors for the currents inactivating with V_h-1 and V_h-2.

α-subunit + $\beta_1\beta_2$	$V_{0.5}$ (mV)	K
Ins1 $Na_V1.3$	-12±1 (31)	8±1 (31)
Ins1 $Na_V1.5$	-35±2 (4)	8±1 (4)
Ins1 $Na_V1.6$	-16±1 (18)	7±1 (18)
Ins1 $Na_V1.7$	-13±1 (39)	8±1(39)
HEK $Na_V1.3$	-14±1 (5)	7±1 (5)
HEK $Na_V1.5$	-35±1 (6)	8±1 (6)
HEK $Na_V1.6$	-5±2 (9)	9±1 (9)
HEK $Na_V1.7$	-12±1 (8)	8±1 (8)

Table 3.2.9.2 - Activation values of $Na_V1.3$, $Na_V1.5$, $Na_V1.6$ and $Na_V1.7$ in Ins1 and HEK cells

Values represent MEAN ± SEM (*n*).

3.2.10 Characterisation of $Na_V1.7$, $Na_V1.3$ and $Na_V1.6$ in human EndoC-βh2 cell line

As previously summarised, the voltage-dependence of Na_V channel inactivation can vary dramatically depending on the β-cell species. Thus far, the literature suggests that negative inactivation of Na_V currents is limited to rodent β-cells (Gopel et al., 1999, Plant, 1988, Lou et al., 2003, Hiriart and Matteson, 1988). Na_V currents in human β-cells inactivate at a V_h of ~-40 mV (Barnett et al., 1995, Braun et al., 2008). However, recent characterisation of Na_V inactivation in human β-cells revealed that some (4/9) cells display a biphasic inactivation with a component that inactivates at a hyperpolarised potential of approximately -105mV (Zhang et al., 2014). Thus, human β-cell Na_V currents can also inactivate at a hyperpolarised membrane potential and can exhibit biphasic inactivation. In order to investigate the species differences of Na_V current inactivation, $Na_V1.7$, $Na_V1.3$ and $Na_V1.6$ channels were co-expressed with β_1- and β_2-subunits in a human β-cell-line,

EndoC-βh2, and current inactivation was characterised, as shown in Figure 3.2.10.1.

All three Na_V current inactivation curves exhibited a significant depolarising shift when expressed in EndoC-βh2 cells compared to their inactivation in Ins1 cells (Figure 3.2.10.1A-C and Supplemetary Table 1). All three Na_V currents expressed in EndoC-βh2 cells inactivated with a single component of inactivation with an average V_h of $Na_V1.7$, $Na_V1.3$ and $Na_V1.6$ is -71±1mV (*n*=10), -61 ± 1 (n=10) and -56±2mV (n=9). The shift in inactivation of $Na_V1.7$ and $Na_V1.6$ currents between the Ins1 and EndoC-βh2 cell is similar to the shift in V_h between Ins1 and HEK cells. Although $Na_V1.3$ currents also produced a depolarising shift in inactivation between Ins1 and EndoC-βh2 cells, the shift in V_h was less than that observed for $Na_V1.6$ and $Na_V1.7$ (Supplementary Table 1). This reflects different modulation of Na_V channel α-subunits in EndoC-βh2 compared to HEK cells.

The average slope factor, *k*, of $Na_V1.7$, $Na_V1.3$ and $Na_V1.6$ is 6±1, 6±1 and 7±1, respectively. Interestingly, the inactivation slopes for Na_V currents were steeper when expressed in EndoC-βh2 cells compared to Ins1 cells (Supplementary Table 1), suggesting a greater sensitivity to the voltage-dependence of inactivation.

A comparison of $Na_V1.7$, $Na_V1.3$ and $Na_V1.6$ reveals a significant difference between the V_h values of the α-subunits expressed in EndoC-βh2 cells (Figure 3.2.10.1D; $P<0.001$, one way ANOVA). However, all three α-subunits have a V_h value that falls within a physiological range. Similar to Ins1 and HEK cells, $Na_V1.7$ expressed in EndoC-βh2 cells inactivated at the most hyperpolarised potential. Meanwhile, $Na_V1.6$ inactivated at the most depolarised membrane potential, which is perhaps not surprising given that it is the predominant α-subunit

expressed in human β-cells (Nica et al., 2013, Braun et al., 2008), which contain Na_V currents that inactivate at approximately -40mV. Taken together these results suggest that the hyperpolarised and biphasic voltage-dependence of inactivation of Na_V currents is specific to rodent β-cells.

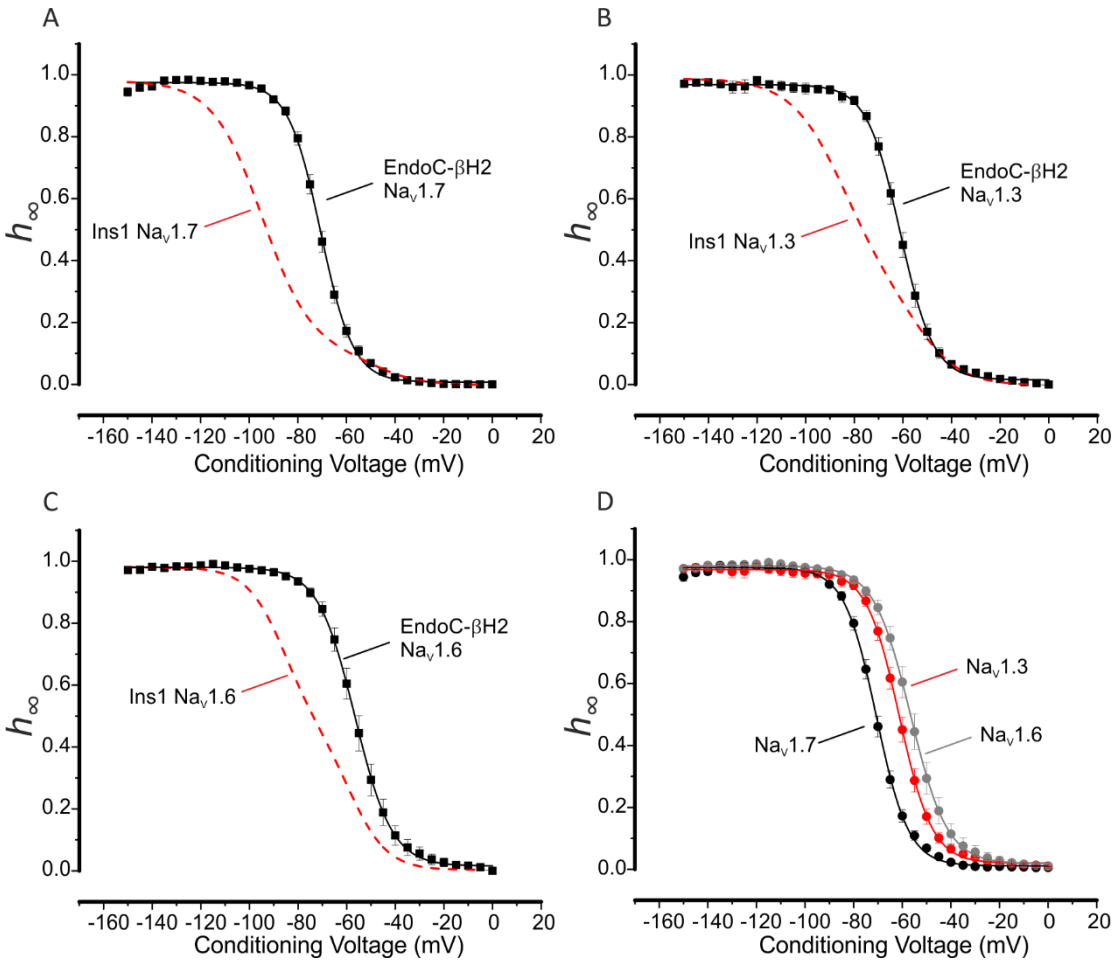


Figure 3.2.10.1- Characterisation of $Na_V1.7$, $Na_V1.3$ and $Na_V1.6$ in EndoC-βh2 cells

A, voltage-dependence of inactivation (h_∞) of $Na_V1.7$ co-expressed with β_1- and β_2-subunit in EndoC-βh2 cells (black; *n*=10). The curve represents a single Boltzmann fit to the data. Dashed red curve represents inactivation of $Na_V1.7$ co-expressed with β_1- and β_2-subunits in Ins1 cells for comparison (same data as in Figure 3.2.3.3). *B*, same as in *A* but for $Na_V1.3$ (black, *n*=10; dashed red curve same data as in Figure 3.2.4.1). *C*, same as in *A* but for $Na_V1.6$ (black, *n*=9; dashed red curve same data as in Figure 3.2.7.1). *D*, voltage-dependence of inactivation of $Na_V1.7$, $Na_V1.3$ and $Na_V1.6$ in EndoC-βh2 cells (same data as in Figure 3.2.10.1A, B and C to facilitate comparison between α-subunits expressed in EndoC-βh2 cells).

3.2.11 Characterisation of $Na_V1.7$, $Na_V1.3$ and $Na_V1.6$ in rodent non-β-cell lines

Given the apparent species difference associated with Na_V channel inactivation, it was important to determine whether the depolarised and monophasic inactivation observed in HEK cells, is not due to the variation in species, but rather the difference in cell-type. In order to assess this the inactivation properties of $Na_V1.3$ and $Na_V1.7$ were characterised in non-β-cells of rodent origin. The two cell lines are a Chinese Hamster Ovary (CHO) cell line and a mouse glucagon-secreting α-cell line, called αTC1-6 cells. Inactivation properties of both $Na_V1.3$ and $Na_V1.7$ expressed in CHO cells were similar to that observed in HEK cells and inactivated at significantly more depolarised membrane potentials compared to Ins1 cells (Figure 3.2.11.1, Table 3.2.11.1 and Supplementary Table 1). In the glucagon-secreting cell line αTC1-6, inactivation of both $Na_V1.3$ and $Na_V1.7$ was more similar to that found in HEK and CHO cells than in the insulin-secreting cells (Figure 3.2.11.1 and Table 3.2.11.1).

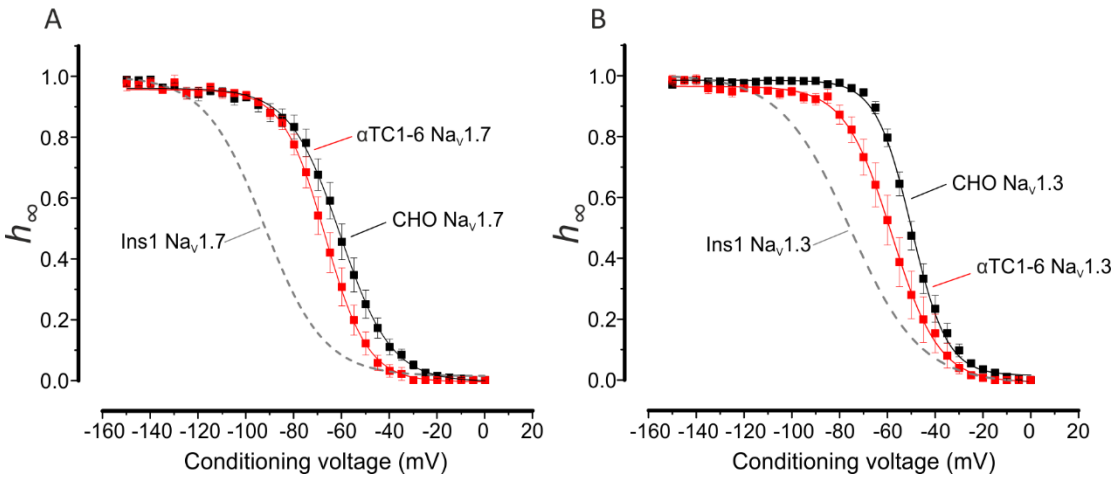


Figure 3.2.11.1 – Characterisation of $Na_v1.7$ and $Na_v1.3$ in αTC1-6 and CHO cells

A, voltage-dependence of inactivation of Nav1.7 currents when the α-subunit is co-expressed with β_1- and β_2- subunits in αTC1-6 (red; n=10) and CHO (black; n=10) cells. The curve represents a single Boltzmann fit to the data and the grey dashed line represents the inactivation of Nav1.7 expressed in Ins1 cells (same as in Figure 3.2.3.3). *B*, same as in *A*, but experiments were conducted with Nav1.3 in αTC1-6 (red; n=10), CHO (black; n=13) and Ins1 cells (grey dashed line; same as in Figure 3.2.4.1).

Cell type	**Nav1.7 V_h (mV)**	***k***	**Nav1.3 V_h (mV)**	***K***
CHO	-61 ± 3 (10)	9 ± 1 (10)	-50 ± 2 (13)	7 ± 0.4 (13)
αTC1-6	-68 ± 3 (10)	7 ± 1 (10)	-59 ± 4 (9)	6 ± 0.5 (9)

Table 3.2.11.1- V_h and k values of Na_v channel inactivation in CHO and αTC1-6 cells

The V_h and *k* values of Nav α-subunits co-expressed with β_1- and β_2-subunits. Values represent mean ± SEM of indicated number of cells (*n*).

3.3 Discussion

To explore the obscure voltage-dependence of inactivation and to understand the contribution of Na_V channel α-subunits, it was important to characterise the current properties of individual α-subunits expressed in β-cells. To this end, TTX-resistant versions of $Na_V1.7$, $Na_V1.3$ and $Na_V1.6$ were generated. Addition of TTX blocked endogenous currents and thus allowed the isolation of expressed TTX-resistant Na_V channels.

3.3.1 Na_V channels inactivate at more negative membrane potentials in Ins1 cells

Ablation of *Scn9a* and *Scn3a* and subsequent characterisation of Na_V currents in β-cells suggested that whilst $Na_V1.3$ inactivates at physiologically relevant membrane potentials in β-cells, similar to other cell types, $Na_V1.7$ is modulated in a β-cell specific manner and inactivates at a more hyperpolarised membrane potentials compared to other cell types (Zhang et al., 2014). However, contrary to expectation, all of the Na_V channel α-subunits expressed in β-cells ($Na_V1.7$, $Na_V1.3$ and $Na_V1.6$) inactivated at a significantly more hyperpolarised potential in Ins1 cells compared to HEK cells. Indeed, an early indication that $Na_V1.7$ is not the only α-subunit that inactivates at hyperpolarised membrane potentials was shown when endogenous Na_V currents in Ins1 cells exhibited a hyperpolarised inactivation without endogenous expression of $Na_V1.7$.

All α-subunits exhibited a 20-30mV hyperpolarising shift in their inactivation between Ins1 and HEK cells, without a significant change in their voltage-dependence of activation. $Na_V1.6$ was an exception and displayed a

significant difference in $V_{0.5}$ between Ins1 and HEK cells. However the 11mV hyperpolarising shift in the $V_{0.5}$ is much smaller than the ~30mV hyperpolarising shift in the V_h of Na$_V$1.6 between Ins1 cells and HEK cells. Interestingly, the Na$_V$ channel α-subunit, Na$_V$1.5, which is not expressed in β-cells and is amongst the α-subunits that share the least homology with Na$_V$1.7 (Table 1.3.1.1) also exhibited a ~22mV hyperpolarising shift in the voltage-dependence of inactivation between Ins1 and HEK cells with no significant difference in the voltage-dependence of activation. This therefore suggests that the hyperpolarised inactivation of Na$_V$ channels is mainly due to modulation by the β-cell environment rather than to sequence variation between α-subunits.

3.3.2 Individual Na$_V$ subtypes exhibit two distinct inactivation behaviours

The biphasic inactivation of Na$_V$ currents in primary rodent β-cells was previously postulated to reflect the expression and different inactivation of Na$_V$ channel α-subunits in β-cells (Vignali et al., 2006, Zhang et al., 2014). However biphasic inactivation of Na$_V$ currents that represent a single type of α-subunit (Na$_V$1.7, Na$_V$1.3 and Na$_V$1.6 expressed individually) also inactivates at both depolarised and hyperpolarised membrane potentials. Interestingly, the depolarised V_h values recorded from Ins1 cells were very similar to that recorded from HEK cells. In Ins1 cells biphasic inactivation of Na$_V$1.7 was significantly less frequent (19%) than found for Na$_V$1.3 (76%) and Na$_V$1.6 (71%), which in addition to it consistently inactivating at significantly more hyperpolarised potentials compared to Na$_V$1.3 and Na$_V$1.6 in all cell types could be the reason why Na$_V$1.7 is the less physiologically relevant α-subunit in β-cells (Zhang et al., 2014).

The biphasic inactivation of individual Na_V α-subunits can be extended to primary rodent β-cells. Net $Na_V1.3$ current from primary β-cells calculated by subtracting the Na_V currents recorded from *Scn3a*$^{+/-}$ and *Scn3a*$^{-/-}$ β-cells likewise revealed a biphasic voltage-dependence of inactivation. Thus, it appears that although different α-subunits can contribute to the biphasic inactivation of Na_V currents, an additional cell-specific modulation occurs whereby individual α-subunits exhibit two distinct voltage-dependences of inactivation.

Biphasic inactivation of $Na_V1.6$ has previously been reported in TsA201 cells, a human embryonic kidney cell line, (Shirahata et al., 2006). The biphasic inactivation was attributed to large persistent currents that became undetectable upon co-expression of ankyrin-G, a member of the ankyrin family of adaptor proteins that facilitate the attachment of integral membrane proteins to the cytoskeleton. However, $Na_V1.7$, $Na_V1.3$ and $Na_V1.6$ did not exhibit persistent currents in Ins1 cells, as shown by families of voltage clamp current traces. Moreover, ankyrin-G, which abolished the persistent current of $Na_V1.6$, is expressed in pancreatic islet cells (Komada and Soriano, 2002). It is therefore unlikely that the biphasic inactivation is due to persistent Na_V currents in Ins1 cells.

It is also unlikely that the biphasic inactivation of Na_V currents observed in Ins1 cells reflects the saturation of a limited pool of a specific factor that modulates the Na_V channels to inactivate negatively because the current density of $Na_V1.7$, $Na_V1.3$ and $Na_V1.6$, had no bearing on the V_h or the monophasic/biphasic inactivation of the current.

A plausible explanation for the biphasic inactivation of Na_V currents in β-cells is that the multiple β-subunits expressed in Ins1 cells, including the transfected β_1- and β_2-subunits and the endogenous β_3-subunit, can modulate inactivation of Na_V α-subunits differentially. Therefore, it is possible that the formation of different heterodimers, and the subsequent variation of channel gating between different heterodimers causes biphasic inactivation of Na_V currents in β-cells. This possibility will be explored in Chapter 4.

3.3.3 Species- and cell-specific regulation of Na_V channels

We investigated whether the hyperpolarised and biphasic inactivation of Na_V currents in rodent β-cells can be extended to human β-cells by characterising the inactivation properties of $Na_V1.7$, $Na_V1.3$ and $Na_V1.6$ expressed in a human β-cell line EndoC-βh2 cells. All three α-subunits displayed a monophasic inactivation over physiologically relevant membrane potentials in the EndoC-βh2 cell and exhibited a depolarising shift compared to their inactivation in Ins1 cells, suggesting that the hyperpolarised and biphasic inactivation of Na_V currents is specific to rodent β-cells.

It was ascertained that the hyperpolarised inactivation in the Ins1 cell (rat) compared to the HEK cell (human) is not due to the species difference between the two cell types. This is because the difference in the V_h of $Na_V1.3$ and $Na_V1.7$ was present between Ins1 cells and non-β-cells of rodent origin: CHO cells (hamster) and αTC1-6 cells (mouse). Na_V currents in CHO and glucagon-secreting αTC1-6 cells did not exhibit biphasic inactivation, suggesting that this is also specific to rodent β-cells. Indeed, the appearance of biphasic Na_V current

inactivation has been described upon conversion of mouse α-cells to β-cells (Chakravarthy et al., 2017).

Characterisation of Na_V currents from αTC1-6 cells, also revealed important information on the properties of Na_V currents in α-cells. Unlike β-cells, the importance of Na_V channels in the regulation of glucagon secretion has been recognised in both human and mouse α-cells (Zhang et al., 2013, MacDonald et al., 2007). In both species, α-cells evoke large inward Na^+ currents in response to a depolarisation from a physiological membrane potential (Ramracheya et al., 2010, Barg et al., 2000). Na_V current is crucial to stimulation of glucagon secretion at low glucose and inhibition of the current by TTX (and high glucose concentrations) significantly reduces glucagon secretion (Zhang et al., 2013, Ramracheya et al., 2010, MacDonald et al., 2007). In both species, α-cells have shown to inactivate within the normal physiological range, with a V_h of approximately -45mV (Ramracheya et al., 2010, Zhang et al., 2013, Gopel et al., 2000, Barg et al., 2000).

However characterisation of Na_V current from primary mouse α-cells has previously shown both hyperpolarised inactivation (-106 mv) and biphasic inactivation of the current (Vignali et al., 2006, Zhang et al., 2014). In the paper by Zhang et al., all α-cells displayed a biphasic inactivation. The more negative component had a V_h of −84±5mV and accounted for only 26±3% of the total Na^+ current. Meanwhile, the principal component, comprising of 74±3% of the total current had a V_h of −47±1mV (Zhang et al., 2014). Genetic ablation of *Scn3a* and *Scn9a*, resulted in a single component of inactivation, with an average V_h of -94±7mV and a V_h of ∼-35mV, respectively. This would suggest that $Na_V1.7$

inactivates at a hyperpolarised membrane potential in α-cells, whilst $Na_V1.3$ inactivates at a depolarised membrane potential. It was reasoned that because $Na_V1.3$ is the predominant Na_V channel expressed in α-cells (ablation of *Scn3a* reduced the Na^+ current density by 80%), Na_V currents are able to contribute to the regulation of glucagon secretion, despite expressing $Na_V1.7$, which inactivates negatively.

Contrary to the data by Zhang et al. the results from this chapter demonstrate that $Na_V1.7$ inactivates at a depolarised potential (-68 mV), which is significantly depolarised compared to its inactivation in Ins1 cells. However, the results support previous findings that Na_V currents inactivate with a single component of inactivation, within a physiological range (Ramracheya et al., 2010, Zhang et al., 2013, Gopel et al., 2000, Barg et al., 2000), which is not surprising given the importance of Na_V currents to the regulation of glucagon secretion (Zhang et al., 2013, MacDonald et al., 2007, Ramracheya et al., 2010).

3.2.4 Biphasic and hyperpolarised inactivation of Na_V currents in Ins1 cells

In this chapter we investigated the contribution of different Na_V channel α-subunits to the hyperpolarised inactivation of Na_V currents in Ins1 cells compared to other cell types. We have identified that all Na_V channels expressed in β-cells can exhibit two distinct inactivation behaviours at positive and negative membrane potentials. The hyperpolarised and biphasic inactivation in Ins1 cells was specific to rodent β-cells, as these characteristic features were not observed in EndoC-βh2, HEK, CHO or αTC1-6 cells. However, in order to further investigate the regulation of Na_V channels it important to understand the contribution of Na_V

channel β-subunits to the hyperpolarised and biphasic inactivation of Na_V currents.

Chapter 4

Contribution of Na_V channel β-subunits to the biphasic inactivation of Na_V currents in rodent β-cells.

4.1 Introduction

Na_V channel β-subunits were the first auxiliary proteins identified to modulate the voltage-dependence of Na_V current activation and inactivation (Isom et al., 1992, Kruger and Isom, 2016). Co-expression of Na_V channel α-subunit with the β_1-subunit was sufficient to shift the voltage-dependence of inactivation by ~20mV in a hyperpolarising direction compared to α-subunits expressed alone (Isom et al., 1992, Patton et al., 1994).

β-subunits are endogenously expressed in primary rodent β-cells (Adriaenssens et al., 2016, DiGruccio et al., 2016, Benner et al., 2014). However, their contribution to the hyperpolarised inactivation of Na_V currents has received much less attention compared to the pore-forming α-subunits. This is in part due to data in which ablation of *Scn3a* resulted in the remaining Na^+ current (representing $Na_V1.7$) inactivating at a V_h of ~-100mV in both α- and β-cells, despite predominant expression of β_3- and β_1-subunits, respectively (Zhang et al., 2014). Moreover, the hyperpolarised inactivation presented by all Na_V channel α-subunits in Ins1 cells in Chapter 3, despite co-expression with β_1- and β_2-subunits (the β-subunits expressed in DRG neurones (Black et al., 1996)) also militates against the idea that β-subunits have a role in the inactivation behaviour of Na_V channels in β-cells.

However, this reasoning does not take into consideration that modulation of Na_V currents by β-subunits may critically depend on the cell type and/or experimental system in which they are expressed (Meadows and Isom, 2005, Moran et al., 2000, Isom et al., 1992). Cell-specific variation can arise because β-subunits are cell-adhesion molecules (CAMs), which can interact with other CAMs, the

extracellular matrix and the cytoskeleton (Isom, 2002, Malhotra et al., 2000, Wood and Slater, 1998); as such, they can recruit various signalling proteins to the Na_V channel complex that can alter channel behaviour, (Kruger and Isom, 2016, Malhotra et al., 2000). With different cell types, the presence of partner proteins vary and naturally the influence of the β-subunit on Na_V current behaviour also varies (Komada and Soriano, 2002). In addition, mature β-subunits contain three to four *N*-linked glycosylation sites (McCormick et al., 1998, Isom et al., 1992) and the negative charge of sialic acid residues at these sites can affect Na_V current gating properties (Johnson et al., 2004, Johnson and Bennett, 2006). As glycosylation varies during the course of development and among cell types, it introduces heterogeneity in β-subunit mediated modulation of Na_V currents (Stocker and Bennett, 2006). Finally, phosphorylation of β-subunits and recruitment of cytoskeletal proteins (Malhotra et al., 2002, Malhotra et al., 2004) known to regulate Na_V current inactivation (Shirahata et al., 2006) can also serve as another mechanism for the cell-dependent effects associated with β-subunits.

Therefore, that modulation of Na_V channels is mediated by β-cell specific post-translational modification of β-subunits or their recruitment of different partner proteins to the Na_V complex still remains a possibility. Accordingly the biphasic Na_V inactivation presented in Ins1 cells may be due to the formation of heterodimers or heterotrimers consisting of a single type of α-subunit with different β-subunits, which have different effects on the voltage-dependence of inactivation. Here we explore the possible regulation of Na_V current inactivation in Ins1 cells by Na_V channel β-subunits.

4.2 Results

4.2.1 Effect of endogenous β3-subunit knockdown on NaV channel current properties in Ins1 cells

To test the possibility that β-subunits mediate the inactivation properties of α-subunits, it was essential to characterise Na_V currents in Ins1 cells in the absence of β-subunit expression. However, as Ins1 cells express the β_3-subunit (Figure 4.2.1.1A), siRNA mediated knockdown was required. A 71% knockdown of *Scn3b* was achieved at the mRNA level without a compensatory change in the gene expression of *Scn1b*, *Scn2b* and *Scn4b*. However, the inactivation curve of endogenous Ins1 Na_V currents after knockdown of the β_3-subunit was essentially superimposable with control Ins1 cells (Figure 4.2.1.1B). The V_h and k values are summarised in Table 4.2.1.1. There was no significant difference in the V_h of currents transfected with scrambled control and β_3 siRNA. Nor was there was a significant difference in the number of cells displaying monophasic or biphasic inactivation and amongst cells that exhibited biphasic inactivation there was no significant difference in the proportion of the current inactivating at hyperpolarised or depolarised membrane potentials.

There was also no significant difference in the voltage-dependence of activation, the I-V relationship or current density after knockdown of the β_3-subunit (Figure 4.2.1.1C and D).

These results suggest that β-subunits, and indeed the β_3-subunit, does not contribute to the hyperpolarised inactivation of Na_V currents in Ins1 cells. In order to conclusively confirm this the expression of the β_3-subunit at the protein level (using western blot), after knockdown would be required. However, with the

finding that 71% knockdown was not associated with any significant changes to inactivation, it seems justified to conclude that β-subunits do not contribute to the hyperpolarised inactivation of Na_V currents in Ins1 cells.

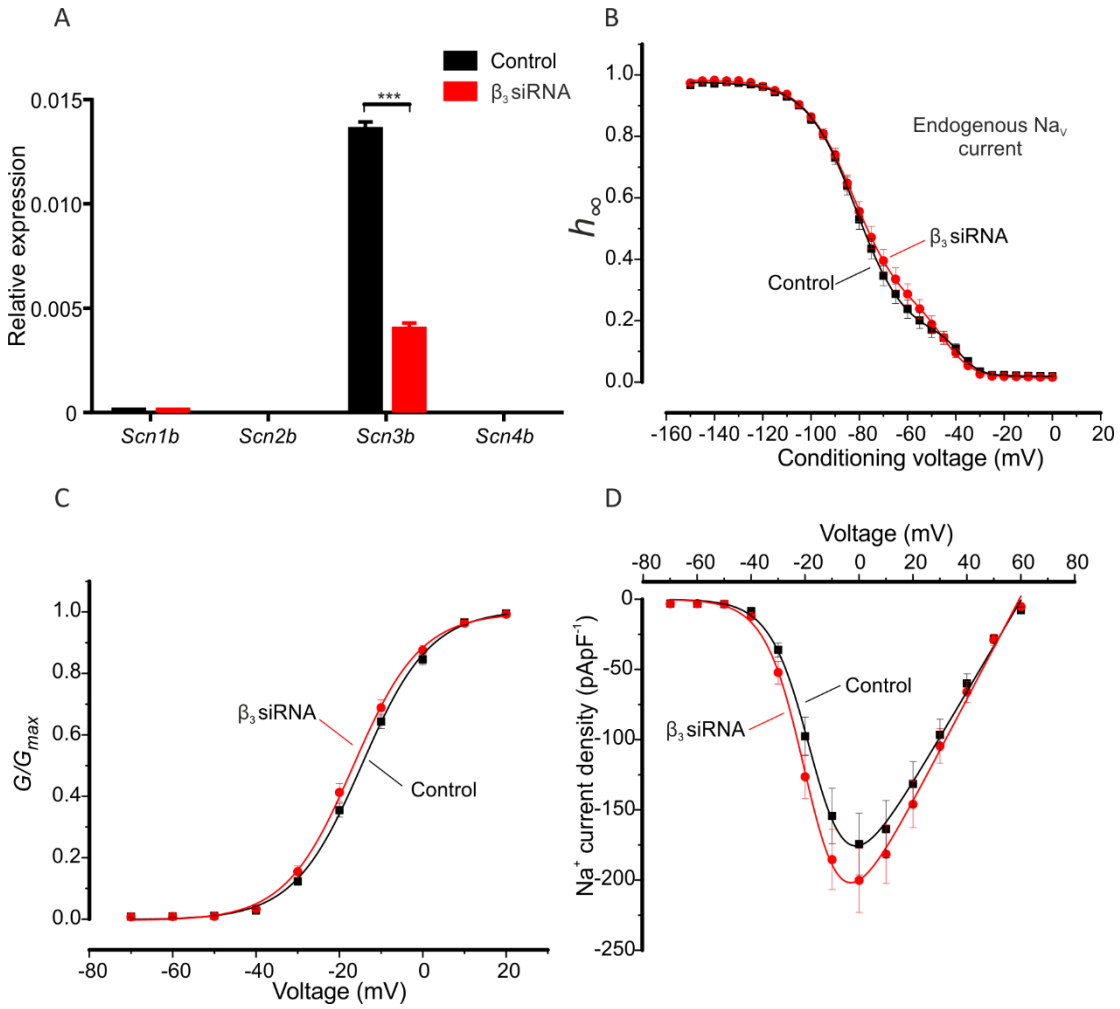


Figure 4.2.1.1 – Effect of β3 knockdown on endogenous Nav current in Ins1 cells

A, relative mRNA expression of *Scn1b*, *Scn2b*, *Scn3b* and *Scn4b* in control Ins1 cells transfected with a scramble siRNA or β3 siRNA (*n*= 3 preparations). *B*, voltage-dependence of inactivation (h_∞) of endogenous Nav currents from control (black; n=22, from 3 preparations) and β3 siRNA treated Ins1 cells (red; n=26 from 3 preparations). The curves represent a double Boltzmann fit to the data. *C*, voltage-dependence of activation (G/G_{max}) of endogenous Nav currents from control (black; n=19, from 3 preparations) and β3 siRNA treated Ins1 cells (red; n=24 from 3 preparations). The curves represent a single Boltzmann fit to the data. *D*, I-V relationship of endogenous Nav currents from control (black; n=19, from 3 preparations) and β3 siRNA treated Ins1 cells (red; n=24 from 3 preparations).

Na_V current	Monophasic V_h (mV)	*k*	Biphasic V_h-1 (mV)	% V_h-1	*k1*	Biphasic V_h-2 (mV)	% V_h-2	*k2*
Control	-81±2 (11)	11±1 (11)	-81±1 (11)	67±5 (11)	9±1 (11)	-43±3 (11)	33±6 (11)	6±2 (11)
β_3 siRNA	-82±3 (9)	10±1 (9)	-83±2 (17)	60±5 (17)	10±1 (17)	-47±2 (17)	40±5 (17)	6±1 (17)

Table 4.2.1.1–Effect of β_3 knockdown on endogenous Na_V current inactivation in Ins1 cells

Values represent mean values ± SEM of indicated number of cells (*n*). See Figure 4.2.1.1. V_h represents membrane potential at which inactivation is half-maximal in cells with monophasic inactivation and *k* represents the slope factor. In cells with biphasic inactivation, V_h-1 and V_h-2 represent the membrane potential at which inactivation is half-maximal for the current components inactivating at negative and positive membrane potentials, respectively. *k1*, *k2*, and %V_h-1, %V_h-2, represent the slope factor and proportion of the current inactivating with V_h-1 and V_h-2, respectively.

4.2.2 Effect of single β-subunit expression on the biphasic inactivation of Na_V currents in Ins1 cells

Since different β-subunits can modulate Na_V current inactivation differently, it could be possible that α-subunit formation of heterotrimers with different β-subunits is responsible for the biphasic inactivation observed in β-cells. To test this possibility, the β_3-subunit was co-expressed with $Na_V1.7$, $Na_V1.3$ and $Na_V1.6$ in Ins1 cells, so that all Na_V channel α-subunits would form heterotrimers with only a single type of β-subunit.

The inactivation of $Na_V1.7$, $Na_V1.3$ and $Na_V1.6$ currents co-expressed with the β_3-subunit in Ins1 cells is shown in Figure 4.2.2.1A-C and summarised in Table 4.2.2.1. The dashed red line represents the inactivation curves of the α-subunits

co-expressed with β_1- and β_2- subunits for comparison (see also Supplementary Table 1). It is clear from the inactivation curves that expression of Na_V channel α-subunits with a single β-subunit (β_3) does not abolish the biphasic inactivation of Na_V currents, suggesting that formation of heterotrimers with different β-subunits does not underpin the biphasic inactivation observed in β-cells. In fact biphasic inactivation was even more prominent when $Na_V1.3$ and $Na_V1.6$ was co-expressed with the β_3-subunit. Moreover, amongst the three cells in which $Na_V1.3$ currents inactivated with a monophasic inactivation the V_h proceeded at negative (-80 and -84mV) and more positive (-52mV) membrane potentials.

The voltage-dependence of activation of $Na_V1.3$ and $Na_V1.6$ subunits when co-expressed with the β_3-subunit was essentially identical to when co-expressed with the β_1- and β_2-subunit (Supplementary Table 2). However, co-expression of $Na_V1.7$ with the β_3-subunit produced a significant 5mV depolarising shift in $V_{0.5}$ (Figure 4.2.2.1D and Supplementary Table 2).

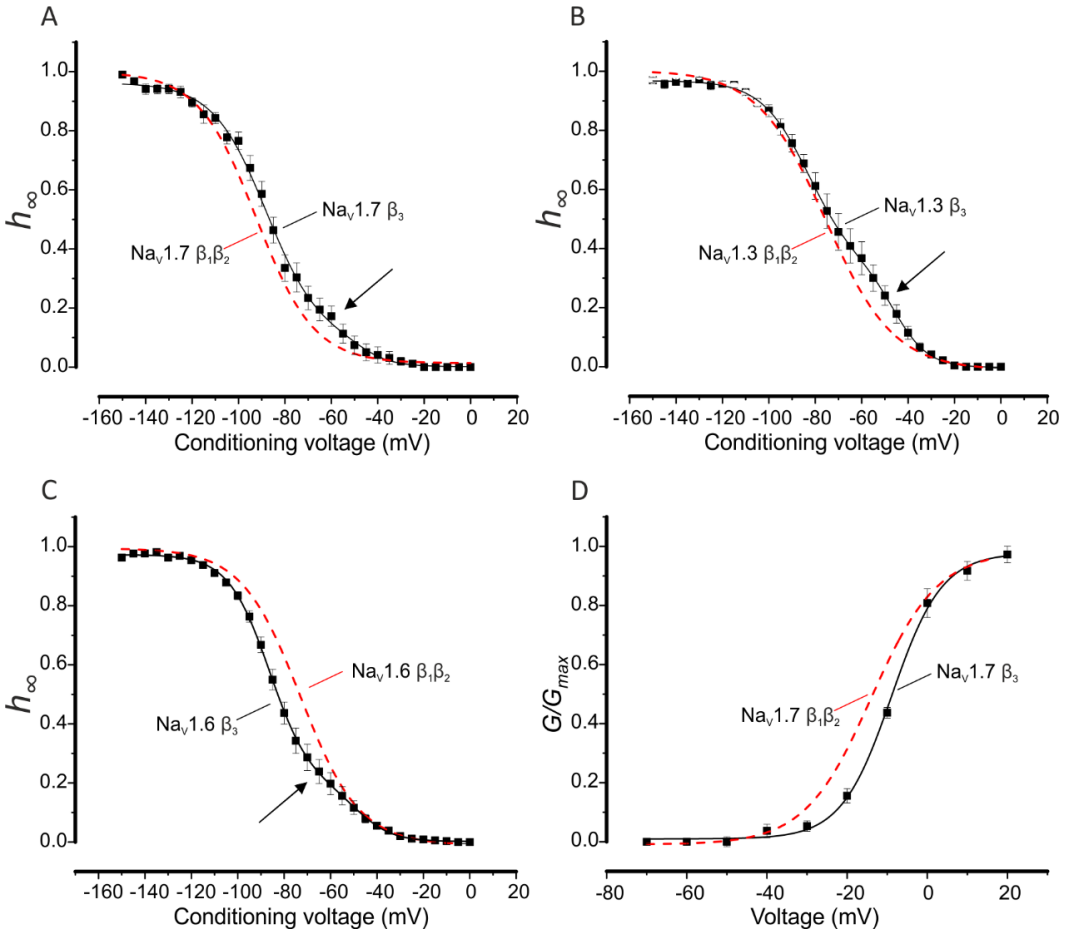


Figure 4.2.2.1- Characterisation of Nav1.7, Nav1.3 and Nav1.6 currents co-expressed with the β3-subunit

A, voltage-dependence of Nav1.7 current inactivation when the α-subunit is co-expressed with β3-subunit (black; *n*=9) in Ins1 cells. Dashed red curve represents voltage-dependence of Nav1.7 current inactivation when the α-subunit is co-expressed with β1- and β2-subunits in Ins1 cells (data shown in Figure 3.2.3.3). The curves represent a double Boltzmann fit to the data. Arrow indicates a component of inactivation occurring at positive membrane potentials. *B*, same as in *A* but for Nav1.3 (black, *n*=11; dashed red line Figure 3.2.4.1). *C*, same as in *A* but for Nav1.6 (black, *n*=18; dashed red line Figure 3.2.7.1). *D*, voltage-dependence of activation (G/G_{max}) of Nav1.7 co-expressed with β3-subunit (black; *n*=5). The curve represents a single Boltzmann fit to the data. Dashed red curve represents voltage-dependence of Nav1.7 current activation when the α-subunit is co-expressed with β1- and β2-subunits in Ins1 cells (data shown in Figure 3.2.3.2).

Na_V current	Monophasic V_h (mV)	*K*	Biphasic V_h-1 (mV)	% V_h-1	*k1*	Biphasic V_h-2 (mV)	% V_h-2	*k2*
$Na_V1.7$	-89±2 (8)	11±1 (8)	-86 (1)	28% (1)	6 (1)	-68 (1)	72% (1)	14 (1)
$Na_V1.3$	-72±10 (3)	9±2 (3)	-84±2 (8)	66±5% (8)	11±1 (8)	-46±2 (8)	34±4% (8)	5±1 (8)
$Na_V1.6$	-86±1 (11)	9±1 (11)	-87±2 (7)	59±9% (7)	9±1 (7)	-54±2 (7)	41±9% (7)	5±1 (7)

Table 4.2.2.1 – V_h and *k* values of $Na_V1.7$, $Na_V1.3$ and $Na_V1.6$ co-expressed with the β_3-subunit in Ins1 cells

Values represent mean values ± SEM of indicated number of cells (*n*). See Figure 4.2.2.1. V_h represents membrane potential at which inactivation is half-maximal in cells with monophasic inactivation and *k* represents the slope factor. In cells with biphasic inactivation, V_h-1 and V_h-2 represent the membrane potential at which inactivation is half-maximal for the current components inactivating at negative and positive membrane potentials, respectively. *k1*, *k2*, and %V_h-1, %V_h-2, represent the slope factor and proportion of the current inactivating with V_h-1 and V_h-2, respectively.

4.2.3 Effect of β_3-subunit expression on Na_V current in HEK cells

Despite a more prominent biphasic inactivation upon overexpression of the β_3-subunits, it is unlikely that the β_3-subunit contributes to the biphasic inactivation of Na_V currents because knockdown of *Scn3b* did not decrease the number of cells exhibiting biphasic inactivation nor did it change the proportion of currents inactivating at different membrane potentials. However, in order to confirm that monophasic inactivation of Na_V currents in HEK cells is not due to a lack of β_3-subunit expression (endogenously expressed in Ins1 cells), Na_V channel

α-subunits were co-expressed with the β_3-subunit and were compared to co-expression with GFP. It was ascertained that HEK cells do not express any endogenous β-subunits (data not shown).

The voltage-dependence of $Na_V1.7$ and $Na_V1.3$ current inactivation and activation when co-expressed with GFP or β_3, is shown in Figure 4.2.3.1. $Na_V1.7$ currents inactivated with a single component of inactivation with a V_h of -66±2mV (n=12) and -70±3mV (n=9), when co-expressed with GFP or the β_3-subunit, respectively (Figure 4.2.3.1A). The V_h values were not significantly different from each other nor were they significantly different from the V_h of $Na_V1.7$ co-expressed with β_1- and β_2-subunits. Unlike $Na_V1.7$, $Na_V1.3$ demonstrated a significant difference in the inactivation when expressed with GFP compared to β_3 subunits, as shown in Figure 4.2.3.1C and summarised in Table 4.2.3.1. $Na_V1.3$ co-expressed with GFP, inactivated at ~10 mV more hyperpolarised potential compared to $Na_V1.3$ co-expressed with β_3-subunit. The inactivation of $Na_V1.3$ co-expressed with GFP is also significantly more hyperpolarised (~10mV) compared to $Na_V1.3$ co-expressed with $\beta_1\beta_2$, thus demonstrating the importance of β-subunits to the regulation of $Na_V1.3$ currents. It is important to note, however, that the hyperpolarising shift obtained without co-expression of β-subunits is still significantly less than when the channel is expressed in Ins1 cells.

There was a significant difference in the voltage-dependence of activation of $Na_V1.7$ and $Na_V1.3$ when co-expressed with the β_3-subunit compared to GFP. Co-expression of $Na_V1.7$ and $Na_V1.3$ currents with the β_3-subunit compared to co-expression with GFP produced a (~6mV) hyperpolarising and depolarising shift in the voltage-dependence of activation, respectively (Figure 4.2.3.1B and D).

Moreover co-expression of $Na_V1.3$ with the β_3-subunit significantly decreased the peak current density to -43±14pApF^{-1} (n=9) from -125±28pApF^{-1} (n=11) when co-expressed with GFP (P<0.05, one way ANOVA, data not shown).

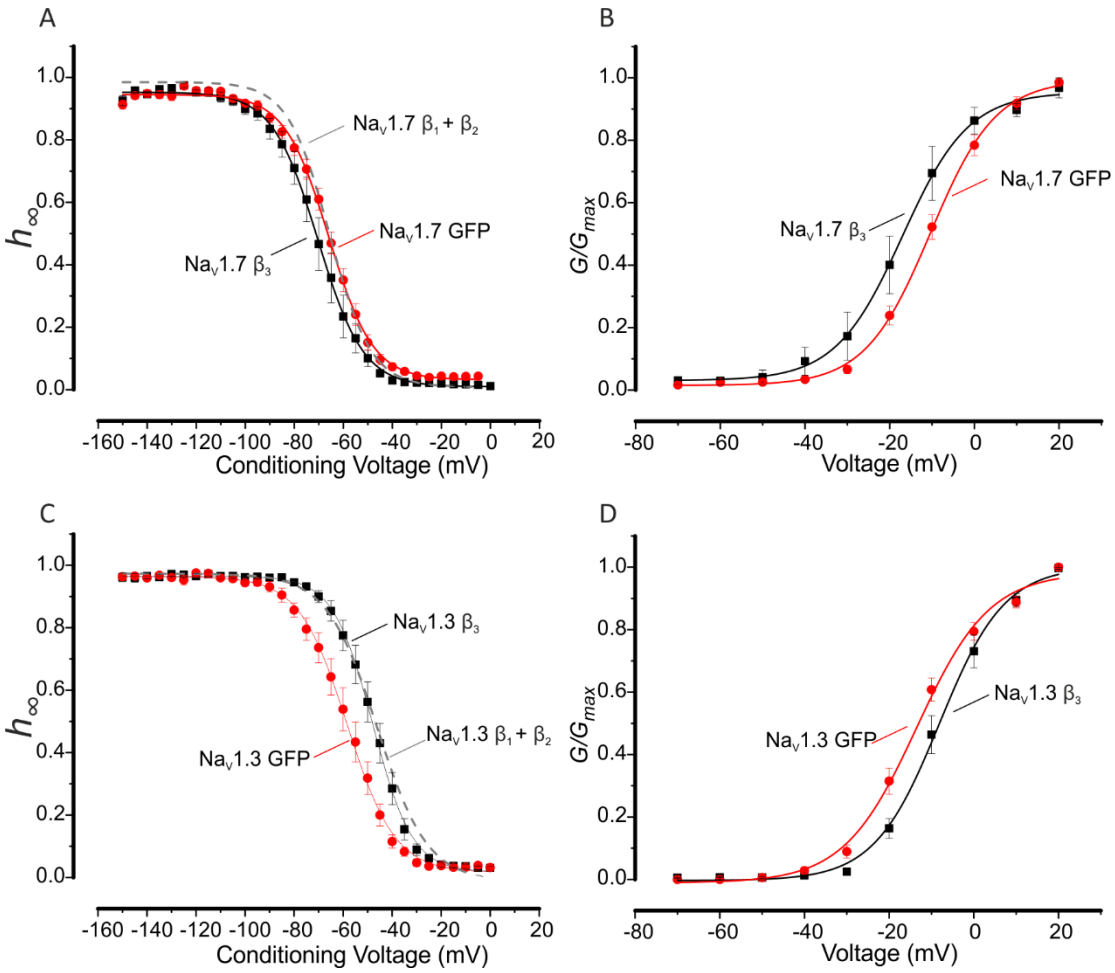


Figure 4.2.3.1- Characterisation of Nav1.7 and Nav1.3 co-expressed with the β3-subunit and GFP in HEK cells

A, voltage-dependence of inactivation (h_∞) of NaV1.7 co-expressed with the β3-subunit (black; *n*=9), GFP (red; *n*=12) and the β1- and β2-subunits (dashed curve; same data as in Figure 3.2.3.2) in HEK cells. The curves represent a single Boltzmann fit to the data. *B*, voltage-dependence of activation (G/G_{max}) of NaV1.7 co-expressed with the β3-subunit (black; *n*=6) and GFP (red; *n*=11) currents in HEK cells. The curves represent a single Boltzmann fit to the data. *C*, same as in *A* but for NaV1.3 (black, *n*=12; red, *n*=10; dashed curve, same data as in Figure 3.2.6.1). *D*, same as in *B* but for NaV1.3 (black, *n*=11; red, *n*=9).

Na_V current	V_h (mV)	K
$Na_V1.7$ + GFP	-66±2 (12)	9±1 (12)
$Na_V1.7$ + β_3	-70±3 (9)	8±1 (9)
$Na_V1.3$ + GFP	-59±3 (10)	8±1 (10)
$Na_V1.3$ + β_3	-48±2 (12)	7±1 (12)

Table 4.2.3.1- Inactivation V_h and k values of $Na_v1.7$ and $Na_v1.3$ co-expressed with the β_3-subunit or GFP in HEK cells

Values represent mean ± SEM of indicated number of cells (n). See Figure 4.2.3.1 . V_h represents membrane potential at which inactivation is half-maximal in cells with monophasic inactivation and k represents the slope factor.

4.3 Discussion

Although, α-subunits are capable of conducting current independently, β-subunits can affect the voltage-dependence of activation and inactivation depending on the α/β-subunits expressed and the host cell in which they are expressed in. In this chapter we investigated the contribution of β-subunits to biphasic and hyperpolarised voltage-dependence of Na_V current inactivation in Ins1 cells. The data indicate that the hyperpolarised and biphasic inactivation exhibited in Ins1 cells is unlikely to be due to cell-specific modulation of β-subunits or the formation of heterodimers/trimers with different combinations of β-subunits.

Knockdown of the β_3-subunits had no effect on the hyperpolarised and biphasic inactivation of endogenous Na_V currents in Ins1 cells. This confirmed that the characteristic features of Na_V current inactivation observed in rodent β-cells is not regulated by β-cell-specific modulation of β-subunits. Moreover, knockdown of

the β_3-subunit also had no effect on the activation or peak Na^+ current density of endogenous Ins1 Na_V currents, which according to mRNA expression primarily represents $Na_V1.3$ current. In contrast, $Na_V1.3$ inactivation, activation and peak Na^+ current density in HEK cells was significantly different when $Na_V1.3$ was co-expressed with GFP compared to the β_3-subunit. The contrasting effect of the β_3-subunit between Ins1 and HEK cells on the same Na_V channel α-subunit, demonstrates the variable cell-dependent effects that β_3-subunits can have on Na_V channel gating and cell surface expression.

As mentioned, in HEK cells the voltage-dependence of inactivation of $Na_V1.3$ shifted to hyperpolarised membrane potentials when co-expressed with GFP compared to its co-expression with the β_3 subunit or the β_1- and β_2-subunits, which could suggest that modulation of the β-subunits are essential for the depolarised inactivation of Na_V currents in non-β-cells. However, this is unlikely, as $Na_V1.7$ current inactivation was unaffected by the lack of β-subunit expression. Moreover, the ~10mV shift observed in $Na_V1.3$ inactivation in the absence of β-subunit expression in HEK cells is significantly less than the ~30 mV shift observed when $Na_V1.3$ is expressed in Ins1 cells. Furthermore, the hyperpolarising shift of $Na_V1.3$ co-expressed with GFP, occurred with a simultaneous hyperpolarising shift in the voltage-dependence of activation. This is different to the modulation of $Na_V1.3$ in Ins1 cells, where a hyperpolarising shift in the voltage-dependence of inactivation occurred without a significant change to the voltage-dependence of activation. Together, this suggests that the regulation of $Na_V1.3$ in the absence of β-subunits in HEK cells is not similar to the regulation of $Na_V1.3$ in Ins1 cells, despite the hyperpolarising shift in inactivation.

In Chapter 3, the effect of the endogenously expressed β_3-subunits in Ins1 cells on the inactivation properties of Na_V channel α-subunits was not taken into consideration. The biphasic inactivation of Na_V currents in Ins1 cells could have been due to the different combinations of heterodimers and/or heterotrimers formed with different β-subunits or due to expression of the β_3-subunit, which is not endogenously expressed in HEK cells. However, co-expression of only the β_3-subunit still exhibited a biphasic voltage-dependence of inactivation for all Na_V channel α-subunits in Ins1 cells. Moreover, knockdown of the β_3-subunit did not abolish the biphasic inactivation of endogenous Ins1 currents, suggesting that the β_3-subunit does not modulate the hyperpolarised or biphasic inactivation of Na_V currents in Ins1 cells. In support of this, co-expression of $Na_V1.7$ and $Na_V1.3$ with the β_3-subunit in HEK cells did not shift the inactivation curve in a hyperpolarising direction nor did it cause a biphasic voltage-dependence of inactivation.

The results from this chapter confirm that the inactivation of Na_V currents in β-cells is due to cell-specific modulation of α-subunits, rather than the β-subunits. The kinetics and voltage-dependence of Na_V currents are subject to modulation by various mechanisms which provide a means for altering cell excitability to meet the physiological demands of the cell. We next explored the involvement of some of these mechanisms in the regulation of Na_V inactivation in Ins1 cells.

Chapter 5

Factors modulating voltage-dependence of Na_V channel inactivation in rodent β-cells

5.1 Introduction

The voltage-dependence of Na_V channel inactivation is subject to cell- and subtype-specific modulation in rodent β-cells. $Na_V1.7$, $Na_V1.3$ and $Na_V1.6$ all exhibited a 20-30mV hyperpolarising shift in the voltage-dependence of inactivation in Ins1 cells compared to expression in HEK cells. Differences in α-subunit regulation were apparent as $Na_V1.3$ and $Na_V1.6$ inactivated at more depolarised membrane potentials and principally exhibited biphasic inactivation, whereas, $Na_V1.7$ inactivated at more hyperpolarised membrane potentials and predominantly inactivated with a monophasic inactivation. It is possible that the cell- and subtype-specific modulation is mediated via post-translational modifications (PTMs) (Pei et al., 2017), protein-protein interactions (Abriel, 2010) and/or Ca^{2+}-dependent regulation mediated directly by binding of intracellular free Ca^{2+} to an EF-hand domain in the C-terminus (Wingo et al., 2004) or indirectly via phosphorylation by Ca^{2+}-dependent protein kinases (Maltsev et al., 2008). We explored the contribution of these factors to the behaviour of Na_V current inactivation in insulin-secreting cells.

5.2 Results

5.2.1 Regulation of Na_V channels is unlikely to be mediated through the cytoplasmic domains

Human $Na_V1.7$ and $Na_V1.3$ channels share 77% amino acid sequence similarity (Table 1.3.1.1), yet their inactivation in Ins1 cells is significantly different. As mentioned, $Na_V1.7$ predominantly displays a single component of inactivation at

a hyperpolarised potential, whereas, Na$_V$1.3 predominantly displays two components of inactivation at both negative and positive membrane potentials in Ins1 cells. It is tempting to speculate that the hyperpolarised V_h of Na$_V$1.7 and Na$_V$1.3 is regulated by the same mechanism. However, due to differences in the amino acid sequence between the two α-subunits, Na$_V$1.7 is more prone to inactivate at hyperpolarised membrane potentials than Na$_V$1.3. Hence a single component of inactivation is observed rather than the predominantly biphasic inactivation observed with Na$_V$1.3. Therefore, the sequence dissimilarities between Na$_V$1.7 and Na$_V$1.3 could be used to identify a site at which Na$_V$ channels are modulated. Regions of considerable sequence dissimilarity are found in the intracellular loops and termini of the protein.

Chimeric channel constructs were generated based on the Na$_V$1.7 backbone by replacing the N-terminal domain, L1 and L2, the C-terminal domain or L3 sequences with the corresponding sequences of Na$_V$1.3 (Figure 5.2.1.1, see also appendix). The chimeras were expressed in Ins1 and HEK cells and the voltage-dependence of inactivation was compared to control Na$_V$1.7. If Na$_V$1.7 modulation occurs at a particular intracellular domain, it would be expected that replacement with the equivalent sequence of Na$_V$1.3 would either (1) cause a depolarising shift in V_h (which would be absent in HEK cells), (2) change the proportion of current inactivating with a biphasic inactivation, or (3) change the proportion of currents inactivating at hyperpolarised and depolarised membrane potentials. However, no significant difference could be observed in any of the given parameters (shown in Figure 5.2.1.1A-D and summarised in Table 5.2.1.1) suggesting that modulation of Na$_V$ channels does not occur at the cytoplasmic domain.

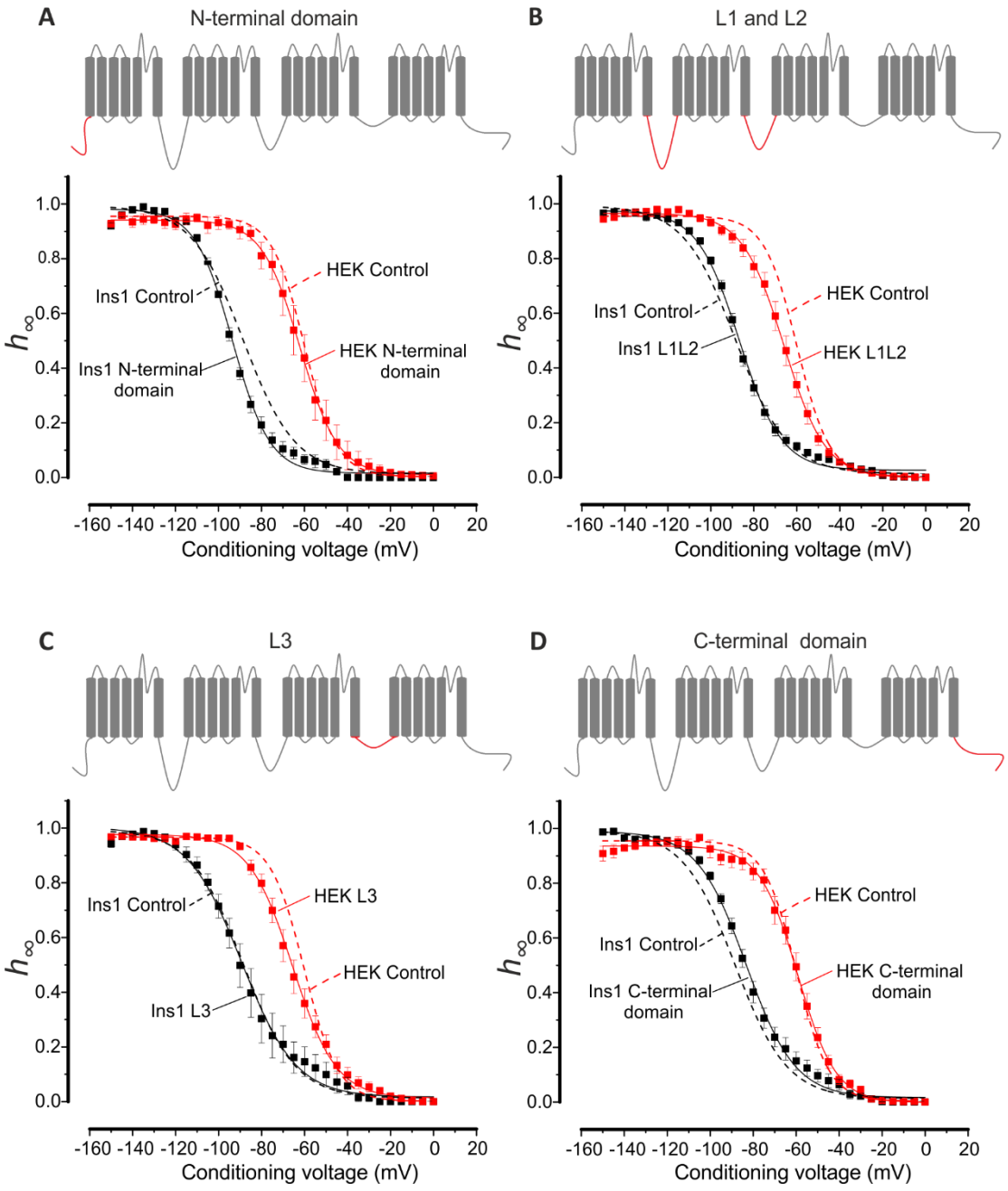


Figure 5.2.1.1- Nav1.7 and Nav1.3 chimera hybrids

A, schematic representation of the N-terminal chimera. Regions of Nav1.7 are depicted in grey, and those of Nav1.3 in red. Below is the voltage-dependence of inactivation of the N-terminal chimera currents when the α-subunit is co-expressed with β_1- and β_2-subunits in Ins1 (black; *n*=9) and HEK cells (red; *n*=6); and control TTX-resistant Nav1.7 currents when the α-subunit is co-expressed with β_1 and β_2 -subunits in Ins1 (dashed black line; *n*=37) and HEK cells (dashed red line; *n*=6). *B,* as in *A,* but for L1L2 chimera currents (black, *n*=15; red, *n*=9); and the same controls as in *A. C,* as in *A,* but for L3 chimera currents (black, *n*=16; red, *n*=11) and the same controls as in *A. D*, as in *A,*

but for C-terminal chimera currents (black, *n*=7; red, *n*=8) and the same controls as in *A.* V_h and *k* values are given in the Table 5.2.1.1 and Supplementary Table 3. See appendix for details on generation of $Na_V1.7$ and $Na_V1.3$ chimera hybrids.

Cell type	Na_V current of $Na_V1.7/1.3$ chimeras	Monophasic V_h (mV)	Biphasic V_h-1 (mV)	Biphasic V_h-2 (mV)	% V_h-1	% V_h-2	% of cells with biphasic inactivation
Ins1	$Na_V1.7$ Control	-90±2 (28)	-94±4 (9)	-63±5 (9)	62±7%	38±7%	25%
Ins1	N-terminal domain	-95±1 (7)	-98±1 (2)	-67±1 (2)	63±1%	37±3%	28%
Ins1	L1L2	-88±1 (12)	-86±1 (3)	-49±5 (3)	71±6%	29±4%	20%
Ins1	L3	-96±3 (12)	-98±3 (4)	-50±5 (4)	64±8%	36±7%	25%
Ins1	C-terminal domain	-86±1 (5)	-84±1 (2)	-50±6 (2)	69±6%	31±3%	28%
HEK	$Na_V1.7$ Control	-60±1 (6)	n/a	n/a	n/a	n/a	n/a
HEK	N-terminal domain	-61±4 (6)	n/a	n/a	n/a	n/a	n/a
HEK	L1L2	-66±2 (9)	n/a	n/a	n/a	n/a	n/a
HEK	L3	-67±3 (11)	n/a	n/a	n/a	n/a	n/a
HEK	C-terminal domain	-60±2 (8)	n/a	n/a	n/a	n/a	n/a

Table 5.2.1.1 - $Na_V1.7/Na_V1.3$ chimeras expressed in Ins1 and HEK cells

V_h and *k* value for the indicated Na_V currents. Values represent mean values ± SEM of indicated number of cells (*n*). Inactivation curves are presented in Figure 5.2.1.1. V_h represents membrane potential at which inactivation is half-maximal in cells with monophasic inactivation. In cells with biphasic inactivation, V_h-1 and V_h-2 represent the membrane potential at which inactivation is half-maximal for the current components inactivating at negative and positive membrane potentials, respectively. %V_h-1 and %V_h-2 represent the proportion of current inactivating with V_h-1 and V_h-2.

5.2.2 Regulation of Na_V current inactivation by cytosolic factors present in rodent β-cells

It is possible that the arcane inactivation observed in rodent β-cells is due to the presence of a cytosolic factor present only in β-cells that interacts with the channels to modulate channel behaviour. To test this possibility, the voltage-dependence of inactivation of $Na_V1.7$ and $Na_V1.3$ expressed in Ins1 and CHO cells was measured in a cell-attached configuration where the channels remain in an intact cell environment. Subsequent recordings were made in the inside-out configuration at various time points after patch excision to promote 'washout' of cytosolic factors that may interact with the channels.

In order to obtain detectable $Na_V1.7$ and $Na_V1.3$ currents in the cell-attached and inside-out configuration the experiments required a high level of channel expression. The currents recorded in Ins1 cells are shown in Figure 5.2.2.1A and B. The corresponding I-V curves of Na_V currents recorded in Ins1 cells are shown in Figure 5.2.2.1C and D, respectively. The shape of the I-V curve indicates good voltage clamp in the cell-attached and inside-out configuration.

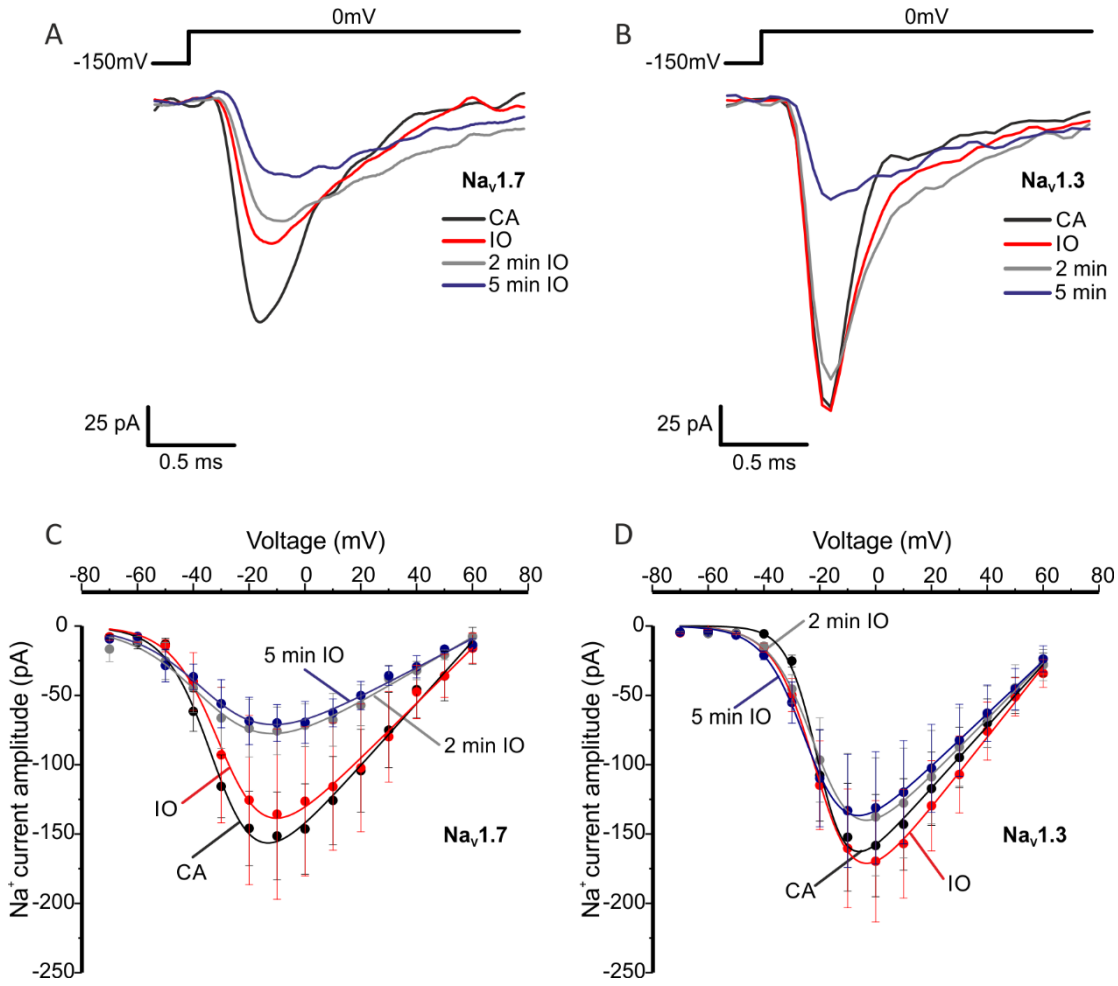


Figure 5.2.2.1 - Na$_v$1.7 and Na$_v$1.3 currents in cell-attached and inside-out configuration

A, Na$_v$1.7 currents when the α subunit is co-expressed with β_1 and β_2 in Ins1 cells in response to a step depolarisation from -150mV to 0mV in cell-attached (CA), inside-out (IO) patch immediately after excision and 2 and 5 minutes after excision. *B*, same as in *A*, but with Na$_v$1.3 currents in Ins1 cells. *C*, I-V relationship of Na$_v$1.7 currents recorded from Ins1 cells in CA (black; n=14), IO patch immediately after excision (red; n=6), 2 minutes after excision (grey; n=6) and 5 minutes after excision (blue; n=5). *D*, same as in *C*, but for Na$_v$1.3 currents recorded in CA (black; n=16), IO patch immediately after excision (red; n=11), 2 minutes after excision (grey; n=7) and 5 minutes after excision (blue; n=7).

Unlike the inactivation curves recorded in whole-cell configuration, inactivation of Na$_v$1.3 and Na$_v$1.7 was invariably monophasic in both cell-attached and

inside-out patches (Figure 5.2.2.2A). The cumulative distribution of V_h measured in cell-attached membrane patches (each represented by a single data point) in Ins1 cells expressing $Na_V1.7$ and $Na_V1.3$ are shown in Figure 5.2.2.2B. Whereas the cumulative distribution of $Na_V1.7$ in cell-attached patches is monophasic with a V_h of -93mV, the distribution of $Na_V1.3$ is biphasic and consists of two components of inactivation with V_h values of -74mV and -58mV. Therefore, although biphasic inactivation was not observed in individual cell-attached and inside-out recordings, the distribution of V_h reflects the predominant monophasic and biphasic inactivation of $Na_V1.7$ and $Na_V1.3$ recorded in whole-cell configuration, respectively. Five of the 18 (28%) membrane patches expressing $Na_V1.3$ had V_h values more positive than -60mV and 2/23 cells (9%) expressing $Na_V1.7$ inactivated at membrane potentials more positive than -65mV. Again, this reflects the capacity of individual Na_V channel α-subunits to undergo inactivation at vastly different membrane potentials in Ins1 cells.

The V_h of $Na_V1.7$ measured in the cell-attached configuration proceeded at -93±3mV (n=23) and -74±4mV (n=15) in Ins1 and CHO cells, respectively (Figure 5.2.2.2D). The corresponding values for $Na_V1.3$ were -69±2mV (n=18) and -56±5mV (n=6) in Ins1 and CHO cells, respectively (Figure 5.2.2.2C). These values are not identical to those recorded in whole-cell configuration and may reflect an improper cancellation of the membrane potential to 0mV when the cells were immersed in high $[K^+]_o$ medium. This idea is supported by the observation that following excision of the patches, there was an immediate ~5-10mV hyperpolarising shift in the voltage-dependence of inactivation and activation (shown in Figure 5.2.2.2E and F). Regardless of the possible voltage errors, $Na_V1.7$ and $Na_V1.3$ maintained a hyperpolarised V_h in Ins1 cells compared to CHO cells

and the inactivation of $Na_V1.7$ was still significantly more hyperpolarised compared to $Na_V1.3$ in Ins1 and CHO cells consistent with data obtained from whole-cell recordings.

As the membrane patches were maintained in the extracellular medium following patch excision and inside-out patch formation, the V_h of $Na_V1.7$ and $Na_V1.3$ channels expressed in both cell types displayed a hyperpolarising shift in the voltage-dependence of activation (Figure 5.2.2.2E and F). This shift in the voltage-dependence of activation may contribute to the reduction in Na^+ current amplitude as observed when the cells are maintained in an inside-out configuration (Figure 5.2.2.1).

The reason for the time-dependent shift in the voltage-dependence of inactivation in the inside-out configuration is not known(Figure 5.2.2.2C and D). However a time-dependent shift has been previously described for endogenous Na_V currents expressed in cardiac cells and $Na_V1.7$ expressed in HEK cells (Cachelin et al., 1983, Jo and Bean, 2014). Since Na_V channels expressed in all cell types appear to exhibit the hyperpolarising shift in inactivation, one would expect that if Na_V channel behaviour in Ins1 cells is regulated by a diffusible cytosolic factor, the V_h of channels expressed in Ins1 and CHO cells would converge, as an additional factor contributing to the hyperpolarised inactivation is displaced. However, a ~10-20mV difference is maintained between the V_h values of the channels expressed in Ins1 and CHO cells, which suggests that Na_V inactivation behaviour in Ins1 cells is not regulated by a diffusible cytosolic factor in Ins1 cells.

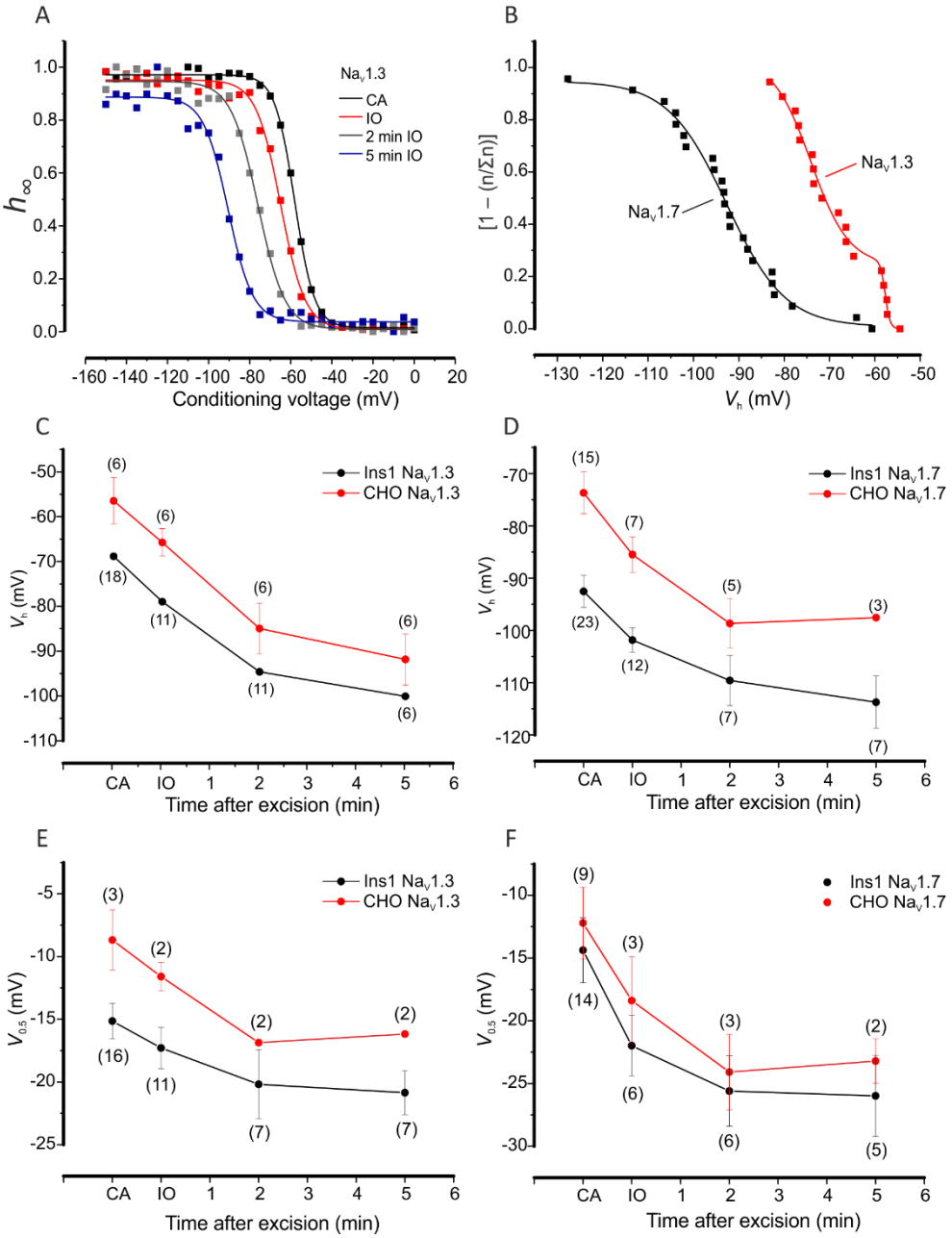


Figure 5.2.2.2– Voltage-dependence of Nav1.7 and Nav1.3 current inactivation and activation in the cell-attached and inside-out configuration.

A, voltage-dependence of inactivation of Nav1.3 currents recorded from Ins1 cells in CA, IO patch immediately after excision and 2 and 5 minutes after excision. Inactivation curves have been fit to a single Boltzmann function. *B*, cumulative distribution of Nav1.3 (red) and Nav1.7 (black) V_h recorded in cell-attached patches from the Ins1 cell. Data have been normalized (n/∑n) to the total number of patches (n=18 patches for Nav1.3 and n=23 patches for Nav1.7). For display and to facilitate comparison with inactivation curves, data are shown as (1-[n/∑n]). The cumulative

distributions have been fit to a double Boltzmann for $Na_V1.3$ and a single Boltzmann for $Na_V1.7$. Arrows indicate the cells inactivating at potentials more positive than -65mV. *C*, summarized voltage-dependence of inactivation of $Na_V1.3$ currents in Ins1 (black) and CHO cells (red) of indicated number of patches/cells (*n*). *D*, same as in *C* but for $Na_V1.7$. *E*, summarized voltage-dependence of activation of $Na_V1.3$ currents co-expressed with β_1- and β_2-subunits in Ins1 (black) and CHO cells (red) of indicated number of patches/cells (*n*). *F*, same as in *E* but for $Na_V1.7$.

5.2.3 Hyperpolarised inactivation of Na_V currents due to absence of cytosolic factors in rodent β-cells

The alternative hypothesis that inactivation of Na_V currents is more negative in Ins1 cells due to the absence of a factor was also tested. $Na_V1.7$ currents were again recorded in a cell-attached patch configuration in Ins1 cells. The patch was subsequently excised and inside-out patches were formed before 'cramming' the membrane into neighbouring HEK cells (Figure 5.2.3.1A). The 'macroscopic' currents and the corresponding inactivation curves recorded in cell-attached patch and immediately after insertion into HEK cells is shown in Figure 5.2.3.1B and C. However a similar time-dependent shift in the voltage-dependence of inactivation (Figure 5.2.3.1D) and activation (Figure 5.2.3.1E) could be observed to when the membrane patch was left in the extracellular medium, suggesting that the modulation of Na_V channel inactivation in Ins1 cells is not due to a diffusible intracellular factor absent in Ins1 cells and present in HEK cells.

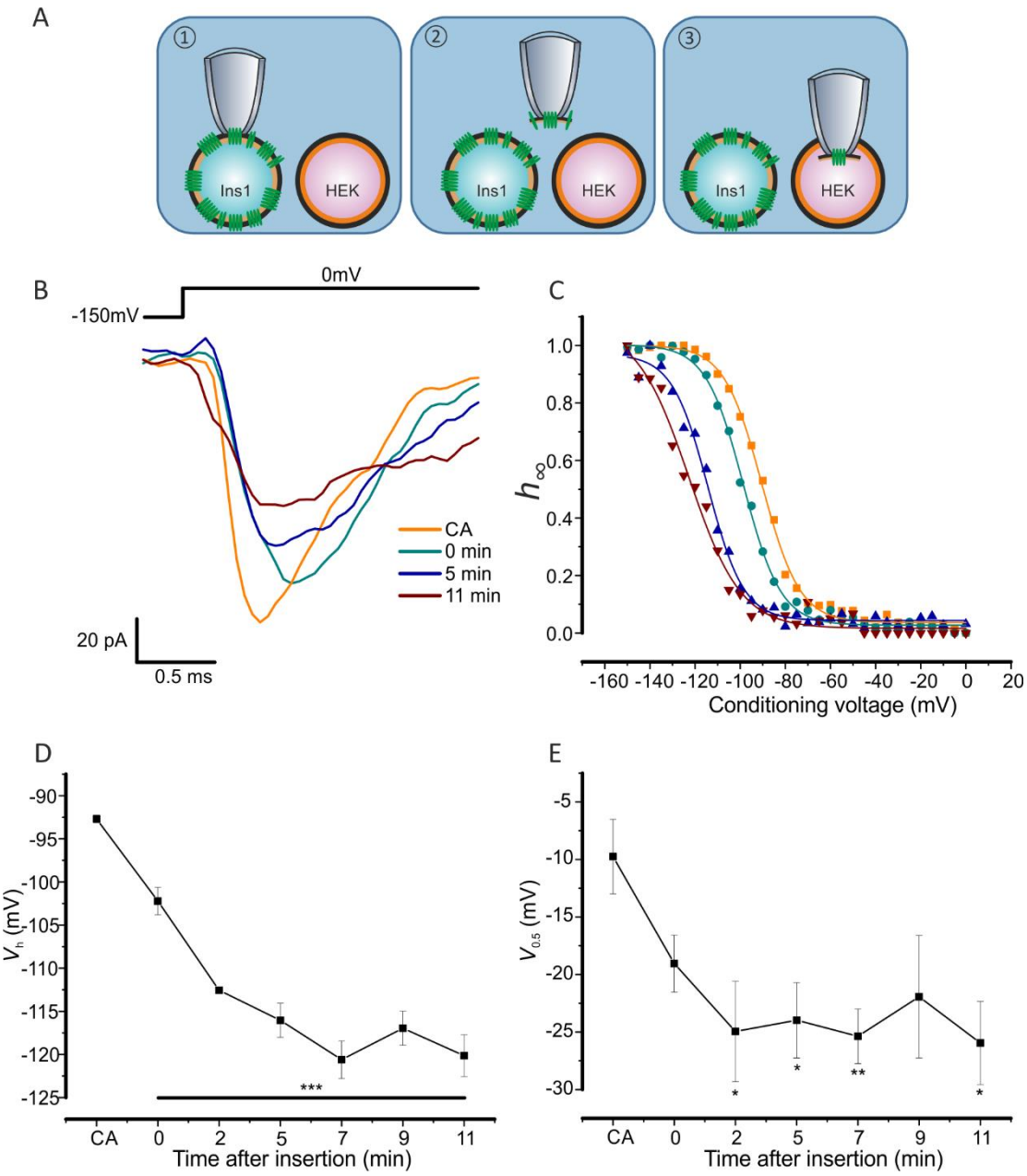


Figure 5.2.3.1- Patch cramming of $Na_V1.7$ channels expressed in Ins1 into HEK cells

A, schematic of patch cramming procedure. $Na_V1.7$ channels were expressed in Ins1 cells and a cell-attached patch was formed (①); the patch of membrane was excised (②) and immediately crammed into HEK cells (③). *B*, represents $Na_V1.7$ currents when the α-subunit is co-expressed with β_1- and β_2-subunits in response to a step depolarisation from -150mV to 0mV in cell-attached (CA) configuration in Ins1 cells, immediately after excision and cramming into HEK cells (0 min) and 5 and 11 minutes after insertion of the membrane into HEK cells. *C*, voltage-dependence of

inactivation for $Na_V1.7$ currents shown in *B* with same colour coding. *D*, summarised voltage-dependence of inactivation of $Na_V1.7$ currents in cell-attached configuration and after cramming into HEK cells (n=4). ***P<0.001 for each time point compared to CA, using a one-way ANOVA. *E*, same as in *D* but voltage-dependence of activation. *P<0.05 or **P<0.01 for each time point compared to CA, using a one-way ANOVA.

5.2.4 Ca^{2+}- and PKC dependent regulation of Na_V channels in rodent β-cells

The results from Figure 5.2.3.1 and Figure 5.2.2.2 suggest that modulation of Na_V channels is not due to a diffusible factor but rather a more permanent modification that still results in a hyperpolarised inactivation even when the channel is removed from the cell environment. Modulation of Na_V channels directly by intracellular free Ca^{2+}, in addition to its effects on the conventional subfamily of PKC, could provide a dynamic mechanism for regulation of cell excitability in insulin-secreting cells. The binding of Ca^{2+} to an EF-hand domain in the C-terminus of $Na_V1.5$ shifts inactivation to more positive membrane potentials, thus providing a positive feedback mechanism for increasing cardiac cell excitability (Wingo et al., 2004).

To test Ca^{2+}-dependent regulation of Na_V channels in β-cells, Ins1 cells were incubated with 20μM BAPTA-AM (a Ca^{2+}chelator) for 20min in a Ca^{2+}-free extracellular medium prior to whole-cell voltage clamp recordings of endogenous Na_V currents in Ins1 cells. If the channels are modulated in a Ca^{2+}-dependent manner to inactivate at a hyperpolarised potential, incubation with BAPTA-AM should reverse this, and therefore produce a depolarising shift compared to the control. However as shown in Figure 5.2.4.1 and summarised in Supplementary Table 3, treatment with BAPTA-AM had no significant effect on Na_V current

inactivation. In the control and BAPTA-AM treated group 5/11 cells and 8/13 cells, respectively, inactivated with a single component with an average V_h of -84±5mV and -92±3mV. The remaining 6/11 control cells and 5/13 BAPTA-AM treated cells exhibited a biphasic inactivation with an average V_h of -86±5mV and -46±4mV, comprising 59±9% and 41±9% of the total current and -89±3mV and -46±2mV, comprising 73±6% and 27±6% of the total current, respectively. Moreover, the voltage-dependence of activation was also not significantly different between control and BAPTA-AM treated endogenous Nav currents, which had a $V_{0.5}$ -14±3mV (n=11) and -18±2mV (n=13), respectively.

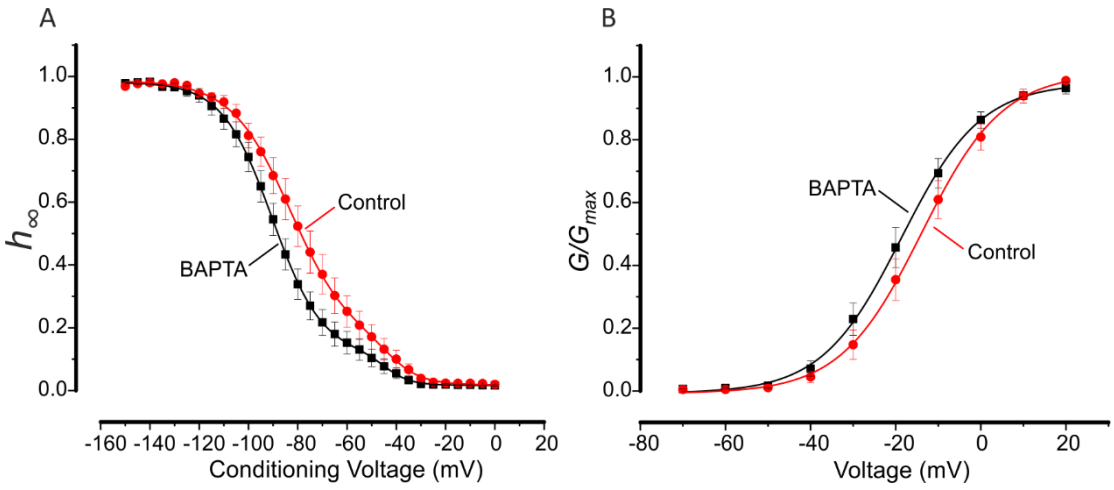


Figure 5.2.4.1- Effect of 20μM BAPTA-AM on endogenous Na_V currents in Ins1 cells

A, voltage-dependence of endogenous Na_V current inactivation (h_∞) in control (red; *n*=11) and 20μM BAPTA-AM treated (black; *n*=13) Ins1 cells. The curves represent a double Boltzmann fit to the data. *B*, voltage-dependence of endogenous Na_V current activation (G/G_{max}) in control (red; *n*=11) and 20μM BAPTA-AM treated (black; *n*=13) Ins1 cells. The curves represent a single Boltzmann fit to the data.

We also investigated the effect of downregulation of protein kinase C (PKC) by long-term exposure to PMA (Srivastava et al., 2002, Johnson et al., 1995) on Na_V current inactivation. Chronic (48h) treatment with 10nM PMA reduced Na^+ current density with no effect on Ca^{2+} current density in insulin-producing RINm5F cells (Rorsman et al., 1986), which was also replicated in Ins1 cells (Figure 5.2.4.2A-D). Whether the reduction in Na_V current density is due to reduced expression of Na_V channels or a hyperpolarising shift in inactivation has yet to be determined. The voltage-dependence of endogenous Na_V current inactivation when cells were chronically treated with 10nM PMA was essentially superimposable with control Ins1 cells (Figure 5.2.4.2E), suggesting that the reduction in current density is not due to a hyperpolarining shift in the voltage-dependence of inactivation. Of the control and PMA treated Ins1 cells, 2/4 and 6/11 Na_V currents inactivated with a single component of inactivation with an average V_h of -94±6mV and -91±2mV, respectively. The average V_h of control cells inactivating with two components of inactivation (2/4 cells) is -94±1mV and -45±5mV, comprising 75±12% and 25±13% of the total current, respectively. Meanwhile, the average V_h of PMA treated cells inactivating with two components of inactivation (5/11 cells) is -92±2mV and -46±2mV, comprising 79±6% and 21±5% of the total current, respectively. There was also no significant difference in the voltage-dependence of activation (data not shown).

PKC phosphorylation of $Na_V1.7$ exhibits a depolarising effect on the voltage-dependence of inactivation in some (Tan et al., 2014) but not all cell types (Vijayaragavan et al., 2004). Moreover, $Na_V1.3$ and $Na_V1.6$ contain a putative PKC phosphorylation site in the same L3 region. We therefore tested the effect of acute activation or inhibition of PKC by application of PMA (10nM) or the inhibitor

BIM23056 (100nM) on $Na_V1.7$ inactivation. However, neither compound affected $Na_V1.7$ inactivation (Figure 5.2.4.2F). The V_h of $Na_V1.7$ in control, BIM and PMA treated Ins1 cells is -96±1mV (n=5), -90±2mV (n=5) and -96±4mV (n=5), respectively.

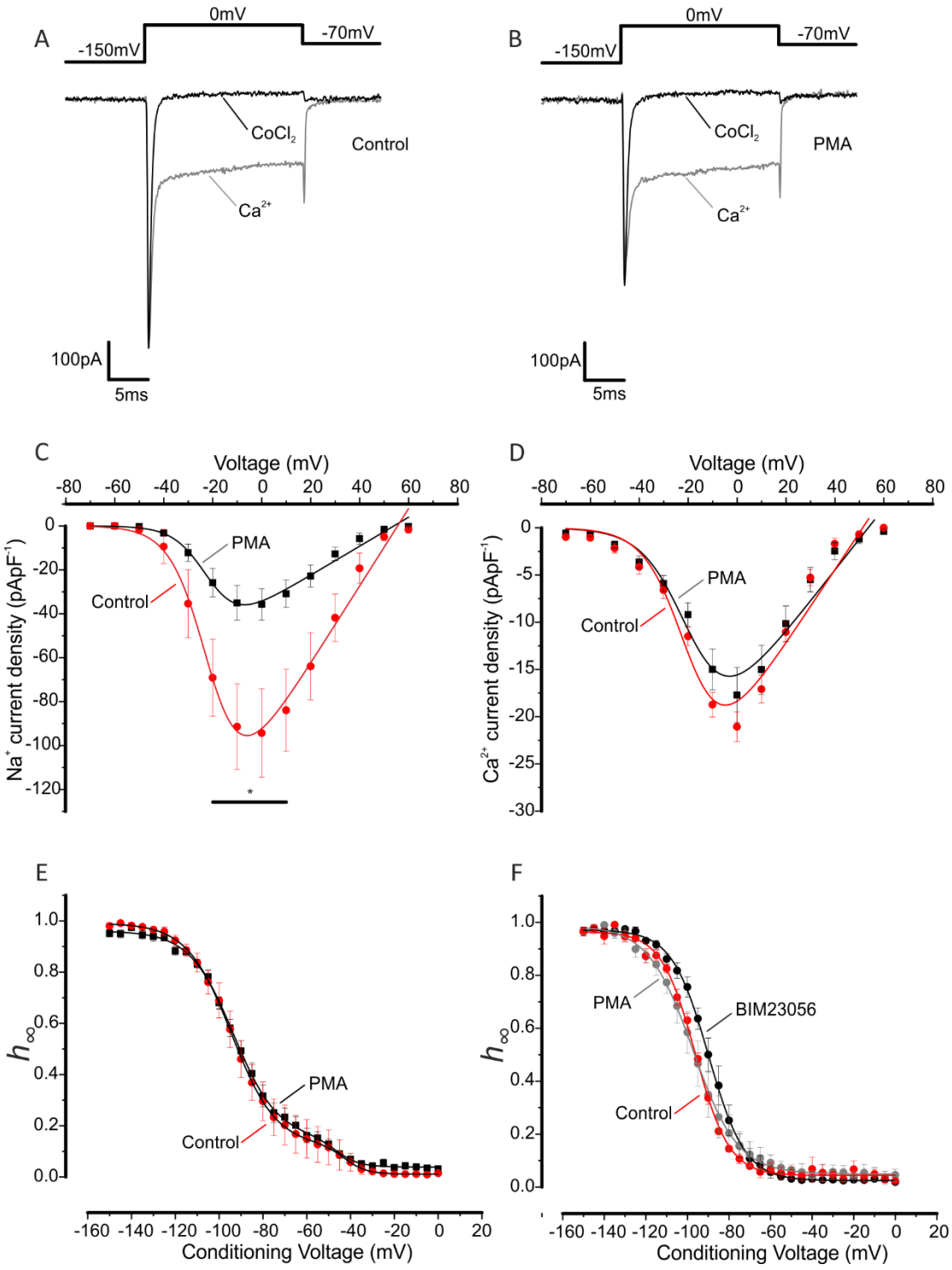


Figure 5.2.4.2 – PKC-dependent regulation of Na_V current inactivation

A, endogenous current from Ins1 cells in response to a step depolarisation from -150mV to 0mV in the presence of extracellular Ca^{2+}, which was subsequently replaced with $CoCl_2$ (Ca^{2+} channel blocker). The sustained current represents Ca^{2+} current, which is abolished upon addition of $CoCl_2$ The rapid activating and inactivating current represent Na_V, which is maintained after the addition

of $CoCl_2$. *B*, same as in *A* but for Ins1 cells treated with 10nM PMA for 48h. Note the reduction in Na_V current compared to control Ins1 cells in *A*. *C*, I-V relationship of Na_V currents from control Ins1 (red; *n*=4) and 10nM PMA treated Ins1 cells (black; *n*=10). **P*<0.05, one way ANOVA between Na^+ current density of control and 10nM PMA treated Ins1 cells at -20, -10, 0 and 10mV. *D*, I-V relationship of voltage-dependent Ca^{2+} currents from control Ins1 (red; *n*=9) and 10nM PMA treated Ins1 cells (black; *n*=13). *E*, voltage-dependence of inactivation (h_∞) of Na_V currents in control Ins1 (red; *n*=4) and 10nM PMA treated Ins1 cells (black; *n*=11). The curves represent a double Boltzmann fit to the data. *F*, voltage-dependence of inactivation of $Na_V1.7$ channels co-expressed with β_1- and β_2-subunis in control Ins 1 cells (red; *n*=4) or Ins1 cells acutely (1h) treated with 100nM BIM23056 (black; *n*=5), or 10nM PMA (grey; *n*=5). The curves represent a single Boltzmann fit to the data.

5.2.5 Regulation of Na_V channels via the insulin receptor signalling pathway

Insulin-secreting cells are naturally exposed to high levels of insulin. Insulin acts on receptor tyrosine kinases which are known to be potent modulators of ion channels (Davis et al., 2001). Indeed, insulin has been shown to alter the voltage-dependence of steady state inactivation without altering the voltage-dependence of activation in HEK cells (Ahern et al., 2005). We investigated the possibility that Na_V channels are modulated by a process downstream of the insulin signalling pathway by measuring the V_h of $Na_V1.7$ expressed in Ins1 cells that were chronically (48h) incubated with 100µM diazoxide (a K_{ATP} channel activator) to prevent insulin secretion. However, there was no significant difference between the control and the diazoxide treated group (Figure 5.2.5.1A). Five out of 6 control cells and 7/9 cells treated with diazoxide inactivated with a monophasic inactivation with an average V_h of -97±7mV and -106±3mV, respectively. In the control group one cell inactivated at a positive

membrane potential with a V_h of -67mV hence the large variation. The remaining control cell had a biphasic inactivation with a V_h of -106mV and -75mV comprising 30% and 70% of the current, respectively, and the remaining 2/9 diazoxide treated cells inactivated with a V_h of -99±6mV and -72±6mV comprising 83±1% and 17±1%mV of the current, respectively.

In the previous experiments, we did not measure the concentration of insulin in the medium after treatment with diazoxide. Therefore we also tested whether inhibition of insulin action using the insulin receptor antagonist, S961, would affect $Na_V1.7$ inactivation. We observed no effect (Figure 5.2.5.1B and Supplementary Table 3). The V_h of control and S961 treated Ins1 cells is -97±1mV (n=2) and -97±1mV (n=3), respectively.

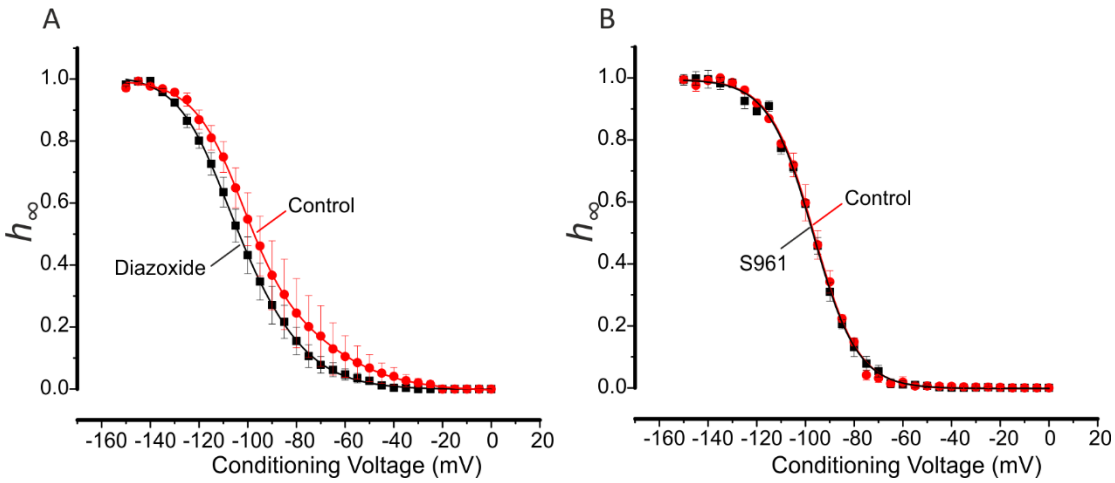


Figure 5.2.5.1- Effect of diazoxide and S961 on Na_V inactivation

A, voltage-dependence of inactivation of $Na_V1.7$ α-subunit co-expressed with β_1- and β_2-subunits in control Ins1 cells (red; *n*=6) and Ins1 cells chronically (48h) treated with 100μM diazoxide (black; *n*=9). The curves represent a double Boltzmann fit to the data. *B*, same as in *A* but for control Ins1 cells (red; *n*=2) and Ins1 cells treated with 10μM S961 for 24h (black; *n*=3).). The curves represent a single Boltzmann fit to the data.

5.2.6 Effect of phosphatidylinositol 4,5-bisphosphate (PIP_2) on Na_V channel inactivation

K_{ATP} channels are more active in β-cells than other cell types (Ashcroft and Rorsman, 2013). It is possible that this may be due to higher levels of PIP_2 in β-cells, which reduces the sensitivity of K_{ATP} channels to ATP (Baukrowitz et al., 1998, Shyng and Nichols, 1998). We therefore explored the possibility that differences in PIP_2 content could underlie the differences in $Na_V1.7$ inactivation between Ins1 and HEK cells. However inclusion of 50μM diC8 in the intracellular pipette solution had no significant effect on $Na_V1.7$ inactivation in Ins1 cells (Figure 5.2.6.1A). The V_h of $Na_V1.7$ in control and diC8 treated cells is -99±1mV and -97±2mV, respectively. Inclusion of 50μM neomycin (a polycation), which would shield the negative charges of PIP_2 also had no effect on $Na_V1.7$ expressed

in Ins1 cells (Figure 5.2.6.1B). The V_h of Nav1.7 in control and Neomycin treated cells is -98±3mV and -98±1mV, respectively. Likewise, addition of 50μM diC8 in the intracellular pipette solution had no effect on inactivation in HEK cells, which according to our hypothesis may have low levels of PIP_2 than Ins1 cells (Figure 5.2.6.1B and Supplementary Table 3). The V_h of Nav1.7 in control and PIP_2 diC8 treated cells is -57±1mV and -59±1mV, respectively. We can thus discard the possibility that differences in PIP_2 concentrations underpin the different Nav current inactivation properties in Ins1 and HEK cells. Moreover, as PIP_2 is downstream of the insulin signalling pathway, these results support the lack of effect observed by the insulin receptor antagonist S961.

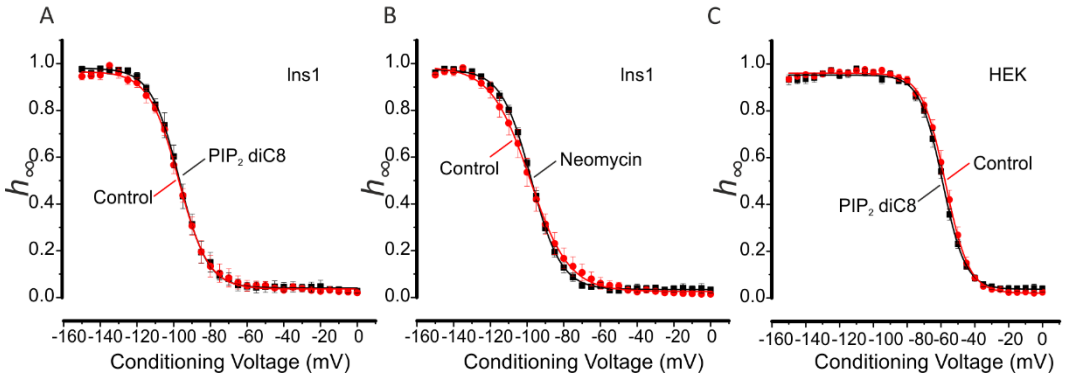


Figure 5.2.6.1- Effect of 50 μM PIP_2 diC8 on Nav current inactivation and activation in Ins1 cells

A, voltage-dependence of inactivation of Nav1.7 α-subunit co-expressed with β_1- and β_2-subunits in control (red; *n*=5) and 50μM PIP_2 diC8 treated (black; *n*=5) Ins1 cells. The curves represent a single Boltzmann fit to the data. *B*, same as in *A* but for control (red; *n*=7) and 50μM neomycin treated (black; *n*=7). *C*, same as in *A* but for HEK cells (red, *n*=8; black, *n*=7).

5.2.7 Effect of chronic and acute differences in the extracellular glucose concentration on the voltage-dependence of Na_V channel inactivation

Rat pancreatic β-cells demonstrate a more significant reduction in insulin secretion in response to TTX as the glucose concentration increases (Hiriart and Matteson, 1988). Although insulin secretion increases with increased glucose concentration, this is still surprising, given that most of the Na_V channels are inactivated at low glucose concentrations in rat β-cells and a greater proportion of them should become inactivated as an increase in glucose concentration depolarises the membrane potential further. One possible explanation for this is that an increase in glucose concentration modifies the voltage-dependence of inactivation to inactivate at more depolarised membrane potentials. Indeed, Na_V current inactivation has been reported to be regulated by the intracellular ATP concentration (Zou et al., 2013) suggestive of metabolic regulation. From a physiological perspective, this would provide an intuitive mechanism for increasing cell excitability and thus insulin secretion upon increases in glucose concentration.

To test this hypothesis, the inactivation of $Na_V1.7$ and $Na_V1.3$ was measured at 1 and 20mM extracellular glucose in Ins1 cells. The perforated patch configuration was used to allow the cell to remain metabolically intact. The inactivation curves of $Na_V1.7$ and $Na_V1.3$ at 1 and 20mM glucose are shown in Figure 5.2.7.1A and B, respectively, and summarisised in Supplementary Table 3. Acute changes in the extracellular glucose concentration had no effect on the inactivation of $Na_V1.7$ or $Na_V1.3$. The average V_h of $Na_V1.7$ at 1 and 20mM glucose is -91$\pm$3mV (n=8) and -92$\pm$2mV (n=8), respectively. Similar to the whole-cell configuration, 3/7 $Na_V1.3$

currents in the perforated patch configuration inactivated with two components, with $Na_V1.3$ currents in the remaining 4 cells inactivating with a single component of inactivation. The average V_h of cells with a single component of inactivation at 1 and 20mM glucose is -46±4mV (n=4) and -49±5mV (n=4), respectively. The V_h of cells inactivating with two components of inactivation at 1mM glucose is -84±2mV and -56±2mV (n=3), comprising of 44±9% and 56±8% of the total current, respectively. At 20mM glucose, the average V_h is -83±1mV and -58±1mV (n=3), comprising 58±11% and 42±10% of the total current, respectively.

As the recordings were done in perforated patch configuration, the series resistance of the recordings were high. However, the voltage error caused by the high series-resistance in this configuration would be the same at 1 and 20 mM glucose as there is no difference between the Na^+ current density (data not shown).

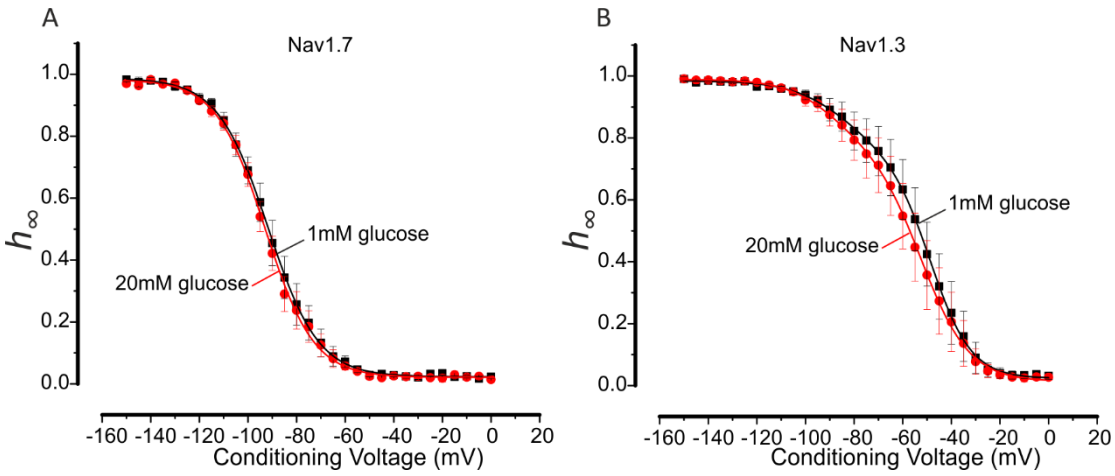


Figure 5.2.7.1 – Effect of acute changes in extracellular glucose concentration on the voltage-dependence of $Na_V1.7$ and $Na_V1.3$ channel inactivation.

A, voltage-dependence of inactivation (h_∞) of $Na_V1.7$ at 1mM (black; *n*=8) and 20mM glucose (red; *n*=8) in Ins1 cells. The curve represents a single Boltzmann fit to the data. *B*, same as in *A* but with $Na_V1.3$ at 1mM (black; *n*=7) and 20mM glucose (red; *n*=7) in Ins1 cells. The curve represents a double Boltzmann fit to the data. *C*, I-V relationship of $Na_V1.7$ at 1mM (black; *n*=6) and 20mM glucose (red; *n*=6) in Ins1 cells. *D*, same as in *C* but with experiments done with $Na_V1.3$ at 1mM (black; *n*=5) and 20mM glucose (red; *n*=5).

$Na_V1.3$ is the major channel expressed during embryogenesis in neurones (Waxman et al., 1994). Its expression is significantly reduced in neonates and undetectable in adult DRG neurones (Waxman et al., 1994). However, in axotomised peripheral DRG neurones, the expression of $Na_V1.3$ is upregulated and is associated with ectopic firing and spontaneous pain (Dib-Hajj et al., 2010, Waxman et al., 1994). We hypothesised that β-cell damage through exposure to chronic high glucose concentrations may also lead to an increased expression of $Na_V1.3$, which could have a beneficial effect on increasing insulin secretion (Zhang et al., 2014). We tested this hypothesis by culturing Ins1 cells at 5mM, 11mM and

25mM extracellular glucose concentrations for 48h, followed by measurements of Na_V channel α- and β-subunit gene expression. Contrary to expectation, a significant glucose-induced and concentration-dependent reduction in the mRNA expression of *Scn3a* could be observed (Figure 5.2.7.2A). However, the reduction of *Scn3a* mRNA expression did not translate into a reduction in Na^+ current density (Figure 5.2.7.2D). of *Scn3a* Ins1 cells do not express $Na_V1.7$ and changes in chronic extracellular glucose had no effect on *Scn9a* gene expression. The inactivation curves of endogenous Na_V currents recorded from Ins1 cells cultured in 5mM, 11mM and 25mM glucose were essentially superimposable (Figure 5.2.7.2B and summarised in Table 5.2.7.1). There was also no significant difference in the voltage-dependence of activation (Figure 5.2.7.2C).

Interestingly, the relative expression of *Scn3b* was also significantly reduced by increasing concentrations of glucose. Thus confirming results from Chapter 4, which show that modulation of Na_V current inactivation in β-cells is not regulated by Na_V channel β-subunits, as again the reduction in *Scn3b* expression was not associated with changes in Na_V current inactivation.

It is well known that glucose increases the intracellular NAD(P)H/NAD(P)-ratio, which would suggest that the redox state does not influence Na_V current inactivation. Although, direct redox sensitivity via cysteine oxidation is still possible and would have to be investigated. Interestingly, intracellular application of pyridine nucleotides such as NADH reduced Na_V currents via a mechanism mediated by PKC and mitochondrial production of reactive oxygen species (Liu et al., 2009, Liu et al., 2010). A similar reduction in Na^+ current density with increased glucose concentration could be observed at 10, 20 and 30mV (Figure

5.2.7.2D), suggesting that despite an increase in NADH there was no significant effect on Na_V current inactivation.

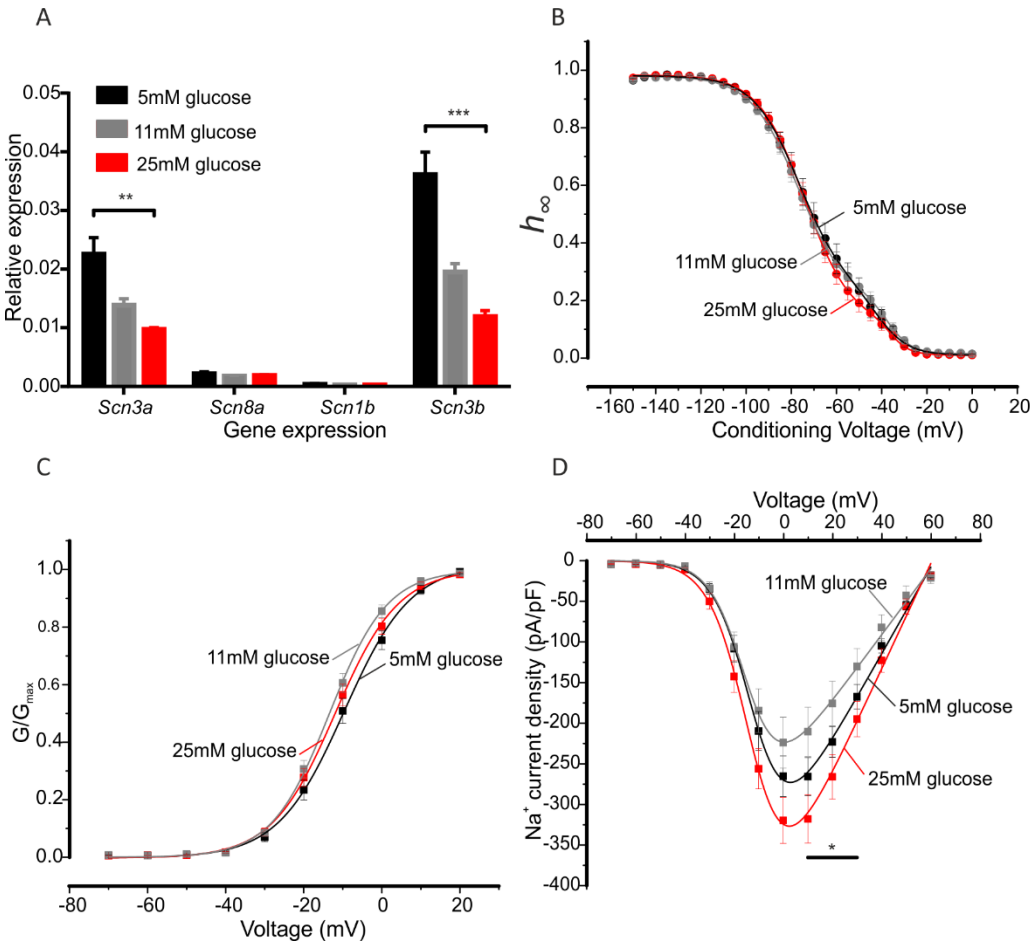


Figure 5.2.7.2 – Effect of chronic changes in glucose on channel inactivation

A, relative gene expression of *Scn3a*, *Scn8a*, *Scn1b* and *Scn3b* in Ins1 cells cultured at 5, 11 and 25mM glucose for 48h (n=3 preparations). ***P*<0.01, one way ANOVA, for relative *Scn3a* mRNA expression between Ins1 cells incubated at 5, 11 and 25mM glucose. ****P* <0.001, one way ANOVA of *Scn3b* mRNA expression between Ins1 cells incubated at 5, 11 and 25mM glucose. *B*, voltage-dependence of endogenous Na_V current inactivation (h_∞) recorded at 5mM glucose from Ins1 cells cultured at 5mM (black; *n*=22), 11mM (grey; *n*=22) and 25mM glucose (red; *n*=18). The curves represent a double Boltzmann fit to the data. *C*, voltage-dependence of endogenous Na_V current activation (G/G_{max}) recorded at 5mM glucose from Ins1 cells cultured at 5mM (black; *n*=21), 11mM (grey; *n*=22) and 25mM glucose (red; *n*=16). The curves represent a single Boltzmann fit to the data. *D*, I-V relationship of endogenous Na_V currents recorded at 5mM glucose from Ins1 cells cultured at 5mM (black; *n*=21), 11mM (grey; *n*=22) and 25mM glucose (red; *n*=16). **P*<0.05, one way ANOVA, for Na^+ current density at 10, 20 and 30mV between Ins1 cells incubated at 5, 11 and 25mM glucose.

Glucose concentration (mM)	Monophasic cells V_h(mV)	Biphasic cells V_h-1 (mV)	Biphasic cells V_h-2 (mV)
5	-70 ± 3 (16)	-80 ± 4 (6)	-41 ± 3 (6)
11	-74 ± 2 (13)	-73 ± 5 (9)	-43 ± 4 (9)
25	-72 ± 4 (7)	-78 ± 2 (11)	-39 ± 2 (11)

Table 5.2.7.1 – Inactivation of endogenous Na_V currents after chronic exposure to 5, 11 and 25mM glucose

Values represent mean ± SEM (*n*). V_h represents membrane potential at which inactivation is half-maximal in cells with monophasic inactivation. In cells with biphasic inactivation, V_h-1 and $V_h\tau 2$ represent the membrane potential at which inactivation is half-maximal for the current components inactivating at negative and positive membrane potentials, respectively.

5.2.8 Surface charge effect of Na_V current inactivation in Ins1 and HEK cells

Next we tested whether there was a difference in surface charge between Ins1 and HEK cells that might influence Na_V channel inactivation. One major source of negative charge is due to glycosylation of extracellular Na_V channel domains that consist of the carbohydrate derivative N-acetylneuraminic acid or sialic acid (Ednie and Bennett, 2012). To explore differences in surface charge we generated inactivation curves for $Na_V1.3$ in the presence of 0.2, 2 and 10mM extracellular Co^{2+} in Ins1 and HEK cells (Bennett et al., 1997; Bennett, 2002). The rationale was to reverse the effect of surface charge by increasing the extracellular concentration of divalent ions. Hypothetically, Na_V channels expressed in Ins1 cells might carry more negative charges than channels expressed in HEK cells (for example due to increased sialylation of the extracellular domains). Accordingly, the voltage difference sensed by the inactivation gate would be reduced and this

might explain the shift in inactivation towards more negative voltages. Figure 5.2.8.1A shows the relationship between the extracellular Co^{2+} concentration and V_h in Ins1 and HEK cells (see also Supplementary Table 3). However increasing the Co^{2+} concentration exhibited the same ~25mV shift in Ins1 and HEK cells and the difference between the two cells persisted. It is also evident that both the positive and negative components of $Na_V1.3$ inactivation in Ins1 cells are both shifted by ~25mV and that V_h values for the positive components superimpose on those obtained in HEK cells for all Co^{2+} concentrations.

The voltage-dependence of activation is the same for $Na_V1.3$ expressed in Ins1 and HEK cells at all extracellular Co^{2+} concentrations and (similar to inactivation) revealed an ~25mV depolarising shift with increasing extracellular cationic strength (Figure 5.2.8.1B). Thus illustrating that differences in extracellular surface charge should shift both the voltage-dependence of inactivation and activation by a similar magnitude.

Collectively, these data suggest that it is unlikely that differences in extracellular surface charges account for the negative Na_V current inactivation in Ins1 cells because (1) increasing the extracellular cationic strength shifted the voltage-dependence of inactivation of $Na_V1.3$ expressed in Ins1 and HEK cells by a similar magnitude and (2) there is no difference between the $V_{0.5}$ of channels expressed between Ins1 and HEK cells.

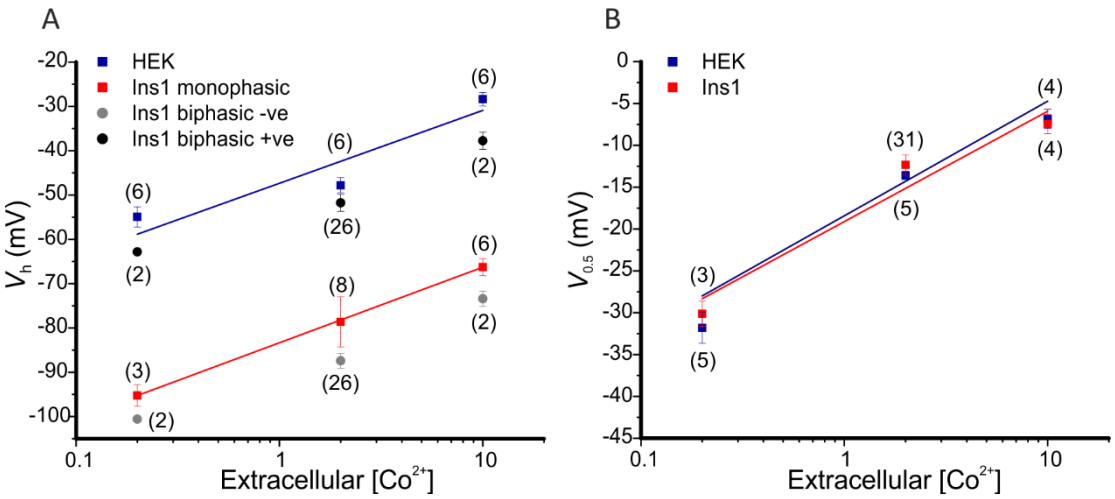


Figure 5.2.8.1- Effect of surface charge on the voltage-dependence of inactivation and activation of Na$_V$1.3 expressed in Ins1 cells

A, summarized voltage-dependence of inactivation of Na$_V$1.3 currents in Ins1 (red, grey and black) and HEK cells (blue) of indicated number of cells (*n*) at increasing concentrations of extracellular Co^{2+} (0.2, 2 and 10mM). The lines represent a linear regression fit to the data. *B*, same as in *A* but for voltage-dependence of activation of Na$_V$1.3 currents in Ins1 (red) and HEK cells (blue).

5.3 Discussion

Here we aimed to identify factors that regulate the hyperpolarised and/or biphasic voltage-dependence of Na$_V$ channel inactivation in rodent β-cells.

5.3.1 Post-translational modification of Na$_V$ channels in Ins1 cells

PTMs are protein modifications that can occur either after ribosome-mediated translation of mRNA or later in the secretory pathway. Modifications can include attachment of biochemical groups (phosphorylation), polypeptides (SUMOylation) or complex molecules (glycosylation) or cleavage of a protein's specific amino acid sequence. The overall effect of PTMs can lead to a modulation of the structure, function or localisation of the protein (Laedermann et al., 2015). Given that Na$_V$ channels maintained their hyperpolarised inactivation properties

upon excision of the membrane, it is possible that the cell-specific regulation of Na_V channel inactivation in insulin-secreting cells is regulated by a PTM.

Na_V channel α-subunits are highly phosphorylated proteins. As an example, 33 in vivo phosphorylation sites were identified on $Na_V1.2$ purified from rat brain (Baek et al., 2014). Phosphate groups each carry 2 negative charges at a physiological pH, which can alter the gating of the channel via an electrostatic effect and can also disrupt binding sites for interaction with other regulatory proteins (Narayanan and Jacobson, 2009). The protein kinases involved in the phosphorylation of Na_V channels include cAMP-dependent protein kinase A (PKA) (Costa et al., 1982, Aromolaran et al., 2017, Laedermann et al., 2015) , PKC (Tan et al., 2014, Vijayaragavan et al., 2004), mitogen-activated protein kinases (MAPKs) (Stamboulian et al., 2010, Wittmack et al., 2005), the Src family of non-receptor tyrosine kinases (Ahern et al., 2005, Francis et al., 2015) and Ca2+/calmodulin-dependent protein kinase II (CAMKII) (Young and Caldwell, 2005, Ben-Johny et al., 2015, Xu et al., 2013).

We investigated a possible involvement of PKC in the hyperpolarised and biphasic inactivation of Na_V currents in Ins1 cells, but observed no significant change to the voltage-dependence of inactivation. Moreover the Ca^{2+} chelator, BAPTA-AM, also produced no significant effect on the voltage-dependence of inactivation, suggesting no involvement of Ca^{2+}-dependent protein kinases, which include the conventional subfamily of PKC and CAMKII. The lack of effect produced by BAPTA-AM also suggests that inactivation is not regulated by a direct action of intracellular free Ca^{2+} binding to an EF-hand domain in the C-terminal of Na_V

channels, an effect described for $Na_V1.5$ that modulated the steady state inactivation of the current (Wingo et al., 2004).

We also explored the possibility that insulin modulates Na_V inactivation downstream of the insulin receptor, however, inhibition of insulin secretion by a K_{ATP} channel activator (diazoxide) and inhibition of insulin action by an insulin receptor antagonist (S961) had no effect on the voltage-dependence of inactivation in Ins1 cells. Moreover, altering the availability of PIP_2, which is downstream of the insulin signalling pathway also had no effect on Na_V inactivation in Ins1 cells.

In addition to phosphorylation, Na_V channels can undergo extensive glycosylation that can account for a remarkable 5% to 30% of the α-subunit's molecular weight (Cohen and Barchi, 1993, Messner and Catterall, 1985). Na_V channels undergo glycosylation steps in the endoplasmic reticulum and Golgi apparatus (Waechter et al., 1983, Schmidt and Catterall, 1987), a process that involves sequential addition of *N*-acteylglucosamines capped by sialic acid residues (Ednie and Bennett, 2012). At a physiological pH, the sialic acid residues are negatively charged and may thus interfere with the transmembrane potential difference detected by the voltage sensor domains. We tested whether a difference in surface charge between Ins1 and HEK cells might influence Na_V channel inactivation by increasing the cationic strength of the extracellular medium to mask the negative charges associated with sialylation. However, we can discard this possibility given that varying the extracellular cationic strength had the same effect in both cell types. In support of this, a difference in cell surface charge between Ins1 and HEK

cells should also produce a simultaneous shift in the voltage-dependence of activation between Ins1 and HEK cells which is not observed.

To specifically confirm that differential glycosylation between Na_V channels expressed in Ins1 and HEK cells does not underlie the difference in inactivation in these cell types, Na_V current inactivation could be compared after application of neuraminidase (Bennett et al., 1997), an enzyme that cleaves sialic acid residues, or after exposure to compounds that inhibit glycosylation, such as castanospermine, and swainsonine (Zhang et al., 1999).

SUMOylation, involving the covalent attachment of small ubiquitin-like modifier (SUMO) proteins has shown to influence the inactivation of voltage sensitive K^+ channel $K_V1.5$ (Benson et al., 2007) and have an indirect effect on $Na_V1.7$ trafficking via axonal collapsin response mediator protein 2 (CRMP2) (Dustrude et al., 2013). Although Na_V channel isoforms contain putative SUMOylation motifs, regulation of channel gating by this PTM remains to be investigated and could potentially underlie the hyperpolarised inactivation of Na_V channels in insulin-secreting cells.

From the experiments that we carried out, we do not have any evidence to show that PTMs are involved in the regulation of Na_V channels in Ins1 cells. However, given the extensive PTMs that Na_V channels undergo, perhaps the best approach to explore differences in PTM between β- and non-β-cells is to conduct mass spectrometry analysis of Na_V channels isolated from Ins1 and HEK cells.

5.3.2 Na_V channels in Ins1 cells are not regulated by a diffusible intracellular factor

We tested whether modulation of Na_V channels involves a diffusible intracellular cytoplasmic factor present in Ins1 cells by measuring the V_h of Na_V currents in an intact cell environment (cell-attached patch) and when the channels were removed from the cell environment (inside-out patch). Both $Na_V1.3$ and $Na_V1.7$ displayed a hyperpolarising shift in the voltage-dependence of inactivation in Ins1 and CHO cells. Since the hyperpolarising shift in V_h appears to be common to all cell types in the inside-out configuration (Cachelin et al., 1983, Jo and Bean, 2014), we would expect the V_h of $Na_V1.7$ and $Na_V1.3$ in Ins1 cells to converge with those expressed in CHO cells, if Ins1 cells did contain a diffusible factor that modulates the behaviour of Na_V currents. However, a ~15-20mV difference in the V_h of $Na_V1.7$ and $Na_V1.3$ persisted between Ins1 and CHO cells at different time points after excision. We also tested the converse hypothesis that HEK cells contain an intracellular factor that modulates the voltage-dependence of inactivation to depolarised potentials. However, insertion of Na_V channels expressed in Ins1 cells into HEK cells produced the same hyperpolarising shift to when the membrane was left in the extracellular solution.

It is possible, that a firmer interaction is maintained with Na_V channels that is not disrupted upon 'wash-out' of binding factors in the inside-out configuration. An example of such interactions may be with other proteins. Na_V channels can be part of multi-protein complexes composed of several interacting proteins, which regulate channel expression and function (Abriel, 2010). Interacting proteins have largely been described for $Na_V1.5$ due to their importance in inherited forms of cardiac arrhythmias (Vatta et al., 2006, Ueda et al., 2008, Wu et al., 2008, London et al., 2007, Valdivia et al., 2009). Proteins known to interact with Na_V channels that are also expressed in mouse β-cells (Benner et al., 2014) include

fibroblast growth factor homologous factor 1B (FHF1B) (Liu et al., 2003), cytosolic acid protein 14-3-3η (Allouis et al., 2006), glycerol-3-phosphate dehydrogenase 1-like protein (London et al., 2007, Valdivia et al., 2009) and plakophilin-2 (Sato et al., 2009). FHF1B influences both the voltage-dependence of activation and inactivation of $Na_V1.5$ via interaction with a proximal acidic rich domain of the C-terminus (Liu et al., 2003), a region of known importance to the regulation of steady-state inactivation (Mantegazza et al., 2001). Meanwhile 14-3-3η demonstrated a hyperpolarising shift in the inactivation of $Na_V1.5$ without any effect on the voltage-dependence of activation (Allouis et al., 2006). Indeed, our characterisation of $Na_V1.5$ in Ins1 and HEK cells also produced a hyperpolarising shift in inactivation without a change to the voltage-dependence of activation. To investigate the differences in protein interaction between β- and non-β-cells, immunoprecipitation of Na_V channels expressed in Ins1 and HEK cells followed by mass spectrometry analysis could be conducted. Yeast two-hybrid screening could also be an efficient method for identifying interacting partners.

We hypothesised that the hyperpolarised and the biphasic inactivation observed in Ins1 cells is regulated by the same mechanism but to different extents between $Na_V1.7$ and $Na_V1.3$. $Na_V1.7$ current inactivation could be more prone to modulation at hyperpolarised potentials than $Na_V1.3$ and hence they exhibit a predominant monophasic and biphasic voltage-dependence of inactivation, respectively. Therefore, we expected that by exploring the apparent differences between the biphasic voltage-dependence of inactivation between $Na_V1.7$ and $Na_V1.3$ we could find a site for Na_V channel modulation. Since the amino acid sequence of $Na_V1.7$ and $Na_V1.3$ is so similar (77%), we expected that the site(s) in which Na_V channels are modulated would be in regions of sequence dissimilarity

that predominantly exist in the cytosolic loops and termini. We generated chimeric channels based on the $Na_V1.7$ backbone by replacing the N-terminal domain, L1 and L2, the C-terminal domain or L3 sequences with the corresponding sequences of $Na_V1.3$. However, we observed no difference in the voltage-dependence of inactivation, the proportion of cells inactivating with a monophasic/biphasic inactivation or the proportion of current inactivating at negative and positive membrane potentials between the chimera and control $Na_V1.7$ channels. These results would suggest that the difference between Ins1 and other cell types is likely to reside within the plasma membrane itself and does not involve cytoplasmic factors.

Chapter 6

Discussion

6.1 Properties of Na_V inactivation in insulin-secreting cells

Pancreatic β-cells are equipped with voltage-gated Na_V channels that inactivate at hyperpolarised membrane potentials, so characteristic that it can be used for functional identification of β-cells (Briant et al., 2017a, Chakravarthy et al., 2017). However, a small Na^+ current component (10-15%) that inactivates over physiological membrane potentials and contributes to action potential firing also exists. The aim of this thesis was to understand the contribution of individual Na_V channel α-subunits to the behaviour of Na_V current inactivation in rodent β-cells and to investigate the underlying mechanism(s) of channel regulation. We generated mutant TTX-resistant Na_V channels, which allowed us to isolate and characterise the expressed channels by blocking the endogenous Na_V channels with TTX.

6.1.1 Hyperpolarised inactivation of $Na_V1.3$, $Na_V1.5$, $Na_V1.6$ and $Na_V1.7$ channels in Ins1 cells vs non-β-cells

Characterisation of individual Na_V channel α-subunits ($Na_V1.3$, $Na_V1.6$, $Na_V1.5$ and $Na_V1.7$) in Ins1 cells compared to three other non-β-cell types (HEK, CHO and αTC1-6 cells), revealed that all four channels inactivate at ~20-30mV more negative membrane potentials when expressed in Ins1 cells. These results are in contrast to that expected from genetic ablation studies in rodent β-cells, in which it was postulated that $Na_V1.7$ is modulated in a rodent β-cell-specific manner to inactivate over hyperpolarised membrane potentials, whilst $Na_V1.3$ inactivates over physiological membrane potentials similar to that observed in other cell types (Zhang et al., 2014). Despite the shift in the voltage-dependence of

inactivation between Ins1 and non-β-cell types, we confirm that inactivation of $Na_V1.7$ occurs at more negative membrane potentials than $Na_V1.3$ and $Na_V1.6$ in Ins1 cells, consistent with the previous study. However, the hyperpolarised inactivation of $Na_V1.7$ is not specific to Ins1 cells as a similar observation was made in HEK, CHO, αTC1-6 and EndoC-βh2 cells. Thus, although the Na_V α-subunit expressed makes a significant difference to the voltage-dependence of inactivation, it appears that there is also an additional cell-specific modulation in Ins1 cells that shifts inactivation of Na_V channels to functionally irrelevant membrane potentials.

The 20-30mV shift in the voltage-dependence of inactivation between Ins1 and HEK cells for all the Na_V channels that we characterised (with the exception of $Na_V1.6$) occurred without a significant difference in the voltage-dependence of activation. Since there is no overlap between the voltage-dependence of inactivation and activation in Ins1 cells, our data does not favour the strict coupling of inactivation to activation proposed by several models (Hille, 2001, Armstrong, 2006). Amino acid substitutions in the voltage sensor which shift the voltage-dependence of inactivation to a hyperpolarised potential and simultaneously shift the voltage-dependence of activation to a depolarised potential also militate against the dependence of inactivation on activation (Kontis and Goldin, 1997, Ulbricht, 2005). Moreover introducing a short (1ms) pre-pulse to -70mV in the inactivation protocol, after a conditioning voltage to hyperpolarised potentials (-150mV) and prior to depolarisation to 0mV, causes a reduction in the peak current amplitude compared to the protocol in which the -70mV pre-pulse is absent. As Na_V currents are not activated at -70mV, it suggests

that inactivation of the current occurs without activation of the channel. The vast difference between the V_h and $V_{0.5}$ (~60-80mV) of Na_V channels expressed in Ins1 cells suggests an alternative mechanism for Na_V inactivation that is independent of activation.

6.1.2 Biphasic inactivation of individual Na_V channel α-subunits

In addition to the different α-subunits contributing to the biphasic inactivation of Na_V currents in insulin-secreting cells, we unexpectedly found that individual Na_V subtypes exhibit two distinct inactivation behaviours. Thus, in >75% of the experiments with $Na_V1.3$ expressed in Ins1 cells, two distinct components of inactivation (each accounting for – on average - ~50% of the total current) separated by ~30mV were observed. Biphasic inactivation was also observed for $Na_V1.7$ (in 20% of experiments) and $Na_V1.6$ (60%) expressed in Ins1 cells. In Ins1 cells that exhibited biphasic inactivation, the V_h for the component inactivating at more depolarised membrane potentials is very similar to that found in HEK or CHO cells, whilst the V_h for the more hyperpolarised component is ~-90mV. In cells that displayed monophasic inactivation, inactivation proceeded within either of the two distinct V_h ranges observed in cells that exhibited biphasic inactivation.

Likewise, primary mouse β-cells also appear to exhibit a biphasic voltage-dependence of inactivation. The net $Na_V1.3$ current isolated by subtracting the currents recorded from the $Na_V1.3$-deficient cells from control cells similarly displayed a biphasic voltage-dependence of inactivation. Importantly, biphasic inactivation was not observed when these channels were instead expressed in HEK, CHO, αTC1-6 or EndoC-βh2 cells. Therefore, similar to

the hyperpolarised inactivation of Na_V currents in Ins1 cells, the biphasic voltage-dependence of inactivation also demonstrates both species and cell-specific modulation.

6.2 Na_V inactivation in Ins1 cells: a possible model

An explanation of these data would have to account both for the fact that inactivation of all studied Na_V subtypes is shifted by 20-30 mV in Ins1 cells relative to that seen in other cell types (HEK, CHO etc.) and the finding that biphasic Na^+ current inactivation is observed also when a single Na_V subtype is expressed. We speculate that the mechanism that underlies the hyperpolarised inactivation of $Na_V1.7$ and the biphasic inactivation of $Na_V1.3$ are the same. However $Na_V1.7$ channels are more prone to modulation at hyperpolarised potentials than $Na_V1.3$ and hence they exhibit a predominant monophasic and biphasic voltage-dependence of inactivation, respectively.

Given that the chimeric channels showed no significant difference compared to $Na_V1.7$ channels and that there was no difference in the change of V_h in the inside-out configuration we speculate that the differences in Na_V channel inactivation between Ins1 and HEK cells is likely to reside within the plasma membrane.

The plasma membrane lipidome is extremely complex and contains >2000 lipid subtypes (Galbiati et al., 2001, Simons and Ehehalt, 2002). The distribution of lipids within the plasma membrane is not uniform but shows considerable regional differences. Indeed, the plasma membrane has been described as a 'patchwork of different lipid environments' (Edidin, 1993). Perhaps the best known example of such lipid aggregates are the lipid rafts that are enriched in

cholesterol. There are many examples that lipid microdomains and cholesterol affect ion channel function (Dart, 2010). For example, depletion of membrane cholesterol in HEK cells results in a ~10mV hyperpolarising shift in $Na_V1.4$ current inactivation, an effect that is partially reversible by subsequent cholesterol enrichment (Lundbaek et al., 2004). Moreover, in β-cells, cholesterol depletion causes a hyperpolarizing shift in the inactivation curve of $K_V2.1$ channels (Xia et al., 2004).

We therefore propose that the lipidome of the rodent β-cell plasma membrane is different from that of HEK and most other cells and that the rodent β-cell membrane contains specialized lipid domains that shift inactivation into very negative membrane potentials. Na^+ channels outside these domains behave exactly as in other cell types. Indeed, in cells showing biphasic Na_V current inactivation, the positive component shows essentially the same voltage-dependence as in non-β-cells (see schematic in Figure 6.1.2.1).

The true nature of these specialised domains remains to be established but that such domains exist is suggested by the cell-attached measurements in which a small part of the cell (1μm^2) is isolated and where channel inactivation was invariably monophasic but with V_h values varying between -80 and -55mV. We speculate that this is because all channels within an individual patch reside in a uniform membrane environment, which may differ between patches. It is interesting that the 'inactivation curve' for $Na_V1.3$ channels reconstructed from the cumulative distribution of V_h in cell-attached patches was biphasic (with V_h values of -75mV and -55mV) and resembled that which can be recorded from individual cells expressing this α-subunit. For $Na_V1.7$, the cumulative distribution

was monophasic with a V_h of ~-90 mV. Notably, 10% of the patches had V_h values ~30mV more positive. This is in agreement with the whole-cell data indicating biphasic inactivation in <20% of the cells expressing Na$_V$1.7. The idea that negative and positive inactivation results from insertion of the α-subunits into membrane domains of different composition might seem in conflict with observation that the fraction of Na$_V$ channels inactivating at negative and positive membrane potentials varied for Nav1.3, Nav1.6 and Nav1.7. However, it is possible that the intracellular trafficking and their association with distinct membrane domains is α-subunit-dependent.

We recognise that not all of our data fits the suggested model for modulation of Na$_V$ channels in rodent β-cells. For example the monophasic inactivation of Na$_V$ currents at negative membrane potentials does not suggest that the rodent β-cell membrane contains 'specialized lipid domains that shift inactivation into very negative membrane potentials'. The model that we propose attempts to consolidate the two observations observed in rodent β-cells: (1) the hyperpolarised voltage-dependence of inactivation of Na$_V$ currents and (2) the biphasic inactivation of Na$_V$ currents. However, it possible that these two observations are regulated by different mechanisms.

This hypothesis remains to be tested and we acknowledge that other mechanisms of Na$_V$ channel modulation by PTM and protein-protein interactions remain possible and can be explored by mass spectrometry and/or yeast-two hybrid screening, respectively.

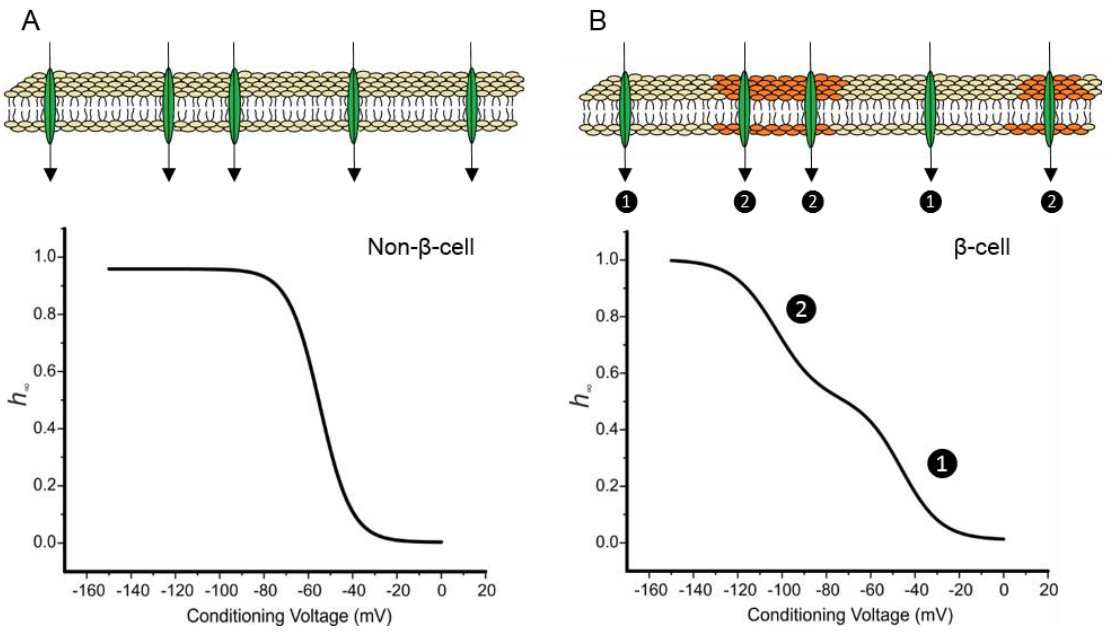


Figure 6.1.2.1- Biphasic inactivation of Na$_V$ currents in Ins1 cells

Schematic of Na$_V$ channel inactivation in non-β-cells (A) and β-cells (B). In non-β-cells, the plasma membrane is uniform in terms of impact on Na$_V$ current inactivation and the relationship between membrane potential and the fraction of activatable Na$_V$ channels (h_∞). However, rodent β-cells contain specialised domains that differ from the rest of the plasma membrane. Na$_V$ channels within these domains undergo inactivation at more negative membrane potentials whereas Na$_V$ channels outside these regions inactivate with the same voltage-dependence as the corresponding Na$_V$ channels when expressed in non-β-cells. Thus, the Ins1 cell will contain two electrophysiologically distinct populations of Na$_V$ channels (❶ and ❷), accounting for the biphasic Na$_V$ current inactivation.

6.3 Physiological significance of Na$_V$ inactivation properties in rodent β-cells

The physiological significance of the hyperpolarised inactivation in rodent β-cells remains to be established. To our knowledge the only other cell type in which Na$_V$ currents inactivate at such hyperpolarised membrane potentials is mouse olfactory sensory neurons (Ahn et al., 2011). These neurons predominantly

express $Na_V1.7$ and the V_h of Na_V currents recorded from this cell type are ~-100mV. Despite the negative inactivation of current, Na_V channels still play a significant role in olfaction as global knockout of *Scn9a* is responsible for generating neonatally lethal mice, which are anosmic and consequently do not feed (Nassar et al., 2004, Goldberg et al., 2007, Nilsen et al., 2009, Weiss et al., 2011). It is possible that Na_V channels have a non-canonical role (Black and Waxman, 2013) in this cell type as they are unlikely to contribute to the excitability of the cell due to their hyperpolarised inactivation. Unlike olfactory sensory neurons, knockdown of $Na_V1.7$ in mouse β-cells exhibited no phenotype to suggest a physiological role of these channels in mouse β-cells.

6.4 Na_V channels in disease

Because of the crucial function of Na_V channels in excitable cells and the complexity of their structure, a large number of genetic diseases are caused by its mutation (Catterall et al., 2008, Lehmann-Horn and Jurkat-Rott, 1999). More than 300 mutations in the *SCN5A* gene, which encodes the cardiac $Na_V1.5$ channel, have been described in association with Brugada syndrome (Meregalli et al., 2009). The genetic disease is characterised by an abnormal electrocardiograph and leads to arrhythmias, ventricular fibrillation and increased risk of sudden death (Brugada, 2016). Mutations in $Na_V1.1$, $Na_V1.2$ and $Na_V1.3$ have been implicated in childhood forms of epilepsy (Holland et al., 2008).

6.4.1 Na_V channels and diabetes

It has been hypothesised that diabetes and peripheral neuropathy (commonly associated with diabetes) occur as a consequence of mutations in $Na_V1.7$ that confer increased susceptibility for both diseases, rather than the more commonly assumed idea that peripheral neuropathy is a consequence of hyperglycaemia associated with diabetes (Hoeijmakers et al., 2014). The mutations in $Na_V1.7$ are suggested to depolarise the membrane potential and lead to β-cell and small nerve fibres injury. However, this hypothesis remains to be tested and Na_V channel α-subunits have not yet been associated with diabetes according to genome-wide association studies.

However, inhibition of the late Na^+ current by the antianginal drug, ranolazine has shown to have anti-diabetic effects. In animal models of diabetes ranolazine reduced postprandial and basal glucagon levels, which was associated with a reduction in hyperglycaemia (Dhalla et al., 2014). The proposed mechanism of action for this is that ranoloazine blocks Na_V channels in pancreatic α-cells, inhibiting their electrical activity and reducing glucagon secretion. However, ranolazine only had an effect on glucose-stimulated insulin secretion when Na_V current was enhanced either pharmacologically by veratridine (a blocker of Na_V channel inactivation) or by long term incubation at high (33mM) glucose (Rizzetto et al., 2015).

6.4.2 Na_V channels and pain

One of the striking examples of Na_V channel mutations leading to disease, is the nonsense mutation in the gene *Scn9a*, which results in a non-functional $Na_V1.7$ channel, and causes a congenital inability to perceive any form of pain (Cox et al.,

2006). $Na_V1.7$ channels are strongly expressed in the nerve terminals of nociceptive DRG neurones (Dib-Hajj et al., 2010). Whilst the channel had already been shown to be involved in nociception in both humans and rodents, this was the first study to show that functional $Na_V1.7$ expression is an essential and non-redundant requirement for nociception in humans (Cox et al., 2006). In contrast, dominantly inherited gain-of-function mutations in $Na_V1.7$ are linked to hypersensitivity to pain, as found in individuals suffering from inherited erythromelalgia (IEM) and paroxysmal extreme pain disorder (PEPD) (Yang et al., 2004, Fertleman et al., 2006). Symptoms of IEM usually appear in childhood and are characterised by severe episodic burning pain, localised to the feet and hands, in response to warm stimuli and exercise (Dib-Hajj et al., 2013). PEPD is distinct from IEM and typically starts in early infancy. It is associated with severe perirectal pain, which is accompanied with skin flushing of the lower or upper body or face, in a harlequin pattern (Dib-Hajj et al., 2013).

To date, functional characterisation of mutations in $Na_V1.7$ that lead to IEM have all shown a shift in the voltage-dependence of activation in a hyperpolarised direction, increase ramp current and slow deactivation, all of which result in enhanced DRG neuron hyperexcitability (Dib-Hajj et al., 2013). Mutations in *SCN9A* that are linked to IEM can also impair slow inactivation, which again enhances DRG neuron hyperexcitability (Sheets et al., 2007). Meanwhile other IEM mutations enhance slow inactivation and therefore attenuate cell excitability (Cheng et al., 2011).

PEPD-associated *SCN9A* mutations produce different effects on $Na_V1.7$ channel gating compared to IEM-linked mutations. PEPD-associated mutations shift the

voltage-dependence of steady state fast inactivation towards a depolarising direction (Fertleman et al., 2006). Since the V_h of most Na_V channels are around the resting membrane potential of a cell, slight depolarising shifts in V_h can cause significant changes leading to a gain of cellular excitability. Furthermore, depending on the specific mutations channel inactivation can be made incomplete, resulting in a persistent Na^+ current (Dib-Hajj et al., 2013). PEPD mutant $Na_V1.7$, can also manifest increased resurgent current (Jarecki et al., 2010). Collectively, these alterations to channel gating in both IEM and PEPD reduce the threshold for single action potentials and increase the frequency of firing in DRG neurones (Dib-Hajj et al., 2013). Hence there is an increased cellular excitability and hypersensitivity to pain as observed in these patients.

Na_V channels also play an important role in non-inherited acquired pain disorders. Nerve fibre damage or dysfunction, is usually accompanied by tissue injury, which can be caused by axotomy of peripheral axons, inflammation and in some cases longstanding hyperglycaemia associated with diabetic disease states. In axotomised peripheral DRG neurones, the expression of $Na_V1.3$ is upregulated and is associated with ectopic firing and spontaneous pain (Dib-Hajj et al., 2010, Waxman et al., 1994). In such cases, $Na_V1.7$ also accumulates in nerve endings and phosphorylation of the channel produces a graded hyperpolarisation of channel activation, suggesting that $Na_V1.7$ also contributes to injury-mediated DRG neuron hyperexcitability (Stamboulian et al., 2010, Dib-Hajj et al., 2013). Moreover, $Na_V1.7$ expression is increased in DRG neurones of diabetic rats (Chattopadhyay et al., 2008, Chattopadhyay et al., 2011). A change that is predicted to contribute to hyperexcitabilty associated with pain, as knockdown of

$Na_V1.7$ attenuates pain in rats with painful diabetic neuropathy (Chattopadhyay et al., 2012).

6.4 Concluding remarks

Rodent pancreatic β-cells present a fascinating environment in which the voltage-dependence of Na_V current inactivation is modified in a cell-specific manner. If the negative shift of inactivation in rodent β-cells could be harnessed, it may provide a novel means of regulating Na_V channel activity. As described $Na_V1.7$ channels play an important role in pain perception (Cox et al., 2006, Dib-Hajj et al., 2013). If the inactivation of the $Na_V1.7$ channels in nociceptive neurons became more like that in rodent β-cells, then the channels would inactivate and thus be unavailable for action potential propagation, which may represent a novel means of pain relief, especially in disease states associated with $Na_V1.7$ hyperexcitability (Dib-Hajj et al., 2008).

Appendix

$Na_v1.7$ and $Na_v1.3$ chimeras constructs.
CLUSTAL format alignment of $Na_v1.7$ (NP_002968) and $Na_v1.3$ (NP_008853) amino acid sequences was performed using MAFFT software. Corresponding residue numbers are labelled on the left. Sequences of the generated chimeric alpha subunits are shown at the bottom. Only partial alignments of the regions where changes were introduced are depicted. $Na_v1.3$ sequences introduced into $Na_v1.7$ backbone are highlighted in yellow.

N-terminal domain chimera

```
Nav1.7       1 M--AMLPPPGPQSFVHFTKQSLALIEQRIAERKSKEPKEEKKDDDEEAPKPSSDLEAGKQ
Nav1.3       1 MAQALLVPPGPESFRLFTRESLAAIEKRAAEEKAKKPKKEQDNDDENKPKPNSDLEAGKN
                 *  *:* ****:**  **::*** **:* **.*:*:**:*:.:***: ***.*******:
N-term           MAQALLVPPGPESFRLFTRESLAAIEKRAAEEKAKKPKKEQDNDDENKPKPNSDLEAGKN

Nav1.7      59 LPFIYGDIPPGMVSEPLEDLDPYYADKKTFIVLNKGKTIFRFNATPALYMLSPFSPLRRI
Nav1.3      61 LPFIYGDIPPEMVSEPLEDLDPYYINKKTFIVMNKGKAIFRFSATSALYILTPLNPVRKI
                 ********** ************ :******:****:****.**.***:*:*:.*:*:*
N-term           LPFIYGDIPPEMVSEPLEDLDPYYINKKTFIVMNKGKAIFRFSATSALYILTPLNPVRKI

Nav1.7     119 SIKILVHSLFSMLIMCTILTNCIFMTMNNPPDWTKNVEYTFTGIYTFESLVKILARGFCV
Nav1.3     121 AIKILVHSLFSMLIMCTILTNCVFMTLSNPPDWTKNVEYTFTGIYTFESLIKILARGFCL
               :**********************:***:.**********************:********:
N-term           AIKILVHSLFSMLIMCTILTNCIFMTMNNPPDWTKNVEYTFTGIYTFESLVKILARGFCV
```

L1L2 chimera

```
Nav1.7     399 AVVAMAYEEQNQANIEEAKQKELEFQQMLDRLKKEQEEAEAIAAAAAEYTSIRRSRIMGL
Nav1.3     421 AVVAMAYEEQNQATLEEAEQKEAEFQQMLEQLKKQQEEAQAVAAASA--ASRDFSGIGGL
               *************.:***:*** ******::***:****:*:***:*  :*   * * **
L1L2             AVVAMAYEEQNQATLEEAEQKEAEFQQMLEQLKKQQEEAQAVAAASA--ASRDFSGIGGL

Nav1.7     459 S---ESSSETSKLSSKSAKERRNRRKKKNQKKLSSGEEKGDAEKLSKSESEDSIRRKSFH
Nav1.3     479 GELLESSSEASKLSSKSAKEWRNRRKKRRQREHLEGNNKGERDSFPKSESEDSVKRSSFL
               .   *****:********** ******:.*::  .*::**: :.:.********::*.**
L1L2             GELLESSSEASKLSSKSAKEWRNRRKKRRQREHLEGNNKGERDSFPKSESEDSVKRSSFL

Nav1.7     516 LGVEGHRRAHEKRLSTPNQSPLSIRGSLFSARRSSRTSLFSFKGRGRDIGSETEFADDEH
Nav1.3     539 FSMDGNRLTSDKKFCSPHQSLLSIRGSLFSPRRNSKTSIFSFRGRAKDVGSENDFADDEH
               :.::*:* : :*::.:*:** *********.**.*:**:***:**.:*:***.:******
L1L2             FSMDGNRLTSDKKFCSPHQSLLSIRGSLFSPRRNSKTSIFSFRGRAKDVGSENDFADDEH

Nav1.7     576 SIFGDNESRRGSLFVPHRPQERRSSNISQASRSP---PMLPVNGKMHSAVDCNGVVSLVD
Nav1.3     599 STFEDSESRRDSLFVPHRHGERRNSNVSQASMSSRMVPGLPANGKMHSTVDCNGVVSLVG
               * * *.****.*******  ***.**:**** *.   * **.******:**********.
L1L2             STFEDSESRRDSLFVPHRHGERRNSNVSQASMSSRMVPGLPANGKMHSTVDCNGVVSLVG

Nav1.7     633 GRSALMLPNGQLLPEGTTNQIH-KKRRCSSYLLSEDMLNDPNLRQRAMSRASILTNTVEE
Nav1.3     659 GPSALTSPTGQLPPEGTTTETEVRKRRLSSYQISMEMLEDSSGRQRAVSIASILTNTMEE
               * ***  *.*** *****.: . :*** *** :* :**:*.. ****:* *******:**
L1L2             GPSALTSPTGQLPPEGTTTETEVRKRRLSSYQISMEMLEDSSGRQRAVSIASILTNTMEE
```

```
Nav1.7    692 LEESRQKCPPWWYRFAHKFLIWNCSPYWIKFKKCIYFIVMDPFVDLAITICIVLNTLFMA
Nav1.3    719 LEESRQKCPPCWYRFANVFLIWDCCDAWLKVKHLVNLIVMDPFVDLAITICIVLNTLFMA
              ********** *****: ****:*.  *:*.*: : :**********************
L1L2          LEESRQKCPPCWYRFANVFLIWDCCDAWLKVKHLVNFIVMDPFVDLAITICIVLNTLFMA


Nav1.7    752 MEHHPMTEEFKNVLAIGNLVFTGIFAAEMVLKLIAMDPYEYFQVGWNIFDSLIVTLSLVE
Nav1.3    779 MEHYPMTEQFSSVLTVGNLVFTGIFTAEMVLKIIAMDPYYYFQEGWNIFDGIIVSLSLME
              ***:****:*..**::*********:******:****** *** ******.:**:***:*
L1L2          MEHHPMTEEFKNVLAIGNLVFTGIFAAEMVLKLIAMDPYEYFQVGWNIFDSLIVTLSLVE


Nav1.7    812 LFLADVEGLSVLRSFRLLRVFKLAKSWPTLNMLIKIIGNSVGALGNLTLVLAIIVFIFAV
Nav1.3    839 LGLSNVEGLSVLRSFRLLRVFKLAKSWPTLNMLIKIIGNSVGALGNLTLVLAIIVFIFAV
              * *::**************************************************
L1L2          LFLADVEGLSVLRSFRLLRVFKLAKSWPTLNMLIKIIGNSVGALGNLTLVLAIIVFIFAV


Nav1.7    872 VGMQLFGKSYKECVCKINDDCTLPRWHMNDFFHSFLIVFRVLCGEWIETMWDCMEVAGQA
Nav1.3    899 VGMQLFGKSYKECVCKINDDCTLPRWHMNDFFHSFLIVFRVLCGEWIETMWDCMEVAGQT
              ************************************************************:
L1L2          VGMQLFGKSYKECVCKINDDCTLPRWHMNDFFHSFLIVFRVLCGEWIETMWDCMEVAGQA


Nav1.7    932 MCLIVYMMVMVIGNLVVLNLFLALLLSSFSSDNLTAIEEDPDANNLQIAVTRIKKGINYV
Nav1.3    959 MCLIVFMLVMVIGNLVVLNLFLALLLSSFSSDNLAATDDDNEMNNLQIAVGRMQKGIDYV
              *****:*:****************************:* ::* : ******* *::***:**
L1L2          MCLIVYMMVMVIGNLVVLNLFLALLLSSFSSDNLAATDDDNEMNNLQIAVGRMQKGIDYV


Nav1.7    992 KQTLREFILKAFSKKPKISREIRQAEDLNTKKENYISNHTLAEMSKGHNFLKEKDKIS--
Nav1.3   1019 KNKMRECFQKAFFRKPKV-IEIHEG----NKIDSCMSNNTGIEISKELNYLRDGNGTTSG
              *:.:** : *** :***:  **::.    .* :. :**:*  *:**  *:*:: :  :
L1L2          KNKMRECFQKAFFRKPKV-IEIHEG----NKIDSCMSNNTGIEISKELNYLRDGNGTTSG


Nav1.7   1050 -GFGSSVDKHLMEDSDGQSFIHNPSLTVTVPIAPGESDLENMNAEELSSDSDSEYSKVRL
Nav1.3   1074 VGTGSSVEKYVIDENDYMSFINNPSLTVTVPIAVGESDFENLNTEEFSSESELEESKEKL
               * ****:*::::::*  ***:*********** ****:**:*:**:**:*: * ** :*
L1L2          VGTGSSVEKYVIDENDYMSFINNPSLTVTVPIAVGESDFENLNTEEFSSESELEESKEKL


Nav1.7   1109 NRSSSSECSTVDNPLPGEGEEAEAEPMNSDEPEACFTDGCVRRFSCCQVNIESGKGKIWW
Nav1.3   1134 NATSSSEGSTVDVVLPREGEQAETEPEEDLKPEACFTEGCIKKFPFCQVSTEEGKGKIWW
              * :**** ****  ** ***:**:** :. :******:**:::*. ***. *.*******
L1L2          NATSSSEGSTVDVVLPREGEQAETEPEEDLKPEACFTEGCIKKFPFCQVSTEEGKGKIWW


Nav1.7   1169 NIRKTCYKIVEHSWFESFIVLMILLSSGALAFEDIYIERKKTIKIILEYADKIFTYIFIL
Nav1.3   1194 NLRKTCYSIVEHNWFETFIVFMILLSSGALAFEDIYIEQRKTIKTMLEYADKVFTYIFIL
              *:*****.****.***:***:*****************::**** :******:*******
L1L2          NLRKTCYSIVEHSWFESFIVLMILLSSGALAFEDIYIERKKTIKIILEYADKIFTYIFIL
```

L3 chimera

```
Nav1.7   1409 NVDKQPKYEYSLYMYIYFVVFIIFGSFFTLNLFIGVIIDNFNQQKKKLGGQDIFMTEEQK
Nav1.3   1431 DVKLQPVYEENLYMYLYFVIFIIFGSFFTLNLFIGVIIDNFNQQKKKFGGQDIFMTEEQK
              :*. ** ** .****:***:**************************:************
L3            NVDKQPKYEYSLYMYIYFVVFIIFGSFFTLNLFIGVIIDNFNQQKKKFGGQDIFMTEEQK

Nav1.7   1409 KYYNAMKKLGSKKPQKPIPRPGNKIQGCIFDLVTNQAFDISIMVLICLNMVTMMVEKEGQ
Nav1.3   1431 KYYNAMKKLGSKKPQKPIPRPANKFQGMVFDFVTRQVFDISIMILICLNMVTMMVETDDQ
              **********************.**:** :**:**.*.******:************.:.*
L3            KYYNAMKKLGSKKPQKPIPRPANKFQGMVFDLVTNQAFDISIMVLICLNMVTMMVEKEGQ
```

C-terminal domain chimera

```
Nav1.7   1829 DILFAFTKRVLGESGEMDSLRSQMEERFMSANPSKVSYEPITTTLKRKQEDVSATVIQRA
Nav1.3   1851 DILFAFTKRVLGESGEMDALRIQMEDRFMASNPSKVSYEPITTTLKRKQEEVSAAIIQRN
              ******************:** ***:***::********************:***::***
C-term        DILFAFTKRVLGESGEMDALRIQMEDRFMASNPSKVSYEPITTTLKRKQEEVSAAIIQRN

Nav1.7   1889 YRRYRLRQNVKNISSIYIKDGDRDD-DLLNKKDMAFDNVNENSSPEKTDATSSTTSPPSY
Nav1.3   1911 FRCYLLKQRLKNISSNYNKEAIKGRIDLPIKQDMIIDKLNGNSTPEKTDGSSSTTSPPSY
              :* * *:*.:***** * *:. :.  **  *:** :*::* **:*****.:*********
C-term        FRCYLLKQRLKNISSNYNKEAIKGRIDLPIKQDMIIDKLNGNSTPEKTDGSSSTTSPPSY

Nav1.7   1948 DSVTKPDKEKYEQDRTEKEDKGKDSKESKK
Nav1.3   1971 DSVTKPDKEKFEKDKPEKESKGKEVRENQK
              **********:*:*:.***.***: :*.:*
C-term        DSVTKPDKEKFEKDKPEKESKGKEVRENQK
```

Cell	α-subunit	β_1- and β_2-subunit V_h (mV)	k	β_1- and β_2-subunit V_h-1 (mV)	k_1	β_1- and β_2-subunit V_h-2 (mV)	k_2	β_3-subunit V_h (mV)	k	β_3-subunit V_h-1 (mV)	k_1	β_3-subunit V_h-2 (mV)	k_2	GFP V_h (mV)	k
Ins1	$Na_V1.3$	-79±6 (8)	9±1 (8)	-87±2(26)	9±1 (26)	-55±2(26)	7±1 (26)	-72±10 (3)	9±2 (3)	-84±2 (8)	11±1 (8)	-46±2 (8)	5±1 (8)		
Ins1	$Na_V1.5$	-99±2 (9)	8±1 (9)	N/A	N/A	N/A	N/A	N/A	N/A	N/A	N/A	N/A	N/A		
Ins1	$Na_V1.6$	-73±4 (10)	8±1 (10)	-86±1(25)	8±1 (25)	-56±1(25)	6±1 (25)	-86±1(11)	9±1 (11)	-87±2 (7)	9±1 (7)	-54±2 (7)	5±1 (7)		
Ins1	$Na_V1.7$	-94±2 (38)	9±1 (38)	-97±4 (9)	8±1 (9)	-67±4 (9)	10±2 (9)	-89±2(8)	11±1 (8)	-86 (1)	6 (1)	-68 (1)	14 (1)		
HEK	$Na_V1.3$ WT	-50±2 (14)	8±1 (14)												
HEK	$Na_V1.5$ WT	-77±1 (10)	6±1 (10)												
HEK	$Na_V1.6$ WT	-53±1 (13)	8±1 (13)												
HEK	$Na_V1.7$ WT	-67±2 (6)	8±1 (6)												
HEK	$Na_V1.3$	-48±1 (7)	10±2 (7)					-48±2 (12)	7±1 (12)					-59±3 (10)	8±1 (10)
HEK	$Na_V1.6$	-53±1 (10)	7±1 (10)												
HEK	$Na_V1.7$	-66±2 (9)	8±1 (9)					-70±3 (9)	8±1 (9)					-66±2 (12)	9±1 (12)
EndoC-βh2	$Na_V1.3$	-61±1(10)	6±1 (10)												
EndoC-βh2	$Na_V1.6$	-56±2(9)	7±1 (9)												
EndoC-βh2	$Na_V1.7$	-71±1(10)	6±1 (10)												
CHO	$Na_V1.3$	-50 ± 2 (13)	7±1 (13)												

Cell	α-subunit	β_1- and β_2-subunit V_h (mV)	k	β_1- and β_2-subunit V_h-1 (mV)	k_1	β_1- and β_2-subunit V_h-2 (mV)	k_2	β_3-subunit V_h (mV)	k	β_3-subunit V_h-1 (mV)	k_1	β_3-subunit V_h-2 (mV)	k_2	GFP V_h (mV)	k
CHO	$Na_V1.7$	-61 ± 3 (10)	9 ± 1 (10)												
αTC1-6	$Na_V1.3$	-59 ± 4 (9)	6 ± 0.5 (9)												
αTC1-6	$Na_V1.7$	-68 ± 3 (10)	7 ± 1 (10)												

Supplementary Table 1- Summary of V_h and k values of wild-type and tetrodotoxin-resistant Na_V channel α-subunits expressed in Ins1, HEK, EndoC-βh2, CHO and αTC1-6 cells

Values represent mean ± SEM of indicated number of cells (n). Note that $Na_V1.3$, $Na_V1.6$ and $Na_V1.7$ refer to the tetrodotoxin-resistant form of the channel. V_h represents membrane potential at which inactivation is half-maximal in cells with monophasic inactivation and k represents the slope factor. In cells with biphasic inactivation, V_h-1 and V_h-2 represent the membrane potential at which inactivation is half-maximal for the current components inactivating at negative and positive membrane potentials, respectively. k_1 and k_2, represent the respective slope factors for the currents inactivating with V_h-1 and V_h-2.

Cell	α-subunit	β_1- and β_2-subunit $V_{0.5}$ (mV)	k	β_3- subunit $V_{0.5}$ (mV)	k	GFP $V_{0.5}$ (mV)	k
Ins1	$Na_V1.3$	-12±1 (31)	8±1 (31)	-14±2 (6)	6±1 (6)		
Ins1	$Na_V1.5$	-35±2 (4)	8±1 (4)				
Ins1	$Na_V1.6$	-16±1 (18)	7±1 (18)	-16±1 (13)	7±1 (13)		
Ins1	$Na_V1.7$	-13±1 (39)	8±1(39)	-8±1 (5)	6±1 (5)		
HEK	$Na_V1.3$ WT	-18±1 (5)	5±1 (5)				
HEK	$Na_V1.5$ WT	-35±1 (6)	8±1 (6)				
HEK	$Na_V1.6$ WT	-9±1 (5)	8±1 (5)				
HEK	$Na_V1.7$ WT	-13±1 (7)	7±1 (7)				
HEK	$Na_V1.3$	-14±1 (7)	7±1 (7)	-8±2 (11)	7±1 (11)	-14±2 (9)	9±1 (9)
HEK	$Na_V1.6$	-5±1 (9)	9±1 (9)				
HEK	$Na_V1.7$	-12±1 (9)	8±1 (9)	-17±3 (6)	7±1 (6)	-10±1 (11)	8±1 (11)
EndoC-βh2	$Na_V1.3$	-17±1 (7)	6±1 (7)				
EndoC-βh2	$Na_V1.6$	-16±2 (8)	6±1 (8)				
EndoC-βh2	$Na_V1.7$	-17±2 (9)	7±2 (9)				
CHO	$Na_V1.3$	-2±1 (12)	7±1 (12)				
CHO	$Na_V1.7$	-6±1 (7)	5±1 (7)				
αTC1-6	$Na_V1.3$	-16±2 (7)	5±1 (7)				
αTC1-6	$Na_V1.7$	-9±2 (3)	8±1 (3)				

Supplementary Table 2- Summary of $V_{0.5}$ and k values of wild-type and tetrodotoxin-resistant Na_V channel α-subunits expressed in Ins1, HEK, EndoC-βh2, CHO and αTC1-6 cells

Values represent mean ± SEM of indicated number of cells (n). Note that $Na_V1.3$, $Na_V1.6$ and $Na_V1.7$ refer to the tetrodotoxin-resistant form of the channel. $V_{0.5}$ represents membrane potential at which activation is half-maximal.

Cell	α-subunit	Treatment condition	Endogenous β-subunit V_h (mV)	k	Endogenous β-subunit V_h-1 (mV)	k_1	Endogenous β-subunit V_h-2 (mV)	k_2	β_1- and β_2-subunit V_h (mV)	K	β_1- and β_2-subunit V_h-1 (mV)	k_1	β_1- and β_2-subunit V_h-2 (mV)	k_2
Ins1	Endogenous Na_V channels	β_3-subunit siRNA control	-81±2 (11)	11±1 (11)	-81±1 (11)	9±1 (11)	-43±3 (11)	6±2 (11)						
Ins1	Endogenous Na_V channels	β_3-subunit siRNA	-82±3 (9)	10±1 (9)	-83±2 (17)	10±1 (17)	-47±2 (17)	6±1 (17)						
Ins1	$Na_V1.7$ Control								-90±2 (28)	9±1 (28)	-94±4 (9)	10±1 (9)	-63±5 (9)	8±1 (2)
Ins1	N-terminal domain								-95±1 (7)	8±1 (7)	-98±1 (2)	9±1 (2)	-67±1 (2)	7±1 (2)
Ins1	L1L2								-88±1 (12)	9±1 (12)	-86±1 (3)	7±1 (3)	-49±5 (3)	13±1 (3)
Ins1	L3								-96±3 (12)	11±3 (12)	-98±3 (4)	13±2 (4)	-50±5 (4)	8±2 (4)
Ins1	C-terminal domain								-86±1 (5)	9±1 (5)	-84±1 (2)	10±1 (2)	-50±6 (2)	10±3 (2)
HEK	$Na_V1.7$ Control								-60±1 (6)	8±1 (6)				
HEK	N-terminal domain								-61±4 (6)	8±1 (6)				
HEK	L1L2								-66±2 (9)	9±1 (9)				
HEK	L3								-67±3 (11)	12±1 (11)				
HEK	C-terminal domain								-60±2 (8)	9±1 (8)				

Cell	α-subunit	Treatment condition	Endogenous β-subunit V_h (mV)	k	Endogenous β-subunit V_h-1 (mV)	k_1	Endogenous β-subunit V_h-2 (mV)	k_2	β_1- and β_2-subunit V_h (mV)	k	β_1- and β_2-subunit V_h-1 (mV)	k_1	β_1- and β_2-subunit V_h-2 (mV)	k_2
Ins1	Endogenous Na_V channels	Control	-84±5 (5)	9±1 (5)	-86±5 (6)	10±1 (6)	-46±4 (6)	5±1 (6)						
Ins1	Endogenous Na_V channels	20μM BAPTA-AM	-92±3 (8)	9±1 (8)	-89±3 (5)	10±1 (5)	-46±2 (5)	5±1 (5)						
Ins1	Endogenous Na_V channels	Control	-94±6 (2)	10±1 (2)	-94 (2)	10 (2)	-45 (2)	4 (2)						
Ins1	Endogenous Na_V channels	Chronic 10nM PMA	-91±2 (6)	11±1 (6)	-92±2 (5)	10±1 (5)	-46±2 (5)	5±1 (5)						
Ins1	$Na_V1.7$	Control							-96±1 (5)	8±1 (5)				
Ins1	$Na_V1.7$	Acute 10nMPMA							-96±4 (5)	10±2 (5)				
Ins1	$Na_V1.7$	Acute 100M BIM23056							-90±2 (5)	8±1 (5)				
Ins1	$Na_V1.7$	Control							-97±7 (5)	10±1 (5)	-106 (1)	4 (1)	-75 (1)	18 (1)
Ins1	$Na_V1.7$	100μM diazoxide							-106±3 (7)	10±1 (7)	-99 (2)	14 (2)	-72 (2)	12 (2)
Ins1	$Na_V1.7$	Control							-97 (2)	9 (2)				
Ins1	$Na_V1.7$	10μM s961							-97±1 (3)	8±1 (3)				
Ins1	$Na_V1.7$	Control							-99±1 (5)	7±1 (5)				

Cell	α-subunit	Treatment condition	Endogenous β-subunit V_h (mV)	k	Endogenous β-subunit V_h-1 (mV)	k_1	Endogenous β-subunit V_h-2 (mV)	k_2	β_1- and β_2-subunit V_h (mV)	k	β_1- and β_2-subunit V_h-1 (mV)	k_1	β_1- and β_2-subunit V_h-2 (mV)	k_2
Ins1	$Na_V1.7$	50μM PIP_2 diC8							-97±2 (5)	7±1 (5)				
Ins1	$Na_V1.7$	Control							-98±3 (7)	11±2 (7)				
Ins1	$Na_V1.7$	50μM Neomycin							-98±1 (7)	8±1 (7)				
HEK	$Na_V1.7$	Control							-57±2 (8)	7±1 (8)				
HEK	$Na_V1.7$	50μM PIP_2 diC8							-59±1 (7)	7±1 (7)				
Ins1	Endogenous Na_V channels	Chronic 5mM glucose	-70 ± 3 (16)	9±1 (16)	-80 ± 4 (6)	9±1 (6)	-41 ± 3 (6)	5±1 (6)						
Ins1	Endogenous Na_V channels	Chronic 11mM glucose	-74 ± 2 (13)	9±1 (13)	-73 ± 5 (9)	9±1 (9)	-43 ± 4 (9)	5±1 (9)						
Ins1	Endogenous Na_V channels	Chronic 25mM glucose	-72 ± 4 (7)	9±1 (7)	-78 ± 2 (11)	11±1 (11)	-39 ± 2 (11)	5±1 (11)						
Ins1	$Na_V1.3$	0.2mM $CoCl_2$							95±2 (3)	8±1 (3)	-100 (2)	9 (2)	-63 (2)	5 (2)
Ins1	$Na_V1.3$	2mM $CoCl_2$							-79±6 (8)	9±1 (8)	-87±2 (26)	9±1 (26)	-55±2 (26)	7±1 (26)
Ins1	$Na_V1.3$	10mM $CoCl_2$							-66±2 (6)	7±1 (6)	-73 (2)	10 (2)	-37 (2)	5 (2)
HEK	$Na_V1.3$	0.2mM $CoCl_2$							-55±2 (6)	8±1 (6)				
HEK	$Na_V1.3$	2mM $CoCl_2$							-47±2 (6)	8±1 (6)				

Cell	α-subunit	Treatment condition	Endogenous β-subunit V_h (mV)	k	Endogenous β-subunit V_h-1 (mV)	k_1	Endogenous β-subunit V_h-2 (mV)	k_2	β_1- and β_2-subunit V_h (mV)	k	β_1- and β_2-subunit V_h-1 (mV)	k_1	β_1- and β_2-subunit V_h-2 (mV)	k_2
HEK	$Na_V1.3$	10mM $CoCl_2$							-28±2 (6)	7±1 (6)				

Supplementary Table 3- Summary of V_h and k values of endogenous, $Na_V1.3$ and/or $Na_V1.7$ currents for the indicated treatment conditions in Ins1 and HEK cells

Values represent mean ± SEM of indicated number of cells (n). V_h represents membrane potential at which inactivation is half-maximal in cells with monophasic inactivation and k represents the slope factor. In cells with biphasic inactivation, V_h-1 and V_h-2 represent the membrane potential at which inactivation is half-maximal for the current components inactivating at negative and positive membrane potentials, respectively. k_1 and k_2, represent the respective slope factors for the currents inactivating with V_h-1 and V_h-2.

References

ABRIEL, H. 2010. Cardiac sodium channel Nav1.5 and interacting proteins: Physiology and pathophysiology. *Journal of Molecular and Cellular Cardiology,* 48**,** 2-11.

ADRIAENSSENS, A. E., SVENDSEN, B., LAM, B. Y. H., YEO, G. S. H., HOLST, J. J., REIMANN, F. & GRIBBLE, F. M. 2016. Transcriptomic profiling of pancreatic alpha, beta and delta cell populations identifies delta cells as a principal target for ghrelin in mouse islets. *Diabetologia,* 59**,** 2156-2165.

AHERN, C. A. 2013. What activates inactivation? *J Gen Physiol,* 142**,** 97-100.

AHERN, C. A., ZHANG, J. F., WOOKALIS, M. J. & HORN, R. 2005. Modulation of the cardiac sodium channel NaV1.5 by Fyn, a Src family tyrosine kinase. *Circ Res,* 96**,** 991-8.

AHN, H. S., BLACK, J. A., ZHAO, P., TYRRELL, L., WAXMAN, S. G. & DIB-HAJJ, S. D. 2011. Nav1.7 is the predominant sodium channel in rodent olfactory sensory neurons. *Mol Pain,* 7**,** 32.

ALBERTI, K. G. & ZIMMET, P. Z. 1998. Definition, diagnosis and classification of diabetes mellitus and its complications. Part 1: diagnosis and classification of diabetes mellitus provisional report of a WHO consultation. *Diabet Med,* 15**,** 539-53.

ALLOUIS, M., LE BOUFFANT, F., WILDERS, R., PEROZ, D., SCHOTT, J. J., NOIREAUD, J., LE MAREC, H., MEROT, J., ESCANDE, D. & BARO, I. 2006. 14-3-3 is a regulator of the cardiac voltage-gated sodium channel Nav1.5. *Circ Res,* 98**,** 1538-46.

ARMSTRONG, C. M. 2006. Na channel inactivation from open and closed states. *Proceedings of the National Academy of Sciences,* 103**,** 17991-17996.

ARMSTRONG, C. M. & BEZANILLA, F. 1973. Currents related to movement of the gating particles of the sodium channels. *Nature,* 242**,** 459-61.

ARMSTRONG, C. M. & BEZANILLA, F. 1974. Charge Movement Associated with the Opening and Closing of the Activation Gates of the Na Channels. *The Journal of General Physiology,* 63**,** 533-552.

ARMSTRONG, C. M. & BEZANILLA, F. 1977. Inactivation of the sodium channel. II. Gating current experiments. *J Gen Physiol,* 70**,** 567-90.

ARMSTRONG, C. M., BEZANILLA, F. & ROJAS, E. 1973. Destruction of sodium conductance inactivation in squid axons perfused with pronase. *J Gen Physiol,* 62**,** 375-91.

AROMOLARAN, A. S., CHAHINE, M. & BOUTJDIR, M. 2017. Regulation of Cardiac Voltage-Gated Sodium Channel by Kinases: Roles of Protein Kinases A and C. *Handb Exp Pharmacol*.

ASHCROFT, F. M., HARRISON, D. E. & ASHCROFT, S. J. 1984. Glucose induces closure of single potassium channels in isolated rat pancreatic beta-cells. *Nature,* 312**,** 446-8.

ASHCROFT, F. M. & RORSMAN, P. 1989. Electrophysiology of the pancreatic beta-cell. *Prog Biophys Mol Biol,* 54**,** 87-143.

ASHCROFT, F. M. & RORSMAN, P. 2013. K(ATP) channels and islet hormone secretion: new insights and controversies. *Nat Rev Endocrinol,* 9**,** 660-9.

BAEK, J. H., RUBINSTEIN, M., SCHEUER, T. & TRIMMER, J. S. 2014. Reciprocal changes in phosphorylation and methylation of mammalian brain sodium channels in response to seizures. *J Biol Chem,* 289**,** 15363-73.

BARG, S., GALVANOVSKIS, J., GOPEL, S. O., RORSMAN, P. & ELIASSON, L. 2000. Tight coupling between electrical activity and exocytosis in mouse glucagon-secreting alpha-cells. *Diabetes,* 49**,** 1500-10.

BARNETT, D. W., PRESSEL, D. M. & MISLER, S. 1995. Voltage-dependent Na+ and Ca2+ currents in human pancreatic islet beta-cells: evidence for roles in the generation of action potentials and insulin secretion. *Pflugers Arch,* 431**,** 272-82.

BAUKROWITZ, T., SCHULTE, U., OLIVER, D., HERLITZE, S., KRAUTER, T., TUCKER, S. J., RUPPERSBERG, J. P. & FAKLER, B. 1998. PIP2 and PIP as determinants for ATP inhibition of KATP channels. *Science,* 282**,** 1141-4.

BEN-JOHNY, M., DICK, I. E., SANG, L., LIMPITIKUL, W. B., KANG, P. W., NIU, J., BANERJEE, R., YANG, W., BABICH, J. S., ISSA, J. B., LEE, S. R., NAMKUNG, H., LI, J., ZHANG, M., YANG, P. S., BAZZAZI, H., ADAMS, P. J., JOSHI-MUKHERJEE, R., YUE, D. N. & YUE, D. T. 2015. Towards a Unified Theory of Calmodulin Regulation (Calmodulation) of Voltage-Gated Calcium and Sodium Channels. *Curr Mol Pharmacol,* 8**,** 188-205.

BENNER, C., VAN DER MEULEN, T., CACERES, E., TIGYI, K., DONALDSON, C. J. & HUISING, M. O. 2014. The transcriptional landscape of mouse beta cells compared to human beta cells reveals notable species differences in long non-coding RNA and protein-coding gene expression. *BMC Genomics,* 15**,** 620.

BENNETT, E., URCAN, M. S., TINKLE, S. S., KOSZOWSKI, A. G. & LEVINSON, S. R. 1997. Contribution of sialic acid to the voltage dependence of sodium channel gating. A possible electrostatic mechanism. *J Gen Physiol,* 109**,** 327-43.

BENSON, M. D., LI, Q. J., KIECKHAFER, K., DUDEK, D., WHORTON, M. R., SUNAHARA, R. K., IÑIGUEZ-LLUHÍ, J. A. & MARTENS, J. R. 2007. SUMO modification regulates inactivation of the voltage-gated potassium channel Kv1.5. *Proc Natl Acad Sci U S A,* 104**,** 1805-10.

BLACK, J. A., DIB-HAJJ, S., MCNABOLA, K., JESTE, S., RIZZO, M. A., KOCSIS, J. D. & WAXMAN, S. G. 1996. Spinal sensory neurons express multiple sodium channel alpha-subunit mRNAs. *Brain Res Mol Brain Res,* 43**,** 117-31.

BLACK, J. A. & WAXMAN, S. G. 2013. Noncanonical roles of voltage-gated sodium channels. *Neuron,* 80**,** 280-91.

BODE, H. P., WEBER, S., FEHMANN, H. C. & GOKE, B. 1999. A nutrient-regulated cytosolic calcium oscillator in endocrine pancreatic glucagon-secreting cells. *Pflugers Arch,* 437**,** 324-34.

BRAUN, M., RAMRACHEYA, R., AMISTEN, S., BENGTSSON, M., MORITOH, Y., ZHANG, Q., JOHNSON, P. R. & RORSMAN, P. 2009. Somatostatin release, electrical activity, membrane currents and exocytosis in human pancreatic delta cells. *Diabetologia,* 52**,** 1566-78.

BRAUN, M., RAMRACHEYA, R., BENGTSSON, M., ZHANG, Q., KARANAUSKAITE, J., PARTRIDGE, C., JOHNSON, P. R. & RORSMAN, P. 2008. Voltage-gated ion channels in human pancreatic beta-cells: electrophysiological characterization and role in insulin secretion. *Diabetes,* 57**,** 1618-28.

BRERETON, M. F., VERGARI, E., ZHANG, Q. & CLARK, A. 2015. Alpha-, Delta- and PP-cells: Are They the Architectural Cornerstones of Islet Structure and Co-ordination? *J Histochem Cytochem,* 63**,** 575-91.
BRIANT, L., SALEHI, A., VERGARI, E., ZHANG, Q. & RORSMAN, P. 2016. Glucagon secretion from pancreatic alpha-cells. *Ups J Med Sci,* 121**,** 113-9.
BRIANT, L. J., ZHANG, Q., VERGARI, E., KELLARD, J. A., RODRIGUEZ, B., ASHCROFT, F. M. & RORSMAN, P. 2017a. Functional identification of islet cell types by electrophysiological fingerprinting. *J R Soc Interface,* 14.
BRIANT, L. J. B., REINBOTHE, T. M., SPILIOTIS, I., MIRANDA, C., RODRIGUEZ, B. & RORSMAN, P. 2017b. delta-cells and beta-cells are electrically coupled and regulate alpha-cell activity via somatostatin. *J Physiol*.
BRIANT, L. J. B., REINBOTHE, T. M., SPILIOTIS, I., MIRANDA, C., RODRIGUEZ, B. & RORSMAN, P. 2018. δ-cells and β-cells are electrically coupled and regulate α-cell activity via somatostatin. *The Journal of Physiology,* 596**,** 197-215.
BRUGADA, P. 2016. Brugada syndrome: More than 20 years of scientific excitement. *Journal of Cardiology,* 67**,** 215-220.
CABRERA, O., BERMAN, D. M., KENYON, N. S., RICORDI, C., BERGGREN, P. O. & CAICEDO, A. 2006. The unique cytoarchitecture of human pancreatic islets has implications for islet cell function. *Proc Natl Acad Sci U S A,* 103**,** 2334-9.
CACHELIN, A. B., DE PEYER, J. E., KOKUBUN, S. & REUTER, H. 1983. Sodium channels in cultured cardiac cells. *J Physiol,* 340**,** 389-401.
CALHOUN, J. D. & ISOM, L. L. 2014. The role of non-pore-forming beta subunits in physiology and pathophysiology of voltage-gated sodium channels. *Handb Exp Pharmacol,* 221**,** 51-89.
CAMPBELL, J. E. & DRUCKER, D. J. 2015. Islet alpha cells and glucagon--critical regulators of energy homeostasis. *Nat Rev Endocrinol,* 11**,** 329-38.
CATTERALL, W. A. 2000. From ionic currents to molecular mechanisms: the structure and function of voltage-gated sodium channels. *Neuron,* 26**,** 13-25.
CATTERALL, W. A. 2014. Structure and function of voltage-gated sodium channels at atomic resolution. *Exp Physiol,* 99**,** 35-51.
CATTERALL, W. A., DIB-HAJJ, S., MEISLER, M. H. & PIETROBON, D. 2008. Inherited neuronal ion channelopathies: new windows on complex neurological diseases. *J Neurosci,* 28**,** 11768-77.
CATTERALL, W. A., GOLDIN, A. L. & WAXMAN, S. G. 2005. International Union of Pharmacology. XLVII. Nomenclature and structure-function relationships of voltage-gated sodium channels. *Pharmacol Rev,* 57**,** 397-409.
CATTERALL, W. A., WISEDCHAISRI, G. & ZHENG, N. 2017. The chemical basis for electrical signaling. *Nat Chem Biol,* 13**,** 455-463.
CHAKRAVARTHY, H., GU, X., ENGE, M., DAI, X., WANG, Y., DAMOND, N., DOWNIE, C., LIU, K., WANG, J., XING, Y., CHERA, S., THOREL, F., QUAKE, S., OBERHOLZER, J., MACDONALD, P. E., HERRERA, P. L. & KIM, S. K. 2017. Converting Adult Pancreatic Islet alpha Cells into beta Cells by Targeting Both Dnmt1 and Arx. *Cell Metab,* 25**,** 622-634.
CHATTOPADHYAY, M., MATA, M. & FINK, D. J. 2008. Continuous delta-opioid receptor activation reduces neuronal voltage-gated sodium channel

(NaV1.7) levels through activation of protein kinase C in painful diabetic neuropathy. *J Neurosci,* 28**,** 6652-8.
CHATTOPADHYAY, M., MATA, M. & FINK, D. J. 2011. Vector-mediated release of GABA attenuates pain-related behaviors and reduces Na(V)1.7 in DRG neurons. *Eur J Pain,* 15**,** 913-20.
CHATTOPADHYAY, M., ZHOU, Z., HAO, S., MATA, M. & FINK, D. J. 2012. Reduction of voltage gated sodium channel protein in DRG by vector mediated miRNA reduces pain in rats with painful diabetic neuropathy. *Mol Pain,* 8**,** 17.
CHENG, X., DIB-HAJJ, S. D., TYRRELL, L., TE MORSCHE, R. H., DRENTH, J. P. & WAXMAN, S. G. 2011. Deletion mutation of sodium channel Na(V)1.7 in inherited erythromelalgia: enhanced slow inactivation modulates dorsal root ganglion neuron hyperexcitability. *Brain,* 134**,** 1972-86.
COHEN, S. A. & BARCHI, R. L. 1993. Voltage-dependent sodium channels. *Int Rev Cytol,* 137c**,** 55-103.
COPENHAVER, M. & HOFFMAN, R. P. 2017. Type 1 diabetes: where are we in 2017? *Transl Pediatr,* 6**,** 359-364.
COSTA, M. R., CASNELLIE, J. E. & CATTERALL, W. A. 1982. Selective phosphorylation of the alpha subunit of the sodium channel by cAMP-dependent protein kinase. *J Biol Chem,* 257**,** 7918-21.
COX, J. J., REIMANN, F., NICHOLAS, A. K., THORNTON, G., ROBERTS, E., SPRINGELL, K., KARBANI, G., JAFRI, H., MANNAN, J., RAASHID, Y., AL-GAZALI, L., HAMAMY, H., VALENTE, E. M., GORMAN, S., WILLIAMS, R., MCHALE, D. P., WOOD, J. N., GRIBBLE, F. M. & WOODS, C. G. 2006. An SCN9A channelopathy causes congenital inability to experience pain. *Nature,* 444**,** 894-8.
CUMMINS, T. R., AGLIECO, F., RENGANATHAN, M., HERZOG, R. I., DIB-HAJJ, S. D. & WAXMAN, S. G. 2001. Nav1.3 sodium channels: rapid repriming and slow closed-state inactivation display quantitative differences after expression in a mammalian cell line and in spinal sensory neurons. *J Neurosci,* 21**,** 5952-61.
DART, C. 2010. Lipid microdomains and the regulation of ion channel function. *J Physiol,* 588**,** 3169-78.
DAVIS, M. J., WU, X., NURKIEWICZ, T. R., KAWASAKI, J., GUI, P., HILL, M. A. & WILSON, E. 2001. Regulation of ion channels by protein tyrosine phosphorylation. *Am J Physiol Heart Circ Physiol,* 281**,** H1835-62.
DE MARINIS, Y. Z., SALEHI, A., WARD, C. E., ZHANG, Q., ABDULKADER, F., BENGTSSON, M., BRAHA, O., BRAUN, M., RAMRACHEYA, R., AMISTEN, S., HABIB, A. M., MORITOH, Y., ZHANG, E., REIMANN, F., ROSENGREN, A., SHIBASAKI, T., GRIBBLE, F., RENSTROM, E., SEINO, S., ELIASSON, L. & RORSMAN, P. 2010. GLP-1 inhibits and adrenaline stimulates glucagon release by differential modulation of N- and L-type Ca2+ channel-dependent exocytosis. *Cell Metab,* 11**,** 543-553.
DHALLA, A. K., YANG, M., NING, Y., KAHLIG, K. M., KRAUSE, M., RAJAMANI, S. & BELARDINELLI, L. 2014. Blockade of Na+ channels in pancreatic alpha-cells has antidiabetic effects. *Diabetes,* 63**,** 3545-56.
DIB-HAJJ, S. D., CUMMINS, T. R., BLACK, J. A. & WAXMAN, S. G. 2010. Sodium channels in normal and pathological pain. *Annu Rev Neurosci,* 33**,** 325-47.

DIB-HAJJ, S. D., YANG, Y., BLACK, J. A. & WAXMAN, S. G. 2013. The NaV1.7 sodium channel: from molecule to man. *Nat Rev Neurosci,* 14**,** 49-62.
DIGRUCCIO, M. R., MAWLA, A. M., DONALDSON, C. J., NOGUCHI, G. M., VAUGHAN, J., COWING-ZITRON, C., VAN DER MEULEN, T. & HUISING, M. O. 2016. Comprehensive alpha, beta and delta cell transcriptomes reveal that ghrelin selectively activates delta cells and promotes somatostatin release from pancreatic islets. *Mol Metab,* 5**,** 449-58.
DOLENŠEK, J., RUPNIK, M. S. & STOŽER, A. 2015. Structural similarities and differences between the human and the mouse pancreas. *Islets,* 7.
DUSTRUDE, E. T., WILSON, S. M., JU, W., XIAO, Y. & KHANNA, R. 2013. CRMP2 Protein SUMOylation Modulates NaV1.7 Channel Trafficking. *J Biol Chem,* 288**,** 24316-31.
EDIDIN, M. 1993. Patches and fences: probing for plasma membrane domains. *Journal of Cell Science,* 1993**,** 165.
EDNIE, A. R. & BENNETT, E. S. 2012. Modulation of voltage-gated ion channels by sialylation. *Compr Physiol,* 2**,** 1269-301.
ERNST, S. J., AGUILAR-BRYAN, L. & NOEBELS, J. L. 2009. Sodium channel beta1 regulatory subunit deficiency reduces pancreatic islet glucose-stimulated insulin and glucagon secretion. *Endocrinology,* 150**,** 1132-9.
FEATHERSTONE, D. E., RICHMOND, J. E. & RUBEN, P. C. 1996. Interaction between fast and slow inactivation in Skm1 sodium channels. *Biophys J,* 71**,** 3098-109.
FERNANDEZ, J. M., FOX, A. P. & KRASNE, S. 1984. Membrane patches and whole-cell membranes: a comparison of electrical properties in rat clonal pituitary (GH3) cells. *J Physiol,* 356**,** 565-85.
FERTLEMAN, C. R., BAKER, M. D., PARKER, K. A., MOFFATT, S., ELMSLIE, F. V., ABRAHAMSEN, B., OSTMAN, J., KLUGBAUER, N., WOOD, J. N., GARDINER, R. M. & REES, M. 2006. SCN9A mutations in paroxysmal extreme pain disorder: allelic variants underlie distinct channel defects and phenotypes. *Neuron,* 52**,** 767-74.
FORBES, J. M. & COOPER, M. E. 2013. Mechanisms of diabetic complications. *Physiol Rev,* 93**,** 137-88.
FRANCIS, K. R., WEI, L. & YU, S. P. 2015. SRC tyrosine kinases regulate neuronal differentiation of mouse embryonic stem cells via modulation of voltage-gated sodium channel activity. *Neurochem Res,* 40**,** 674-87.
FRANKLIN, I., GROMADA, J., GJINOVCI, A., THEANDER, S. & WOLLHEIM, C. B. 2005. Beta-cell secretory products activate alpha-cell ATP-dependent potassium channels to inhibit glucagon release. *Diabetes,* 54**,** 1808-15.
GALBIATI, F., RAZANI, B. & LISANTI, M. P. 2001. Emerging themes in lipid rafts and caveolae. *Cell,* 106**,** 403-11.
GOLDBERG, Y. P., MACFARLANE, J., MACDONALD, M. L., THOMPSON, J., DUBE, M. P., MATTICE, M., FRASER, R., YOUNG, C., HOSSAIN, S., PAPE, T., PAYNE, B., RADOMSKI, C., DONALDSON, G., IVES, E., COX, J., YOUNGHUSBAND, H. B., GREEN, R., DUFF, A., BOLTSHAUSER, E., GRINSPAN, G. A., DIMON, J. H., SIBLEY, B. G., ANDRIA, G., TOSCANO, E., KERDRAON, J., BOWSHER, D., PIMSTONE, S. N., SAMUELS, M. E., SHERRINGTON, R. & HAYDEN, M. R. 2007. Loss-of-function mutations in the Nav1.7 gene underlie congenital indifference to pain in multiple human populations. *Clin Genet,* 71**,** 311-9.

GOLDIN, A. L., BARCHI, R. L., CALDWELL, J. H., HOFMANN, F., HOWE, J. R., HUNTER, J. C., KALLEN, R. G., MANDEL, G., MEISLER, M. H., NETTER, Y. B., NODA, M., TAMKUN, M. M., WAXMAN, S. G., WOOD, J. N. & CATTERALL, W. A. 2000. Nomenclature of voltage-gated sodium channels. *Neuron,* 28**,** 365-8.

GONOI, T. & HILLE, B. 1987. Gating of Na channels. Inactivation modifiers discriminate among models. *J Gen Physiol,* 89**,** 253-74.

GOPEL, S., KANNO, T., BARG, S., GALVANOVSKIS, J. & RORSMAN, P. 1999. Voltage-gated and resting membrane currents recorded from B-cells in intact mouse pancreatic islets. *J Physiol,* 521 Pt 3**,** 717-28.

GOPEL, S. O., KANNO, T., BARG, S., WENG, X. G., GROMADA, J. & RORSMAN, P. 2000. Regulation of glucagon release in mouse -cells by KATP channels and inactivation of TTX-sensitive Na+ channels. *J Physiol,* 528**,** 509-20.

GROMADA, J., FRANKLIN, I. & WOLLHEIM, C. B. 2007. Alpha-cells of the endocrine pancreas: 35 years of research but the enigma remains. *Endocr Rev,* 28**,** 84-116.

GRUNDY, S. M. 2008. Metabolic syndrome pandemic. *Arteriosclerosis, Thrombosis, and Vascular Biology,* 28**,** 629-636.

GYLFE, E. 2013. Glucose Control of Glucagon Secretion: There Is More to It Than K(ATP) Channels. *Diabetes,* 62**,** 1391-3.

GYLFE, E. 2016. Glucose control of glucagon secretion-'There's a brand-new gimmick every year'. *Ups J Med Sci,* 121**,** 120-32.

GYLFE, E. & GILON, P. 2014. Glucose regulation of glucagon secretion. *Diabetes Res Clin Pract,* 103**,** 1-10.

HAUGE-EVANS, A. C., KING, A. J., CARMIGNAC, D., RICHARDSON, C. C., ROBINSON, I., LOW, M. J., CHRISTIE, M. R., PERSAUD, S. J. & JONES, P. M. 2009. Somatostatin Secreted by Islet δ-Cells Fulfills Multiple Roles as a Paracrine Regulator of Islet Function. *Diabetes,* 58**,** 403-11.

HERZOG, R. I., CUMMINS, T. R., GHASSEMI, F., DIB-HAJJ, S. D. & WAXMAN, S. G. 2003. Distinct repriming and closed-state inactivation kinetics of Nav1.6 and Nav1.7 sodium channels in mouse spinal sensory neurons. *J Physiol,* 551**,** 741-50.

HILLE, B. 1971. The Permeability of the Sodium Channel to Organic Cations in Myelinated Nerve. *The Journal of General Physiology,* 58**,** 599-619.

HILLE, B. 1972. The Permeability of the Sodium Channel to Metal Cations in Myelinated Nerve. *The Journal of General Physiology,* 59**,** 637-658.

HILLE, B. 2001. *Ion channels of excitable membranes,* Sunderland, Mass., Sinauer.

HIRIART, M. & MATTESON, D. R. 1988. Na channels and two types of Ca channels in rat pancreatic B cells identified with the reverse hemolytic plaque assay. *J Gen Physiol,* 91**,** 617-39.

HIYAMA, T. Y., WATANABE, E., ONO, K., INENAGA, K., TAMKUN, M. M., YOSHIDA, S. & NODA, M. 2002. Na(x) channel involved in CNS sodium-level sensing. *Nat Neurosci,* 5**,** 511-2.

HODGKIN, A. L. & HUXLEY, A. F. 1952. A quantitative description of membrane current and its application to conduction and excitation in nerve. *J Physiol,* 117**,** 500-44.

HOEIJMAKERS, J. G., FABER, C. G., MERKIES, I. S. & WAXMAN, S. G. 2014. Channelopathies, painful neuropathy, and diabetes: which way does the causal arrow point? *Trends Mol Med,* 20**,** 544-50.

HOLLAND, K. D., KEARNEY, J. A., GLAUSER, T. A., BUCK, G., KEDDACHE, M., BLANKSTON, J. R., GLAASER, I. W., KASS, R. S. & MEISLER, M. H. 2008. Mutation of sodium channel SCN3A in a patient with cryptogenic pediatric partial epilepsy. *Neurosci Lett,* 433**,** 65-70.

ISOM, L. L. 2002. The role of sodium channels in cell adhesion. *Front Biosci,* 7**,** 12-23.

ISOM, L. L., DE JONGH, K. S., PATTON, D. E., REBER, B. F., OFFORD, J., CHARBONNEAU, H., WALSH, K., GOLDIN, A. L. & CATTERALL, W. A. 1992. Primary structure and functional expression of the beta 1 subunit of the rat brain sodium channel. *Science,* 256**,** 839-42.

JACOBSON, D. A., WICKSTEED, B. L. & PHILIPSON, L. H. 2009. The α-Cell Conundrum: ATP-Sensitive K(+) Channels and Glucose Sensing. *Diabetes,* 58**,** 304-6.

JARECKI, B. W., PIEKARZ, A. D., JACKSON, J. O., 2ND & CUMMINS, T. R. 2010. Human voltage-gated sodium channel mutations that cause inherited neuronal and muscle channelopathies increase resurgent sodium currents. *J Clin Invest,* 120**,** 369-78.

JO, S. & BEAN, B. P. 2014. Sidedness of carbamazepine accessibility to voltage-gated sodium channels. *Mol Pharmacol,* 85**,** 381-7.

JOHNSON, D. & BENNETT, E. S. 2006. Isoform-specific effects of the beta2 subunit on voltage-gated sodium channel gating. *J Biol Chem,* 281**,** 25875-81.

JOHNSON, D., MONTPETIT, M. L., STOCKER, P. J. & BENNETT, E. S. 2004. The sialic acid component of the beta1 subunit modulates voltage-gated sodium channel function. *J Biol Chem,* 279**,** 44303-10.

JOHNSON, J. A., ADAK, S. & MOCHLY-ROSEN, D. 1995. Prolonged phorbol ester treatment down-regulates protein kinase C isozymes and increases contraction rate in neonatal cardiac myocytes. *Life Sciences,* 57**,** 1027-1038.

KOMADA, M. & SORIANO, P. 2002. βIV-spectrin regulates sodium channel clustering through ankyrin-G at axon initial segments and nodes of Ranvier. *J Cell Biol,* 156**,** 337-48.

KONTIS, K. J. & GOLDIN, A. L. 1997. Sodium Channel Inactivation Is Altered by Substitution of Voltage Sensor Positive Charges. *The Journal of General Physiology,* 110**,** 403.

KRAMER, R. H. 1990. Patch cramming: Monitoring intracellular messengers in intact cells with membrane patches containing detector inn channels. *Neuron,* 4**,** 335-341.

KRUGER, L. C. & ISOM, L. L. 2016. Voltage-Gated Na+ Channels: Not Just for Conduction. *Cold Spring Harb Perspect Biol,* 8.

LAEDERMANN, C. J., ABRIEL, H. & DECOSTERD, I. 2015. Post-translational modifications of voltage-gated sodium channels in chronic pain syndromes. *Front Pharmacol,* 6**,** 263.

LEHMANN-HORN, F. & JURKAT-ROTT, K. 1999. Voltage-gated ion channels and hereditary disease. *Physiol Rev,* 79**,** 1317-72.

LEUNG, Y. M., AHMED, I., SHEU, L., TSUSHIMA, R. G., DIAMANT, N. E., HARA, M. & GAISANO, H. Y. 2005. Electrophysiological characterization of pancreatic islet cells in the mouse insulin promoter-green fluorescent protein mouse. *Endocrinology,* 146**,** 4766-75.

LIU, C. J., DIB-HAJJ, S. D., RENGANATHAN, M., CUMMINS, T. R. & WAXMAN, S. G. 2003. Modulation of the cardiac sodium channel Nav1.5 by fibroblast growth factor homologous factor 1B. *J Biol Chem,* 278**,** 1029-36.

LIU, Y. J., VIEIRA, E. & GYLFE, E. 2004. A store-operated mechanism determines the activity of the electrically excitable glucagon-secreting pancreatic alpha-cell. *Cell Calcium,* 35**,** 357-65.

LONDON, B., MICHALEC, M., MEHDI, H., ZHU, X., KERCHNER, L., SANYAL, S., VISWANATHAN, P. C., PFAHNL, A. E., SHANG, L. L., MADHUSUDANAN, M., BATY, C. J., LAGANA, S., ALEONG, R., GUTMANN, R., ACKERMAN, M. J., MCNAMARA, D. M., WEISS, R. & DUDLEY, S. C., JR. 2007. Mutation in glycerol-3-phosphate dehydrogenase 1 like gene (GPD1-L) decreases cardiac Na+ current and causes inherited arrhythmias. *Circulation,* 116**,** 2260-8.

LOU, X. L., YU, X., CHEN, X. K., DUAN, K. L., HE, L. M., QU, A. L., XU, T. & ZHOU, Z. 2003. Na+ channel inactivation: a comparative study between pancreatic islet beta-cells and adrenal chromaffin cells in rat. *J Physiol,* 548**,** 191-202.

LUNDBAEK, J. A., BIRN, P., HANSEN, A. J., SOGAARD, R., NIELSEN, C., GIRSHMAN, J., BRUNO, M. J., TAPE, S. E., EGEBJERG, J., GREATHOUSE, D. V., MATTICE, G. L., KOEPPE, R. E., 2ND & ANDERSEN, O. S. 2004. Regulation of sodium channel function by bilayer elasticity: the importance of hydrophobic coupling. Effects of Micelle-forming amphiphiles and cholesterol. *J Gen Physiol,* 123**,** 599-621.

MACDONALD, P. E., DE MARINIS, Y. Z., RAMRACHEYA, R., SALEHI, A., MA, X., JOHNSON, P. R., COX, R., ELIASSON, L. & RORSMAN, P. 2007. A K ATP channel-dependent pathway within alpha cells regulates glucagon release from both rodent and human islets of Langerhans. *PLoS Biol,* 5**,** e143.

MALHOTRA, J. D., KAZEN-GILLESPIE, K., HORTSCH, M. & ISOM, L. L. 2000. Sodium channel beta subunits mediate homophilic cell adhesion and recruit ankyrin to points of cell-cell contact. *J Biol Chem,* 275**,** 11383-8.

MALHOTRA, J. D., KOOPMANN, M. C., KAZEN-GILLESPIE, K. A., FETTMAN, N., HORTSCH, M. & ISOM, L. L. 2002. Structural requirements for interaction of sodium channel beta 1 subunits with ankyrin. *J Biol Chem,* 277**,** 26681-8.

MALHOTRA, J. D., THYAGARAJAN, V., CHEN, C. & ISOM, L. L. 2004. Tyrosine-phosphorylated and nonphosphorylated sodium channel beta1 subunits are differentially localized in cardiac myocytes. *J Biol Chem,* 279**,** 40748-54.

MALTSEV, V. A., REZNIKOV, V., UNDROVINAS, N. A., SABBAH, H. N. & UNDROVINAS, A. 2008. Modulation of late sodium current by Ca2+, calmodulin, and CaMKII in normal and failing dog cardiomyocytes: similarities and differences. *Am J Physiol Heart Circ Physiol,* 294**,** H1597-608.

MANTEGAZZA, M., YU, F. H., CATTERALL, W. A. & SCHEUER, T. 2001. Role of the C-terminal domain in inactivation of brain and cardiac sodium channels. *Proc Natl Acad Sci U S A,* 98**,** 15348-53.

MCCARTHY, M. I. 2017. Genetics of T2DM in 2016: Biological and translational insights from T2DM genetics. *Nat Rev Endocrinol,* 13**,** 71-72.

MCCORMICK, K. A., ISOM, L. L., RAGSDALE, D., SMITH, D., SCHEUER, T. & CATTERALL, W. A. 1998. Molecular determinants of Na+ channel function

in the extracellular domain of the beta1 subunit. *J Biol Chem,* 273**,** 3954-62.
MCCUSKER, E. C., BAGNERIS, C., NAYLOR, C. E., COLE, A. R., D'AVANZO, N., NICHOLS, C. G. & WALLACE, B. A. 2012. Structure of a bacterial voltage-gated sodium channel pore reveals mechanisms of opening and closing. *Nat Commun,* 3**,** 1102.
MEADOWS, L. S. & ISOM, L. L. 2005. Sodium channels as macromolecular complexes: implications for inherited arrhythmia syndromes. *Cardiovasc Res,* 67**,** 448-58.
MEREGALLI, P. G., TAN, H. L., PROBST, V., KOOPMANN, T. T., TANCK, M. W., BHUIYAN, Z. A., SACHER, F., KYNDT, F., SCHOTT, J.-J., ALBUISSON, J., MABO, P., BEZZINA, C. R., LE MAREC, H. & WILDE, A. A. M. 2009. Type of SCN5A mutation determines clinical severity and degree of conduction slowing in loss-of-function sodium channelopathies. *Heart Rhythm,* 6**,** 341-348.
MESSNER, D. J. & CATTERALL, W. A. 1985. The sodium channel from rat brain. Separation and characterization of subunits. *J Biol Chem,* 260**,** 10597-604.
MIKI, T., LISS, B., MINAMI, K., SHIUCHI, T., SARAYA, A., KASHIMA, Y., HORIUCHI, M., ASHCROFT, F., MINOKOSHI, Y., ROEPER, J. & SEINO, S. 2001. ATP-sensitive K+ channels in the hypothalamus are essential for the maintenance of glucose homeostasis. *Nat Neurosci,* 4**,** 507-12.
MORAN, O., NIZZARI, M. & CONTI, F. 2000. Endogenous expression of the β1A sodium channel subunit in HEK-293 cells. *FEBS Letters,* 473**,** 132-134.
NAMADURAI, S., YEREDDI, N. R., CUSDIN, F. S., HUANG, C. L. H., CHIRGADZE, D. Y. & JACKSON, A. P. 2015. A new look at sodium channel β subunits. *Open Biol,* 5.
NARAYANAN, A. & JACOBSON, M. P. 2009. Computational studies of protein regulation by post-translational phosphorylation. *Current Opinion in Structural Biology,* 19**,** 156-163.
NASSAR, M. A., STIRLING, L. C., FORLANI, G., BAKER, M. D., MATTHEWS, E. A., DICKENSON, A. H. & WOOD, J. N. 2004. Nociceptor-specific gene deletion reveals a major role for Nav1.7 (PN1) in acute and inflammatory pain. *Proc Natl Acad Sci U S A,* 101**,** 12706-11.
NICA, A. C., ONGEN, H., IRMINGER, J. C., BOSCO, D., BERNEY, T., ANTONARAKIS, S. E., HALBAN, P. A. & DERMITZAKIS, E. T. 2013. Cell-type, allelic, and genetic signatures in the human pancreatic beta cell transcriptome. *Genome Res,* 23**,** 1554-62.
NILSEN, K. B., NICHOLAS, A. K., WOODS, C. G., MELLGREN, S. I., NEBUCHENNYKH, M. & AASLY, J. 2009. Two novel SCN9A mutations causing insensitivity to pain. *Pain,* 143**,** 155-8.
PATTON, D. E., ISOM, L. L., CATTERALL, W. A. & GOLDIN, A. L. 1994. The adult rat brain beta 1 subunit modifies activation and inactivation gating of multiple sodium channel alpha subunits. *J Biol Chem,* 269**,** 17649-55.
PAYANDEH, J., GAMAL EL-DIN, T. M., SCHEUER, T., ZHENG, N. & CATTERALL, W. A. 2012. Crystal structure of a voltage-gated sodium channel in two potentially inactivated states. *Nature,* 486**,** 135-9.
PEI, Z., PAN, Y. & CUMMINS, T. R. 2017. Posttranslational Modification of Sodium Channels. *Handb Exp Pharmacol*.

PLANT, T. D. 1988. Na+ currents in cultured mouse pancreatic B-cells. *Pflügers Archiv,* 411**,** 429-435.
PRESSEL, D. M. & MISLER, S. 1991. Role of voltage-dependent ionic currents in coupling glucose stimulation to insulin secretion in canine pancreatic islet B-cells. *J Membr Biol,* 124**,** 239-53.
RAMRACHEYA, R., WARD, C., SHIGETO, M., WALKER, J. N., AMISTEN, S., ZHANG, Q., JOHNSON, P. R., RORSMAN, P. & BRAUN, M. 2010. Membrane potential-dependent inactivation of voltage-gated ion channels in alpha-cells inhibits glucagon secretion from human islets. *Diabetes,* 59**,** 2198-208.
RAVASSARD, P., HAZHOUZ, Y., PECHBERTY, S., BRICOUT-NEVEU, E., ARMANET, M., CZERNICHOW, P. & SCHARFMANN, R. 2011. A genetically engineered human pancreatic beta cell line exhibiting glucose-inducible insulin secretion. *J Clin Invest,* 121**,** 3589-97.
RAVIER, M. A. & RUTTER, G. A. 2005. Glucose or insulin, but not zinc ions, inhibit glucagon secretion from mouse pancreatic alpha-cells. *Diabetes,* 54**,** 1789-97.
RIZZETTO, R., ROCCHETTI, M., SALA, L., RONCHI, C., VILLA, A., FERRANDI, M., MOLINARI, I., BERTUZZI, F. & ZAZA, A. 2015. Late sodium current (INaL) in pancreatic beta-cells. *Pflugers Arch,* 467**,** 1757-68.
RORSMAN, P., ARKHAMMAR, P. & BERGGREN, P. O. 1986. Voltage-activated Na+ currents and their suppression by phorbol ester in clonal insulin-producing RINm5F cells. *Am J Physiol,* 251**,** C912-9.
RORSMAN, P., RAMRACHEYA, R., RORSMAN, N. J. & ZHANG, Q. 2014. ATP-regulated potassium channels and voltage-gated calcium channels in pancreatic alpha and beta cells: similar functions but reciprocal effects on secretion. *Diabetologia,* 57**,** 1749-61.
RORSMAN, P., SALEHI, S. A., ABDULKADER, F., BRAUN, M. & MACDONALD, P. E. 2008. K(ATP)-channels and glucose-regulated glucagon secretion. *Trends Endocrinol Metab,* 19**,** 277-84.
RORSMAN, P. & TRUBE, G. 1985. Glucose dependent K+-channels in pancreatic beta-cells are regulated by intracellular ATP. *Pflugers Arch,* 405**,** 305-9.
RUDY, B. 1978. Slow inactivation of the sodium conductance in squid giant axons. Pronase resistance. *J Physiol,* 283**,** 1-21.
SATO, P. Y., MUSA, H., COOMBS, W., GUERRERO-SERNA, G., PATINO, G. A., TAFFET, S. M., ISOM, L. L. & DELMAR, M. 2009. Loss of plakophilin-2 expression leads to decreased sodium current and slower conduction velocity in cultured cardiac myocytes. *Circ Res,* 105**,** 523-6.
SCHARFMANN, R., PECHBERTY, S., HAZHOUZ, Y., VON BULOW, M., BRICOUT-NEVEU, E., GRENIER-GODARD, M., GUEZ, F., RACHDI, L., LOHMANN, M., CZERNICHOW, P. & RAVASSARD, P. 2014. Development of a conditionally immortalized human pancreatic beta cell line. *J Clin Invest,* 124**,** 2087-98.
SCHMIDT, J. W. & CATTERALL, W. A. 1987. Palmitylation, sulfation, and glycosylation of the alpha subunit of the sodium channel. Role of post-translational modifications in channel assembly. *J Biol Chem,* 262**,** 13713-23.
SHEETS, P. L., JACKSON, J. O., 2ND, WAXMAN, S. G., DIB-HAJJ, S. D. & CUMMINS, T. R. 2007. A Nav1.7 channel mutation associated with hereditary erythromelalgia contributes to neuronal hyperexcitability and displays reduced lidocaine sensitivity. *J Physiol,* 581**,** 1019-31.

SHEN, H., ZHOU, Q., PAN, X., LI, Z., WU, J. & YAN, N. 2017. Structure of a eukaryotic voltage-gated sodium channel at near-atomic resolution. *Science,* 355.
SHIRAHATA, E., IWASAKI, H., TAKAGI, M., LIN, C., BENNETT, V., OKAMURA, Y. & HAYASAKA, K. 2006. Ankyrin-G regulates inactivation gating of the neuronal sodium channel, Nav1.6. *J Neurophysiol,* 96**,** 1347-57.
SHYNG, S. L. & NICHOLS, C. G. 1998. Membrane phospholipid control of nucleotide sensitivity of KATP channels. *Science,* 282**,** 1138-41.
SILVA, A. M., DICKEY, A. S., BARNETT, D. W. & MISLER, S. 2009. Ion channels underlying stimulus-exocytosis coupling and its cell-to-cell heterogeneity in beta-cells of transplantable porcine islets of Langerhans. *Channels (Austin),* 3**,** 91-100.
SIMONS, K. & EHEHALT, R. 2002. Cholesterol, lipid rafts, and disease. *J Clin Invest,* 110**,** 597-603.
SRIVASTAVA, J., PROCYK, K. J., ITURRIOZ, X. & PARKER, P. J. 2002. Phosphorylation is required for PMA- and cell-cycle-induced degradation of protein kinase Cdelta. *Biochem J,* 368**,** 349-55.
STAMBOULIAN, S., CHOI, J. S., AHN, H. S., CHANG, Y. W., TYRRELL, L., BLACK, J. A., WAXMAN, S. G. & DIB-HAJJ, S. D. 2010. ERK1/2 mitogen-activated protein kinase phosphorylates sodium channel Na(v)1.7 and alters its gating properties. *J Neurosci,* 30**,** 1637-47.
STOCKER, P. J. & BENNETT, E. S. 2006. Differential sialylation modulates voltage-gated Na+ channel gating throughout the developing myocardium. *J Gen Physiol,* 127**,** 253-65.
STRUYK, A. F. & CANNON, S. C. 2002. Slow inactivation does not block the aqueous accessibility to the outer pore of voltage-gated Na channels. *J Gen Physiol,* 120**,** 509-16.
STUHMER, W., CONTI, F., SUZUKI, H., WANG, X., NODA, M., YAHAGI, N., KUBO, H. & NUMA, S. 1989. Structural parts involved in activation and inactivation of the sodium channel. *Nature,* 339**,** 597-603.
TAN, Z. Y., PRIEST, B. T., KRAJEWSKI, J. L., KNOPP, K. L., NISENBAUM, E. S. & CUMMINS, T. R. 2014. Protein kinase C enhances human sodium channel hNav1.7 resurgent currents via a serine residue in the domain III-IV linker. *FEBS Lett,* 588**,** 3964-9.
THORENS, B. 2011. Brain glucose sensing and neural regulation of insulin and glucagon secretion. *Diabetes Obes Metab,* 13 Suppl 1**,** 82-8.
UEDA, K., VALDIVIA, C., MEDEIROS-DOMINGO, A., TESTER, D. J., VATTA, M., FARRUGIA, G., ACKERMAN, M. J. & MAKIELSKI, J. C. 2008. Syntrophin mutation associated with long QT syndrome through activation of the nNOS-SCN5A macromolecular complex. *Proc Natl Acad Sci U S A,* 105**,** 9355-60.
ULBRICHT, W. 2005. Sodium Channel Inactivation: Molecular Determinants and Modulation. *Physiological Reviews,* 85**,** 1271-1301.
VALDIVIA, C. R., UEDA, K., ACKERMAN, M. J. & MAKIELSKI, J. C. 2009. GPD1L links redox state to cardiac excitability by PKC-dependent phosphorylation of the sodium channel SCN5A. *Am J Physiol Heart Circ Physiol,* 297**,** H1446-52.

VASSILEV, P., SCHEUER, T. & CATTERALL, W. A. 1989. Inhibition of inactivation of single sodium channels by a site-directed antibody. *Proc Natl Acad Sci U S A,* 86**,** 8147-51.

VATTA, M., ACKERMAN, M. J., YE, B., MAKIELSKI, J. C., UGHANZE, E. E., TAYLOR, E. W., TESTER, D. J., BALIJEPALLI, R. C., FOELL, J. D., LI, Z., KAMP, T. J. & TOWBIN, J. A. 2006. Mutant caveolin-3 induces persistent late sodium current and is associated with long-QT syndrome. *Circulation,* 114**,** 2104-12.

VIEIRA, E., SALEHI, A. & GYLFE, E. 2007. Glucose inhibits glucagon secretion by a direct effect on mouse pancreatic alpha cells. *Diabetologia,* 50**,** 370-9.

VIGNALI, S., LEISS, V., KARL, R., HOFMANN, F. & WELLING, A. 2006. Characterization of voltage-dependent sodium and calcium channels in mouse pancreatic A- and B-cells. *J Physiol,* 572**,** 691-706.

VIJAYARAGAVAN, K., BOUTJDIR, M. & CHAHINE, M. 2004. Modulation of Nav1.7 and Nav1.8 peripheral nerve sodium channels by protein kinase A and protein kinase C. *J Neurophysiol,* 91**,** 1556-69.

WAECHTER, C. J., SCHMIDT, J. W. & CATTERALL, W. A. 1983. Glycosylation is required for maintenance of functional sodium channels in neuroblastoma cells. *J Biol Chem,* 258**,** 5117-23.

WALKER, J. N., RAMRACHEYA, R., ZHANG, Q., JOHNSON, P. R., BRAUN, M. & RORSMAN, P. 2011. Regulation of glucagon secretion by glucose: paracrine, intrinsic or both? *Diabetes Obes Metab,* 13 Suppl 1**,** 95-105.

WAXMAN, S. G., KOCSIS, J. D. & BLACK, J. A. 1994. Type III sodium channel mRNA is expressed in embryonic but not adult spinal sensory neurons, and is reexpressed following axotomy. *J Neurophysiol,* 72**,** 466-70.

WEISS, J., PYRSKI, M., JACOBI, E., BUFE, B., WILLNECKER, V., SCHICK, B., ZIZZARI, P., GOSSAGE, S. J., GREER, C. A., LEINDERS-ZUFALL, T., WOODS, C. G., WOOD, J. N. & ZUFALL, F. 2011. Loss-of-function mutations in sodium channel Nav1.7 cause anosmia. *Nature,* 472**,** 186-90.

WEST, J. W., PATTON, D. E., SCHEUER, T., WANG, Y., GOLDIN, A. L. & CATTERALL, W. A. 1992. A cluster of hydrophobic amino acid residues required for fast Na(+)-channel inactivation. *Proceedings of the National Academy of Sciences of the United States of America,* 89**,** 10910-10914.

WINGO, T. L., SHAH, V. N., ANDERSON, M. E., LYBRAND, T. P., CHAZIN, W. J. & BALSER, J. R. 2004. An EF-hand in the sodium channel couples intracellular calcium to cardiac excitability. *Nat Struct Mol Biol,* 11**,** 219-25.

WITTMACK, E. K., RUSH, A. M., HUDMON, A., WAXMAN, S. G. & DIB-HAJJ, S. D. 2005. Voltage-gated sodium channel Nav1.6 is modulated by p38 mitogen-activated protein kinase. *J Neurosci,* 25**,** 6621-30.

WOOD, S. & SLATER, C. 1998. β-Spectrin Is Colocalized with Both Voltage-gated Sodium Channels and Ankyrin(G) at the Adult Rat Neuromuscular Junction. *J Cell Biol,* 140**,** 675-84.

WU, G., AI, T., KIM, J. J., MOHAPATRA, B., XI, Y., LI, Z., ABBASI, S., PUREVJAV, E., SAMANI, K., ACKERMAN, M. J., QI, M., MOSS, A. J., SHIMIZU, W., TOWBIN, J. A., CHENG, J. & VATTA, M. 2008. alpha-1-syntrophin mutation and the long-QT syndrome: a disease of sodium channel disruption. *Circ Arrhythm Electrophysiol,* 1**,** 193-201.

XIA, F., GAO, X., KWAN, E., LAM, P. P., CHAN, L., SY, K., SHEU, L., WHEELER, M. B., GAISANO, H. Y. & TSUSHIMA, R. G. 2004. Disruption of pancreatic beta-cell lipid rafts modifies Kv2.1 channel gating and insulin exocytosis. *J Biol Chem,* 279**,** 24685-91.

XU, X., GUO, F., LV, X., FENG, R., MIN, D., MA, L., LIU, Y., ZHAO, J., WANG, L., CHEN, T., SHAW, C., HAO, L. & CAI, J. 2013. Abnormal changes in voltage-gated sodium channels Na(V)1.1, Na(V)1.2, Na(V)1.3, Na(V)1.6 and in calmodulin/calmodulin-dependent protein kinase II, within the brains of spontaneously epileptic rats and tremor rats. *Brain Res Bull,* 96**,** 1-9.

YANG, Y., WANG, Y., LI, S., XU, Z., LI, H., MA, L., FAN, J., BU, D., LIU, B., FAN, Z., WU, G., JIN, J., DING, B., ZHU, X. & SHEN, Y. 2004. Mutations in SCN9A, encoding a sodium channel alpha subunit, in patients with primary erythermalgia. *J Med Genet,* 41**,** 171-4.

YAROV-YAROVOY, V., DECAEN, P. G., WESTENBROEK, R. E., PAN, C. Y., SCHEUER, T., BAKER, D. & CATTERALL, W. A. 2012. Structural basis for gating charge movement in the voltage sensor of a sodium channel. *Proc Natl Acad Sci U S A,* 109**,** E93-102.

YOUNG, K. A. & CALDWELL, J. H. 2005. Modulation of skeletal and cardiac voltage-gated sodium channels by calmodulin. *J Physiol,* 565**,** 349-70.

ZAKON, H. H. 2012. Adaptive evolution of voltage-gated sodium channels: the first 800 million years. *Proc Natl Acad Sci U S A,* 109 Suppl 1**,** 10619-25.

ZHANG, Q., CHIBALINA, M. V., BENGTSSON, M., GROSCHNER, L. N., RAMRACHEYA, R., RORSMAN, N. J., LEISS, V., NASSAR, M. A., WELLING, A., GRIBBLE, F. M., REIMANN, F., HOFMANN, F., WOOD, J. N., ASHCROFT, F. M. & RORSMAN, P. 2014. Na+ current properties in islet alpha- and beta-cells reflect cell-specific Scn3a and Scn9a expression. *J Physiol,* 592**,** 4677-96.

ZHANG, Q., RAMRACHEYA, R., LAHMANN, C., TARASOV, A., BENGTSSON, M., BRAHA, O., BRAUN, M., BRERETON, M., COLLINS, S., GALVANOVSKIS, J., GONZALEZ, A., GROSCHNER L , N., RORSMAN N , J. G., SALEHI, A., TRAVERS M , E., WALKER J , N., GLOYN A , L., GRIBBLE, F., JOHNSON P , R. V., REIMANN, F., ASHCROFT F , M. & RORSMAN, P. 2013. Role of K(ATP) Channels in Glucose-Regulated Glucagon Secretion and Impaired Counterregulation in Type 2 Diabetes. *Cell Metab,* 18**,** 871-82.

ZHANG, X., REN, W., DECAEN, P., YAN, C., TAO, X., TANG, L., WANG, J., HASEGAWA, K., KUMASAKA, T., HE, J., WANG, J., CLAPHAM, D. E. & YAN, N. 2012. Crystal structure of an orthologue of the NaChBac voltage-gated sodium channel. *Nature,* 486**,** 130-4.

ZHANG, Y., HARTMANN, H. A. & SATIN, J. 1999. Glycosylation influences voltage-dependent gating of cardiac and skeletal muscle sodium channels. *J Membr Biol,* 171**,** 195-207.

ZOU, N., WU, X., JIN, Y. Y., HE, M. Z., WANG, X. X., SU, L. D., RUPNIK, M., WU, Z. Y., LIANG, L. & SHEN, Y. 2013. ATP regulates sodium channel kinetics in pancreatic islet beta cells. *J Membr Biol,* 246**,** 101-7.